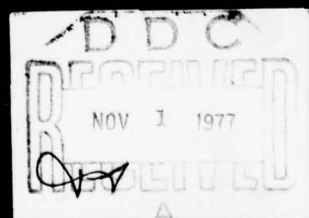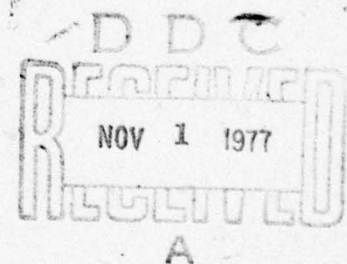DMAAC/RP-76-001

GRAVITATIONAL

MODELING

SEPTEMBER 1976

by
Charles W. Beierle
Walter J. Rothermel
DoD Gravity Correlation Branch

DDC
RECEIVED
NOV 1 1977

A

DEFENSE MAPPING AGENCY
AEROSPACE CENTER
ST LOUIS AIR FORCE STATION, MISSOURI 63118
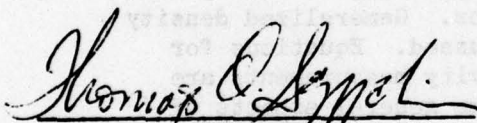
ACKNOWLEDGMENTS

PREFACE

GENERAL: This publication is one of a series of publications on developments relating to mapping, charting, geodesy, and geophysics. Each publication is written by Defense Mapping Agency Aerospace Center scientists and technicians qualified by training and experience to contribute knowledge and technology to the selected subject.

PURPOSE: To set forth a basic and unified approach to gravitational modeling in one publication.
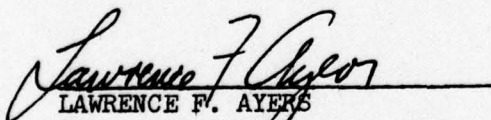
REPRODUCTION: This publication contains in figures 2-14 and 2-17, material that is copyrighted by Dr. Manik Talwani and the Academic Press. Figures 2-14 and 2-17 are reproduced with the full permission and knowledge of the Academic Press and Dr. Talwani. Reproduction of any copyrighted material is not allowed without the written permission of the original copyright owner. Reproduction of all parts except figures 2-14 and 2-17, is permitted for any purpose of the United States Government.

DISTRIBUTION: General public release by the National Technical Information Service, U. S. Department of Commerce, Springfield, Virginia 22151, is approved. Qualified requestors may obtain copies from the Defense Documentation Center.

REVIEWED

THOMAS O. SEPPELIN
Chief, Research Department

LAWRENCE F. AYERS
Technical Director

APPROVED

JAMES H. ST. CLAIR, Colonel, USAF
Director

ABSTRACT

Formulas for computing the gravitational effect of some simple two- and three-dimensional geometric figures are presented in forms suitable for use with digital computers a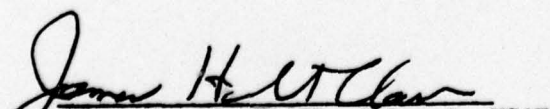nd in many cases, programmable desk calculators. Basic computation schemes are presented for complex two- and three-dimensional bodies of arbitrary shape. Some simple inversion rules or techniques are presented which yield approximations of depth based on simple geometric figures. Such inversion techniques are particularly applicable where gravity measurements and/or other geophysical data are sparse. These techniques yield first approximations of the depth, size, and shape of the mass or masses causing a given residual gravity anomaly. Density or density contrast is independent of depth, size and shape and is discussed separately. Density and porosity are defined by appropriate equations. Generalized density relationships, based on rock types are discussed. Equations for determination of effective density from gravity measurements are presented. The concluding remarks cover some general aspects of gravitational modeling.

CONTENTS

LIST OF FIGURES AND TABLES

TABLES

LIST OF NOTATIONS

The notation is uniform insofar as possible. Any change in the notation listed below is specifically noted. The notation is generally based on the following definitions:

X, Y, Z   = Define the three coordinate axes of a left-handed Cartesian coordinate system in three-dimensional models.

X, Z   = Define the two coordinate axes in two-dimensional models.

x   = The horizontal ground distance along the X-axis, usually from a point above the center of the body to the computation point.

y   = The horizontal ground distance along the Y-axis, usually from a point above the center of the body to the computation point.

z   = The depth from the surface, usually the X, Y plane, to the center of the body.

r   = The distance from the center of the body to the computation point.

R   = The radius of the body.

Δx, Δy, Δz = Thickness of laminar bodies.

K   = Universal constant of gravitation = 6.673×10^{-8} $cm^3/(grams)(sec)^2$.

g_v = Calculated gravitational effect, usually the vertical component of the acceleration of gravity (in milligals)

U   = Gravitational potential

ρ = Volume density or density contrast as a function of x, y, z.

μ = Surface density or density contrast as a function of x, z.

A_s = Cross-sectional area of two-dimensional bodies as a function of x, z.

V   = Volume.

M   = Mass.

GRAVITATIONAL MODELING

1. INTRODUCTION

The purpose of this publication is to present a unified discussion of several widely accepted analytical techniques of gravitational modeling along with some elementary techniques of interpretation in the form of a reference manual. The formulation of these techniques is oriented towards applications compatible with programmable desk calculators and digital computers.

Gravitational modeling refers to the direct problem of determining the mass attraction of a geologic body or structure of known shape, depth, size, and density or density contrast. The reliability of the solution depends on how well the shape of the body or structure is known and how closely it can be approximated by analytical expressions. Thus, the direct problem can be solved only when specific relatively homogeneous geologic bodies or structures can be identified as the gravitating masses.

Such detailed knowledge of geologic structure is limited to features in the upper portion of the earth's crust. The attraction of such bodies is assumed to be an approximation of the local or residual component of the observed gravity anomaly field.

Some common structures which significantly influence the residual gravity anomaly field are: well defined topographic features, sedimentary basins, faults, anticlines, synclines and intrusive bodies of discernible shape.

Gravimetric interpretation refers to the inverse gravimetric problem. The solution to the inverse problem has as its objective the determination of the unknown parameters (i.e., shape, depth, and density or density contrast) from a known residual gravity anomaly field. A unique solution to the inverse problem is theoretically impossible because a given residual gravity anomaly field can be produced by an infinite number of mass configurations.

However, reliable first approximations of the unknown parameters can often be obtained from the shape and magnitude of residual gravity anomaly profiles as well as from various other sources of geologic and geophysical data. Such sources include: field maps, electric logs, seismic profiles, and borehole information. The first approximations of the unknown parameters can then be used in an iterative inversion procedure. In such a procedure, the unknown parameters are then successively adjusted until an observed residual gravity anomaly field is approximated within some predetermined tolerances. The adjusted unknown parameters must then be examined within the context of geologic and geophysical realism. It is often necessary to further constrain the allowable range of any or all of the unknown parameters in successive models.

The inversion of residual gravity anomalies can yield no better results than the residual gravity anomalies themselves. There are certain inherent ambiguities in the separation techniques for computing residual gravity anomalies. The ambiguities are due to the fact that

measuring techniques depict the influences of all the masses within
the measuring range of the instruments. Thus, it is impossible to
completely separate the regional and residual anomaly fields. Therefore,
care must be taken to minimize observational errors and provide the
best possible observed data.

This report contains a relatively complete list of the formulas
and computing schemes which form the basis for the solution of the
direct problem. However, there is only a partial list of formulas
for depth and density determination. Such formulas yield realistic
ranges of depth and density and do not constitute a solution of the
inverse problem. However, they can yield valid first approximations
of depth and density for use in gravitational modeling. Detailed
approaches to the solution of the inverse problem are beyond the purpose
and scope of this publication and can be found in many of the cited
references.

The two-dimensional and three-dimensional formulas are presented
in the general formats used by Heiland (1968) and Talwani (1973). The
functional notation used with the three-dimensional formulas is identi-
cal with that presented by Talwani (1973).

1.1 Mathematical Development

1.1.1 The Three-Dimensional Case

Based on Newton's inverse square law, the gravitational
potential U of a gravitating body of Volume V (Figure 1-1) is given
by:

$$U = K \rho \int_V \int \int \frac{dV}{r} \tag{1-1}$$

where:

$$r = (x^2 + y^2 + z^2)^{1/2} \tag{1-2}$$

$dV = dx \ dy \ dz$ (volume element, Figure 1-2)

Expressed in rectangular coordinates, the **gravitational** potential of V becomes:

$$U = K \rho \int_V \int \int \frac{dx \ dy \ dz}{(x^2 + y^2 + z^2)^{1/2}} \tag{1-3}$$

In spherical coordinates, r, ϕ, α (Figure 1-3), the gravitational potential is then expressed by:

$$U = K \rho \int_V \int \int r \ dr \cos\phi \ d\phi \ d\alpha \tag{1-4}$$

Equation 1-4 is derived by making the following substitutions in equation 1-3:

$$r = (x^2 + y^2 + z^2)^{1/2} \tag{1-5}$$

$r^2 \cos\phi \ dr \ d\phi \ d\alpha = dx \ dy \ dz$ (volume element (Figure 1-2))

$r \sin\phi = z$

The gravitational attraction, g_V, of a gravitating body of volume V is the partial derivative of the potential U with respect to z, and is defined as follows:

$$g_V \equiv \frac{\partial U}{\partial z} = K \rho \int_V \int \int \frac{z}{r^3} \ dV \tag{1-6}$$

4

Figure 1-1

Gravitating Body of Volume, V
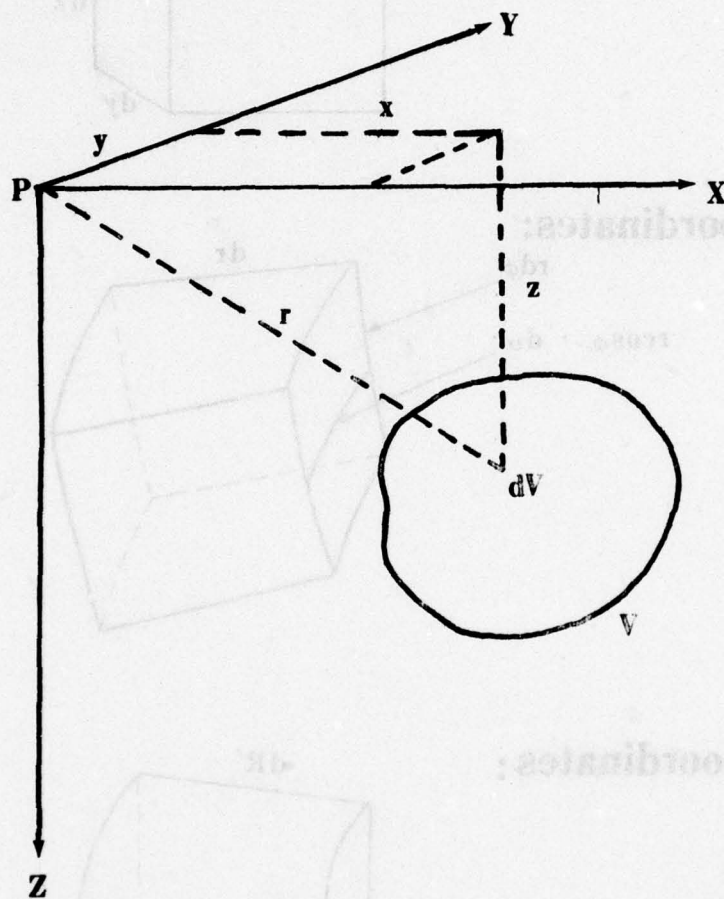
Volume Elements

Cartesian Coordinates

dx

dz

dy

Spherical Coordinates:

$rd\phi$

$r\cos\phi \cdot d\alpha$

dr

Cylindrical Coordinates:

dR'

dz
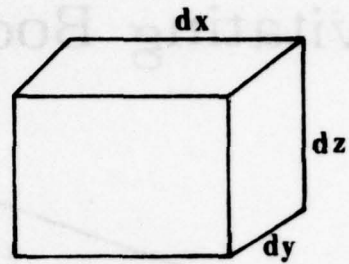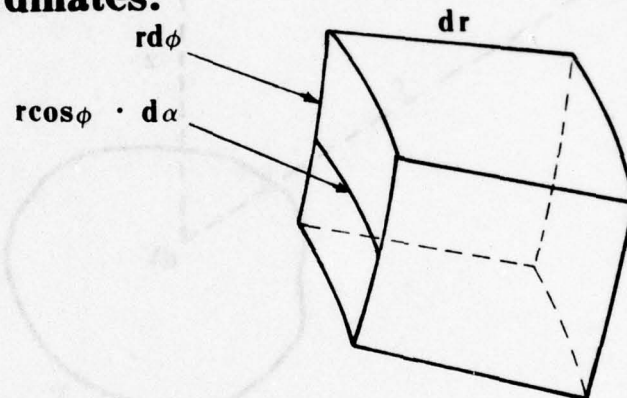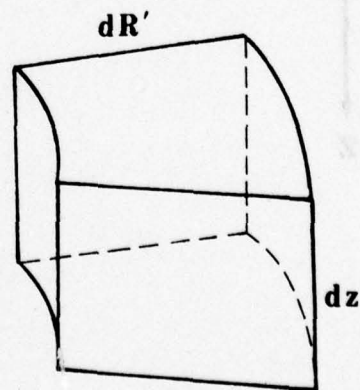
Figure 1–3

Coordinate Systems

P

Y

x

y

R′

α

X

φ

z

r

dV

V

Z
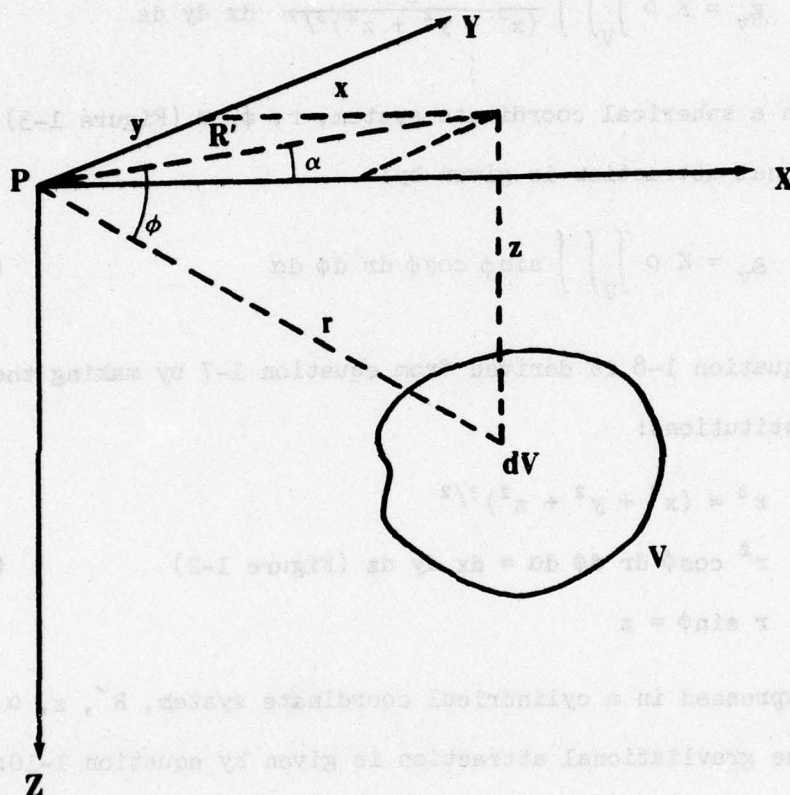
Coordinates:
Cartesian: x,y,z
Spherical: ϕ, r, α
Cylindrical: R′, z, α
Conical: R′, ϕ, α

Expressed in rectangular coordinates, Figure 1-1, equation 1-6 becomes:

$$g_v = K \rho \iiint_V \frac{z}{(x^2 + y^2 + z^2)^{3/2}} \, dx \, dy \, dz \qquad (1-7)$$

In a spherical coordinate system, r, ϕ, α (Figure 1-3), the gravitational attraction is given by:

$$g_v = K \rho \iiint_V \sin\phi \, \cos\phi \, dr \, d\phi \, d\alpha \qquad (1-8)$$

Equation 1-8 is derived from equation 1-7 by making the following substitutions:

$$r^3 = (x^2 + y^2 + z^2)^{3/2}$$
$$r^2 \cos\phi \, dr \, d\phi \, d\alpha = dx \, dy \, dz \text{ (Figure 1-2)} \qquad (1-9)$$
$$r \sin\phi = z$$

Expressed in a cylindrical coordinate system, R', z, α Figure 1-3, the gravitational attraction is given by equation 1-10:

$$g_v = K \rho \iiint_V \frac{R' \, z \, dz \, dR' \, d\alpha}{(R'^2 + z^2)^{3/2}} \qquad (1-10)$$

where, equation 1-10 is derived from equation 1-7 by the following substitutions.

$$(R'^2 + z^2)^{3/2} = (x^2 + y^2 + z^2)^{3/2} \qquad (1-11)$$
$$R' \, z \, dz \, dR' \, d\alpha = z \, dx \, dy \, dz \text{ (Figure 1-2)}$$

In a conical coordinate system R', ϕ, α (Figure 1-3), the

gravitational attraction is then given by equation 1-12.

$$g_v = K \rho \int_V \int \int \sin\phi \; dR' \; d\phi \; d\alpha \qquad (1\text{-}12)$$

Equation 1-12 is derived from equation 1-7 by making the following substitutions:

$$R'^3 = (x^2 + y^2 + z^2)^{3/2} \qquad (1\text{-}13)$$

$$R'^2 \; dR' \; d\phi \; d\alpha = dx \; dy \; dz$$

$$R' \sin\phi = z$$

1.1.2 The Two-Dimensional Case

Many topographic and geologic structures are elongated along their strike. Such structures can often be modeled by two-dimensional approximations. The following paragraphs present the basic mathematical development of the two-dimensional approach.

Two-dimensional structures are modeled by positioning the coordinate axes such that the Y-axis is infinite in extent and is parallel to the strike length, or elongated dimension, of the structure to be modeled. The shape of the structure is then defined by a vertical cross-section of area, A_s, Figure 1-4.

The formula for computing the gravitational attraction of two-dimensional bodies is derived by integrating equation 1-7 with limits from $-\infty$ to $+\infty$ in Y.

$$g_v = K \rho \int \int z \; dx \; dz \int_{-\infty}^{+\infty} \frac{dy}{(x^2 + y^2 + z^2)^{3/2}} \qquad (1\text{-}14)$$

The integral to be evaluated is then rearranged and becomes:

9

Figure 1-4
Two Dimensional Body
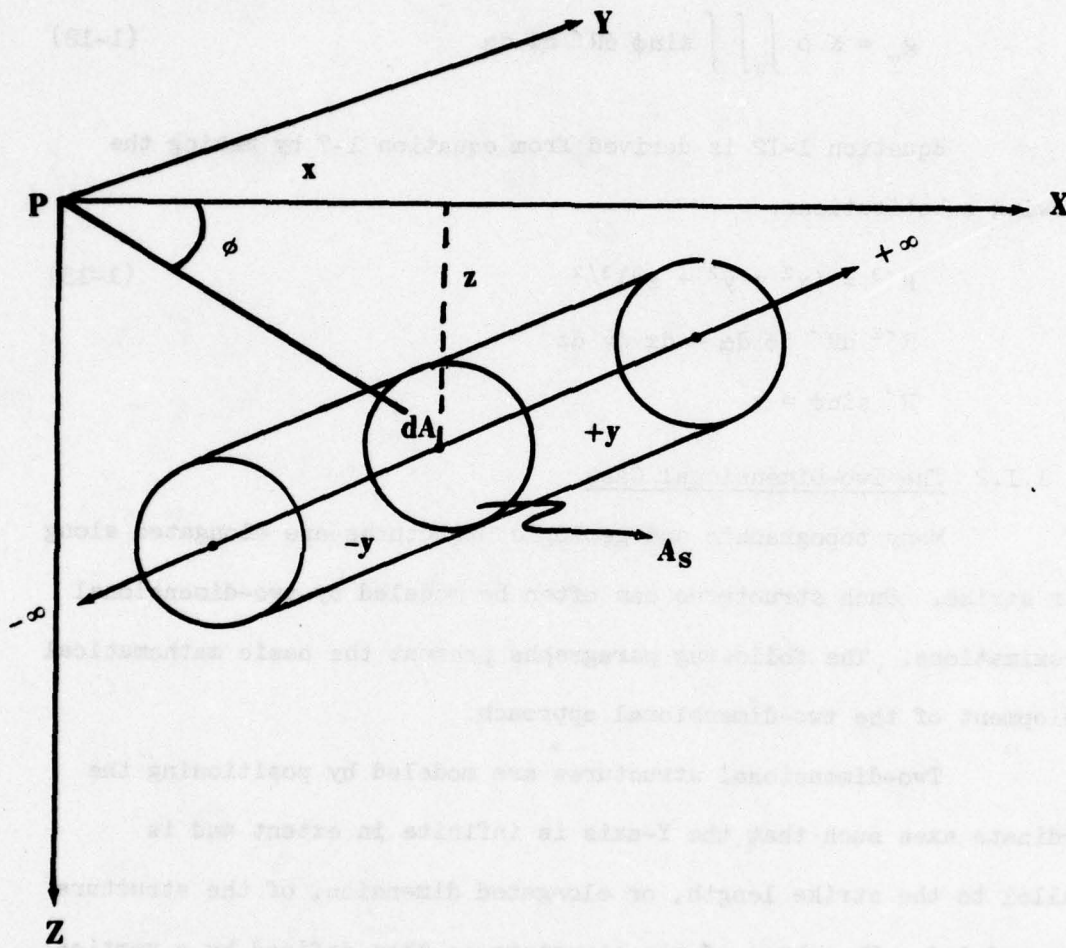
$$T = \int_{-\infty}^{+\infty} \frac{dy}{(x^2 + z^2)^{3/2} \left(1 + \frac{y^2}{x^2 + z^2}\right)^{3/2}} \qquad (1\text{-}15)$$

The following substitutions are made:

$$\tan u = \frac{y}{(x^2 + z^2)^{1/2}} \quad \text{and} \quad \frac{du}{\cos^2 u} = \frac{dy}{(x^2 + z^2)^{1/2}} \qquad (1\text{-}16)$$

Then, equation 1-15 becomes:

$$T = \frac{1}{(x^2 + z^2)} \int_{-\pi/2}^{+\pi/2} \cos u \, du \qquad (1\text{-}17)$$

$$= \frac{2}{(x^2 + z^2)}$$

Equation 1-17 is substituted into equation 1-14 and the resultant formula is:

$$g_v = 2 K \rho \int_A \!\!\int \frac{z}{(x^2 + z^2)} \, dx \, dz \qquad (1\text{-}18)$$

Equation 1-18 expressed in polar coordinates r, ϕ becomes, (Figure 1-4):

$$g_v = 2 K \rho \int_A \!\!\int \sin\phi \, dr \, d\phi \qquad (1\text{-}19)$$

Two-dimensional formulas can be made to closely approximate bodies of finite extent by making "end corrections" for the finite strike length, y (Figure 1-4). The "end correction" for an elongated body of finite strike length is defined by the following integral equation:

$$\delta g_v = 2 K \rho y \int_A \!\!\int \frac{z \, dx \, dz}{(x^2 + z^2) \sqrt{x^2 + z^2 + y^2}} \qquad (1\text{-}20)$$

11

which is given in polar coordinates by:

$$\delta g_v = 2 K \rho y \int_A \int \frac{\cos\phi \, d\phi \, dr}{\sqrt{R^2 + y^2}} \qquad (1-21)$$

Equations 1-20 and 1-21 cannot be integrated in closed form and must be evaluated numerically. The vertical component of the attraction (i.e., gravitational attraction) of the bodies discussed in following sections will be referred to as "gravitational effect."

2. THREE-DIMENSIONAL ATTRACTION FORMULAS

2.1 Some Simple Three-Dimensional Formulas

All the formulas presented in this section are derived from equation 1-6 of the preceeding section on mathematical development. Talwani (1973) shows that many of the formulas can be expressed in functional form as follows:

$$g_v = K \rho \, f(x,y,z) \, F(x/z) \qquad (2-1)$$

where $f(x,y,z)$ is a variable function of x, y, or z and $F(x/z)$ is a dimensionless scaling function. The function $F(x/z)$ is dependent on the variation of x/z from zero to one. Therefore, the evaluation of the formulas can be greatly simplified using plots of $F(x/z)$ against the ratios x/z and z/x.

2.1.1 Rectangular Volume Element

The dimensions of the volume element are given as Δx, Δy, and Δz as shown in Figure 2-1. The gravitational effect of the volume element is given by equation 2-2.

$$g_v = K \rho \, \Delta x \, \Delta y \, \Delta z \, \frac{z}{(x^2 + y^2 + z^2)^{3/2}}$$

$$= K \rho \, \Delta x \, \Delta y \, \Delta z \, z \, \frac{1}{(r^2 + z^2)^{3/2}} \qquad (2-2)$$

where:

$$r = (x^2 + y^2)^{1/2}$$

The function $F_1(r/z)$ is then defined as:

$$F_1(r/z) = (1 + r^2/z^2)^{-3/2} \qquad (2-3)$$

and is plotted in Figure 2-2.

13

Figure 2-1

Rectangular Volume Element
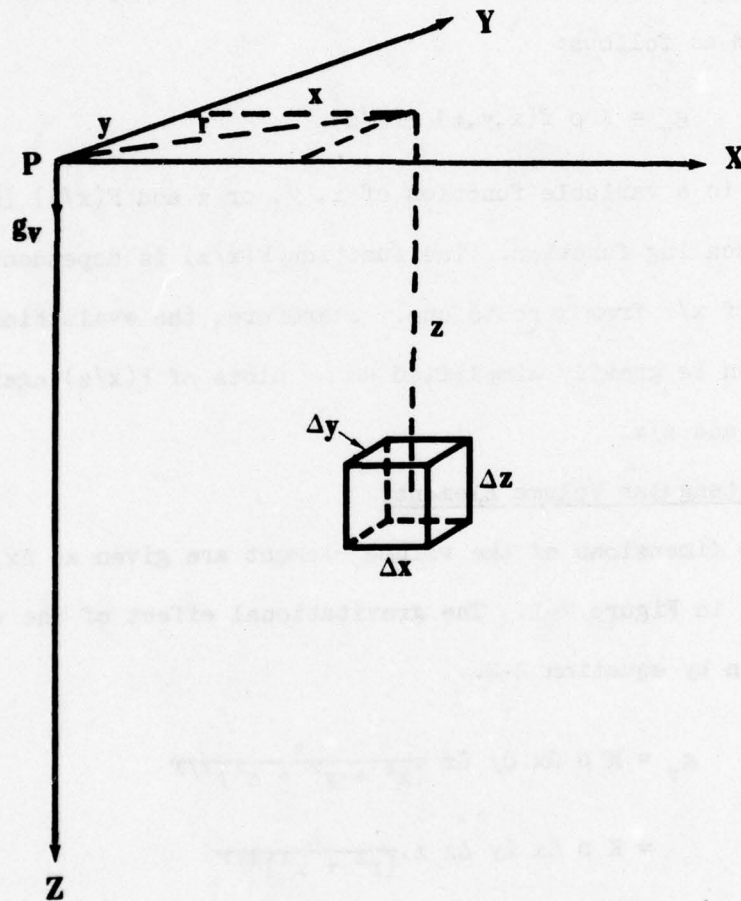
Figure 2-2

Function F1
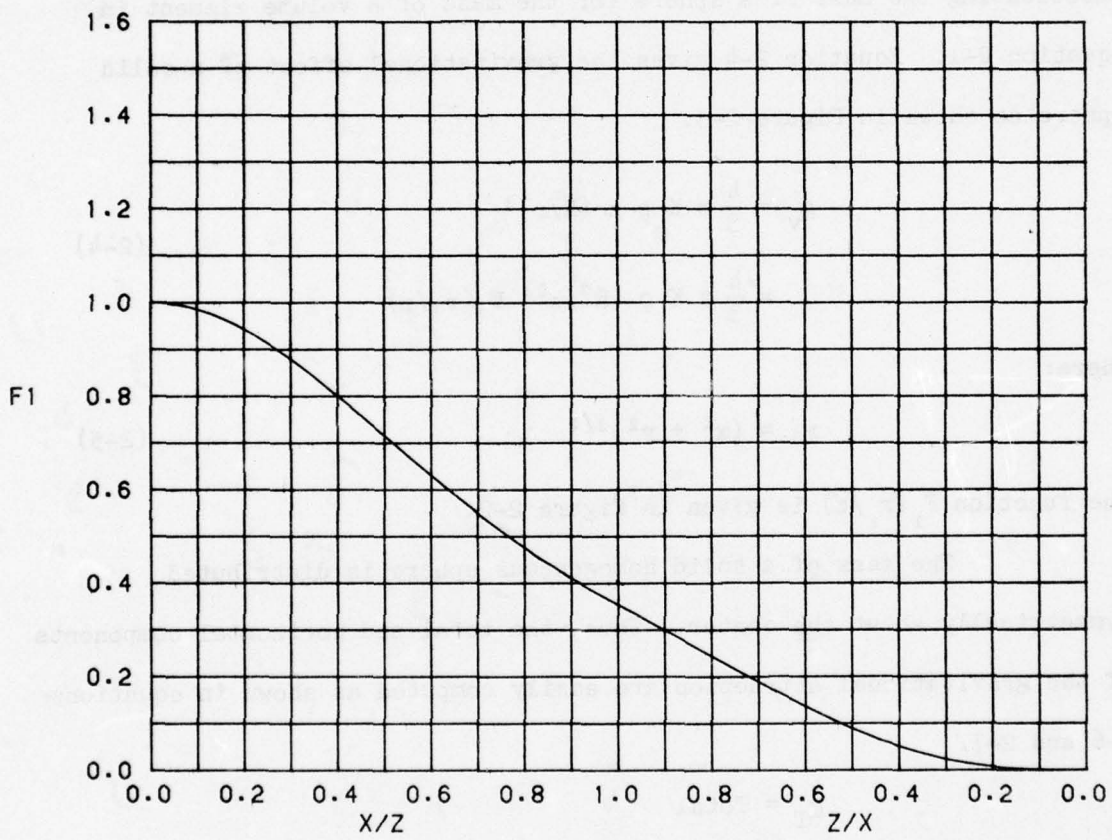
The volume element is not very useful in modeling real geologic bodies or structures. It is included in this discussion for the sake of completeness.

2.1.2 Sphere

The gravitational effect of a solid sphere is derived by substituting the mass of a sphere for the mass of a volume element in equation 2-1. Equation 2-4 gives the gravitational effect of a solid sphere as shown in Figure 2-3.

$$g_v = \frac{4}{3} \pi K \rho z (R/r)^3$$

$$= \frac{4}{3} \pi K \rho (R^3/z^2) F_1(r_1/z) \qquad (2-4)$$

where:

$$r_1 = (x^2 + y^2)^{1/2} \qquad (2-5)$$

The function $F_1(r_1/z)$ is given in Figure 2-2.

The mass of a solid homogeneous sphere is distributed symmetrically about the center. Thus, the total and horizontal components of the gravitational attraction are easily computed as shown in equations 2-6 and 2-7.

$$g_T = \text{Total}$$

$$g_T = g_v (r/z) \qquad (2-6)$$

$$= \frac{g_v}{\cos\theta}$$

16

Figure 2–3
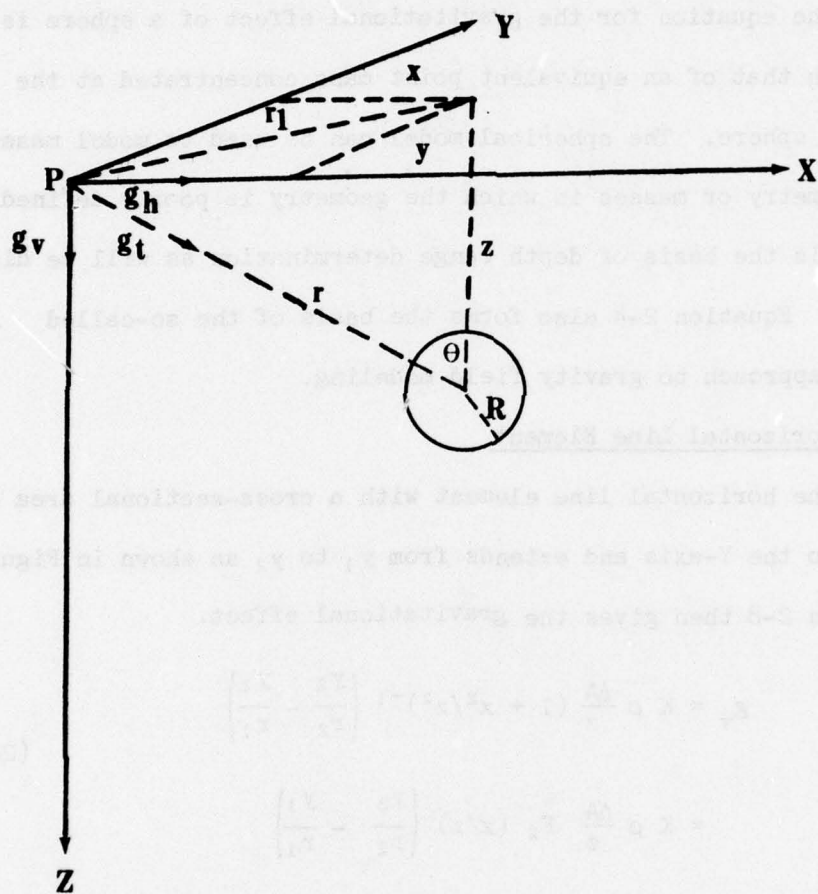
Sphere

$$g_H = \text{Horizontal Component}$$

$$g_H = g_T \, (r_1/r) \tag{2-7}$$

$$= g_T \, \sin\theta$$

The equation for the gravitational effect of a sphere is identical with that of an equivalent point mass concentrated at the center of the sphere. The spherical model can be used to model masses of simple geometry or masses in which the geometry is poorly defined. Equation 2-4 is the basis of depth range determination as will be discussed later. Equation 2-4 also forms the basis of the so-called "point mass" approach to gravity field modeling.

2.1.3 Horizontal Line Element

The horizontal line element with a cross-sectional area ΔA is parallel to the Y-axis and extends from y_1 to y_2 as shown in Figure 2-4. Equation 2-8 then gives the gravitational effect.

$$g_v = K \, \rho \, \frac{\Delta A}{z} \, (1 + x^2/z^2)^{-1} \left(\frac{y_2}{r_2} - \frac{y_1}{r_1} \right)$$

$$\tag{2-8}$$

$$= K \, \rho \, \frac{\Delta A}{z} \, F_2 \, (x/z) \left(\frac{y_2}{r_2} - \frac{y_1}{r_1} \right)$$

where:

$$r_1 = (x^2 + y_1^2 + z^2)^{1/2}$$

$$r_2 = (x^2 + y_2^2 + z^2)^{1/2} \tag{2-9}$$

$$F_2(x/z) = (1 + x^2/z^2)^{-1}$$

The function $F_2(x/z)$ is plotted in Figure 2-5.

18

Figure 2-4

Horizontal Line Element
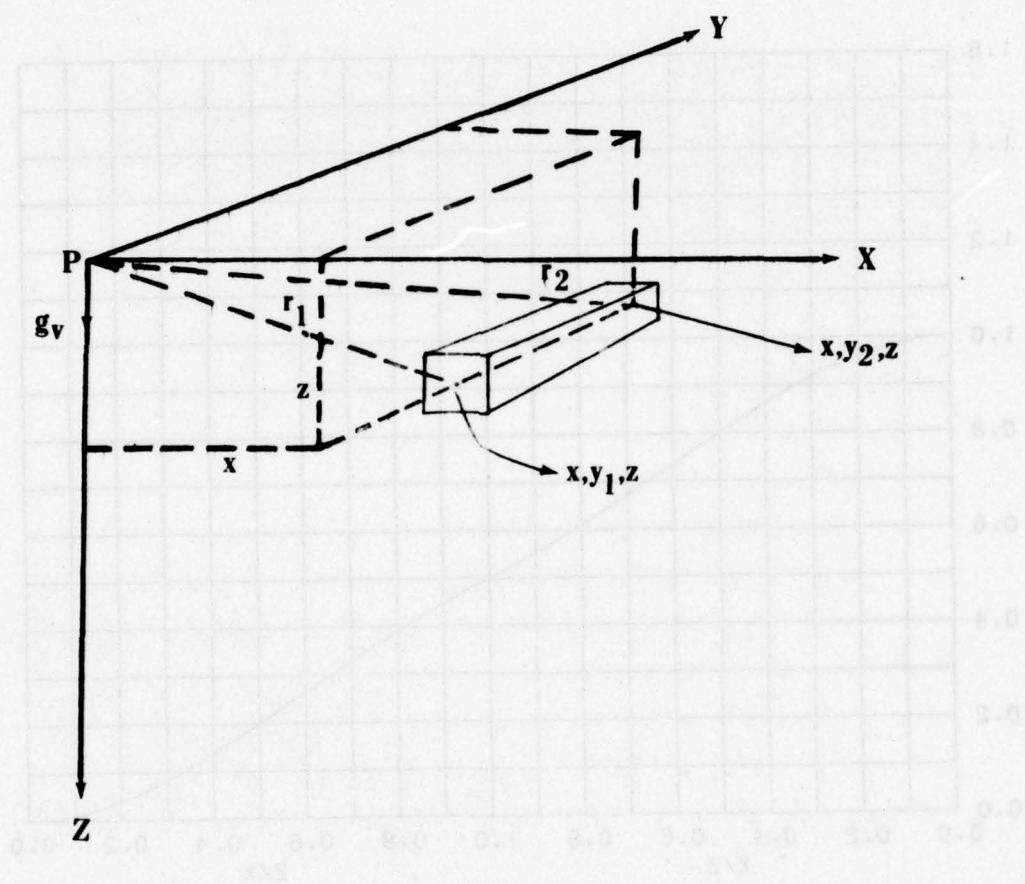
Figure 2-5

Function $F_2(x/z)$
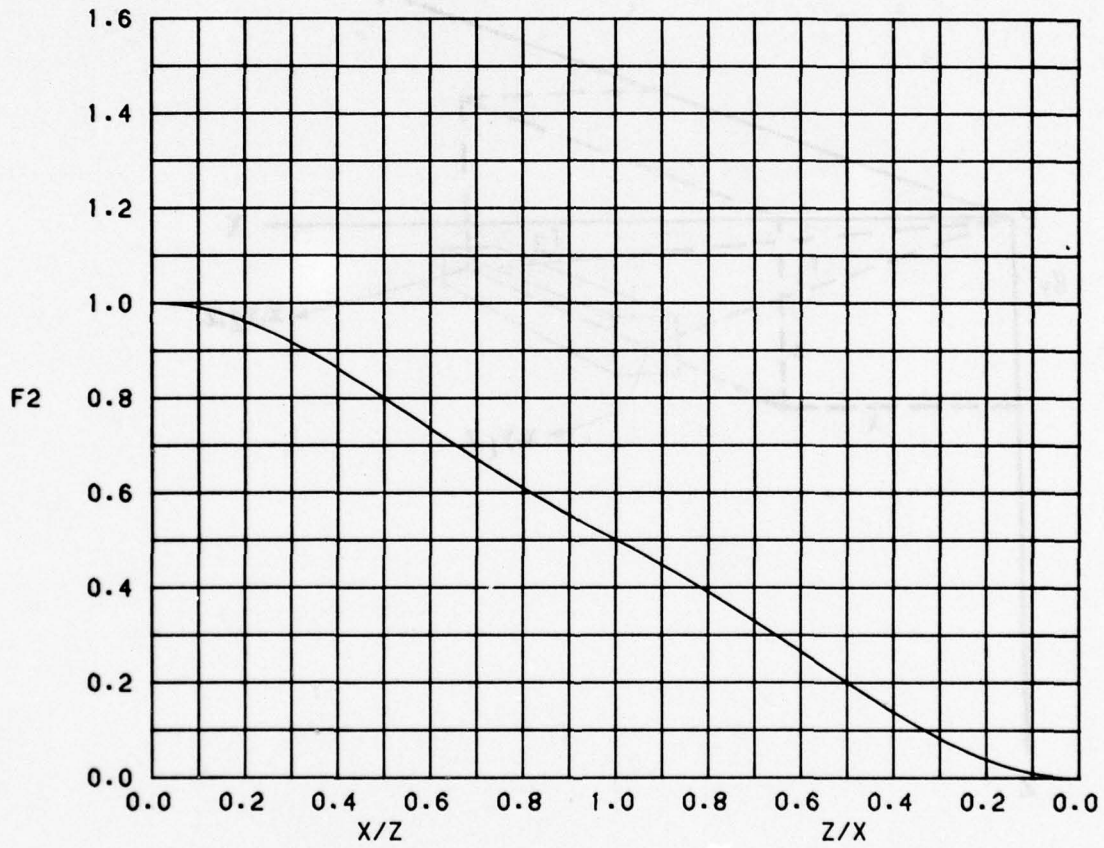
The problem becomes a two-dimensional problem when the line element is infinite in length (i.e., extending from $y = -\infty$ to $y = +\infty$). Equation 2-8 is then reduced to:

$$g_v = 2 K \rho \frac{\Delta A}{z} F_2(x/z) \tag{2-10}$$

Equation 2-10 also applies to an infinite horizontal cylinder of cross-sectional area ΔA.

The horizontal line element is used mainly to determine the two-dimensional criterion as will be shown in later sections.

2.1.4 Vertical Line Element

The vertical line element of cross-sectional area ΔA is oriented parallel to the z-axis and extends from z_1 to z_2 as shown in Figure 2-6. The gravitational effect is given by equation 2-11.

$$
\begin{aligned}
g_v &= K \rho \Delta A \left[\frac{1}{(x^2 + y^2 + z_1^2)^{1/2}} - \frac{1}{(x^2 + y^2 + z_2^2)^{1/2}} \right] \\
&= K \rho \Delta A \left[\frac{1}{(r^2 + z_1^2)^{1/2}} - \frac{1}{(r^2 + z_2^2)^{1/2}} \right] \\
&= \frac{K \rho \Delta A}{r} (\cos\theta_1 - \cos\theta_2)
\end{aligned} \tag{2-11}
$$

where:

$$
\begin{aligned}
r &= (x^2 + y^2)^{1/2} \\
\theta_1 &= \tan^{-1} \frac{z_1}{r} \\
\theta_2 &= \tan^{-1} \frac{z_2}{r}
\end{aligned} \tag{2-12}
$$

If $z_1 = 0$, then equation 2-11 simplifies to:

21

Figure 2-6

Vertical Line Element

$$g_v = K \rho \Delta A \left[\frac{1}{r} - \frac{1}{(r^2 + z_2{}^2)^{1/2}} \right]$$

(2-13)

$$= \frac{K \rho \Delta A}{r} (1 - \cos\theta_2)$$

If $z_2 = \infty$, then equation 2-11 becomes:

$$g_v = K \rho \Delta A \left[\frac{1}{(r^2 + z_1{}^2)^{1/2}} \right]$$

(2-14)

$$= \frac{K \rho \Delta A}{r} \cos\theta_1$$

If $z_1 = 0$ and $z_2 = \infty$, equation 2-11 is further simplified to:

$$g_v = \frac{K \rho \Delta A}{r}$$

(2-15)

The equations for the gravitational effect of a vertical line element can be used to approximate the attraction of right vertical prisms and cylinders (i.e., volcanic plugs and salt domes), as long as the cross-sectional areas, ΔA, are small compared to the other dimensions of the feature.

2.1.5 Vertical Rectangular Lamina

In Figure 2-7, the vertical lamina ab is defined by the opposite corners $a(x,0,0)$ and $b(x,y,z_1)$. Lamina ab is oriented parallel to the YZ plane with dimensions y, z_1 and Δx. The gravitational effect of lamina ab is given by equation 2-16.

$$g_v = K \rho \frac{\Delta x}{2} \ln \left[\frac{\{(x^2 + y^2 + z_1{}^2)^{1/2} - y\} \{(x^2 + y^2)^{1/2} + y\}}{\{(x^2 + y^2 + z_1{}^2)^{1/2} + y\} \{(x^2 + y^2)^{1/2} - y\}} \right]$$

$$= K \rho \Delta x \ln \left[\frac{(x^2 + z_1)^{1/2} \{y + (x^2 + y^2)^{1/2}\}}{x \{y + (x^2 + y^2 + z_1{}^2)^{1/2}\}} \right]$$

(2-16)

The natural logarithm function can be expressed as follows:

Figure 2-7

Vertical Rectangular Lamina
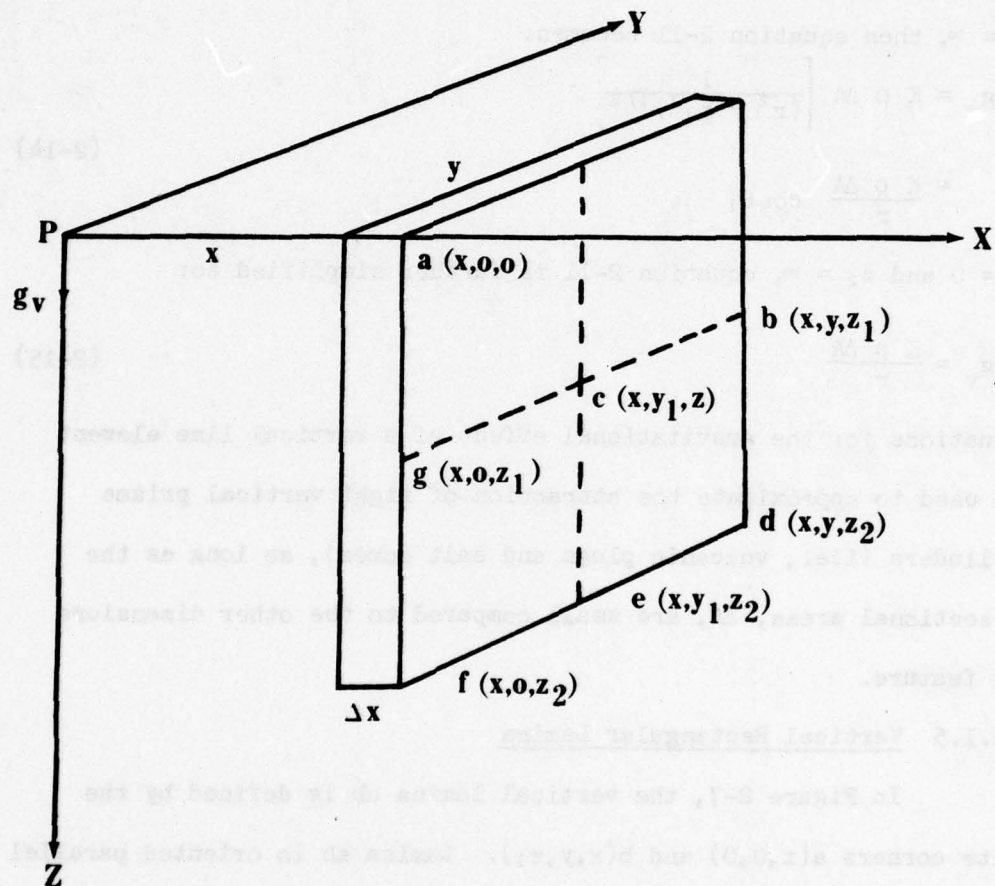
Figure 2-8

Function $G(y/x, z_1/x)$
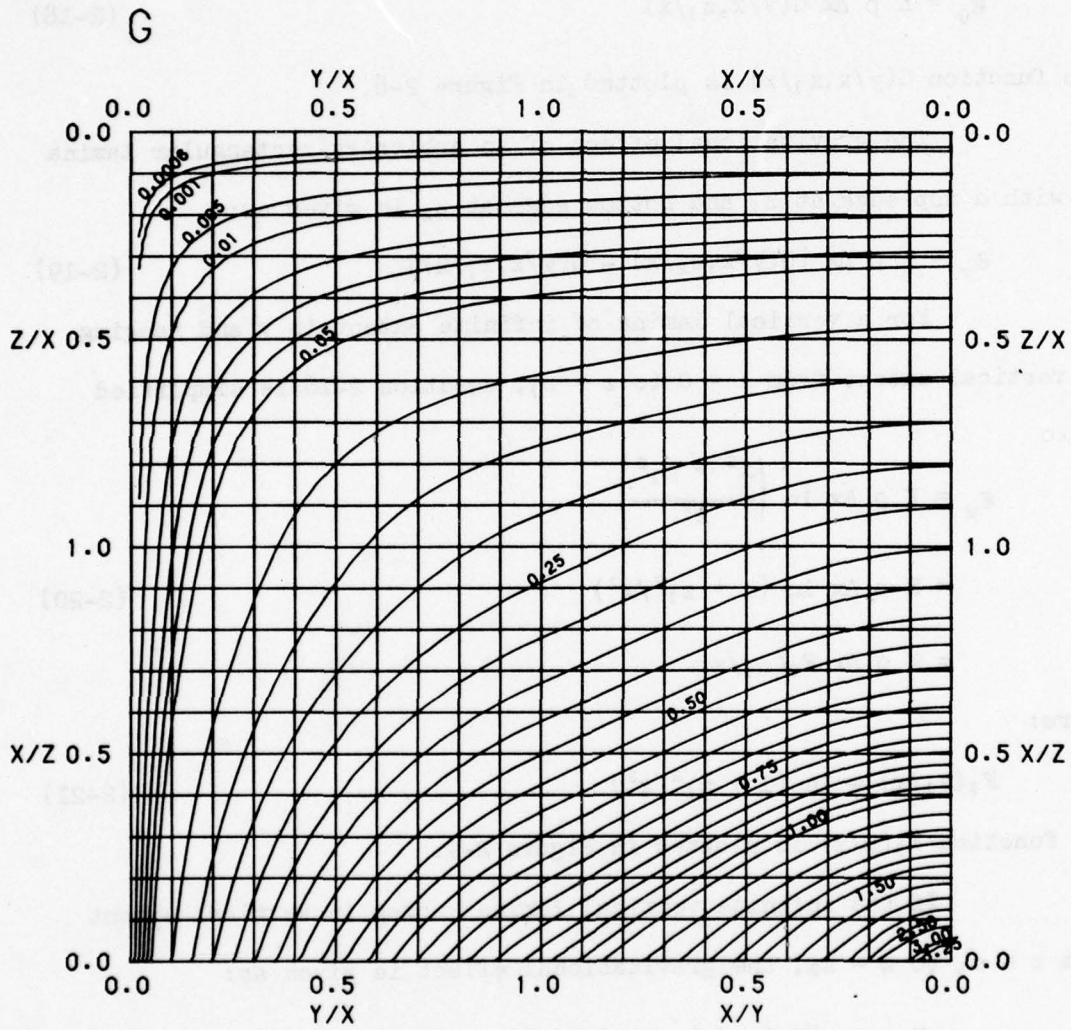
$$G(y/x, z_1/x) = \ln \left[\frac{(1 + z_1^2/x^2)^{1/2} \{1 + (1 + x^2/y^2)^{1/2}\}}{1 + (1 + x^2/y^2 + z_1^2/y^2)^{1/2}} \right] \quad (2\text{-}17)$$

then:

$$g_v = K \rho \Delta x \, G(y/x, z_1/x) \quad (2\text{-}18)$$

The function $G(y/x, z_1/x)$ is plotted in Figure 2-8.

The gravitational effect of an arbitrary rectangular lamina gd with a top edge at z_1 and bottom edge at z_2 is given as:

$$g_v = K \rho \Delta x \, [G(y/x, z_2/x) - G(y/x, z_1/x)] \quad (2\text{-}19)$$

For a vertical lamina of infinite extent in y and ranging in vertical extent from $z = 0$ to $z = z_1$, equation 2-16 is simplified to:

$$g_v = K \rho \Delta x \ln \left(\frac{x^2 + z_1^2}{x^2} \right)$$

$$= K \rho \Delta x \ln (1 + z_1^2/x^2) \quad (2\text{-}20)$$

$$= K \rho \Delta x \, F_3(z_1/x)$$

where:

$$F_3(z_1/x) = \ln (1 + z_1^2/x^2) \quad (2\text{-}21)$$

The function $F_3(z/x)$ is plotted in Figure 2-9.

If the infinite vertical lamina ranges in vertical extent from $z = z_1$ to $z = z_2$, the gravitational effect is given as:

$$g_v = K \rho \Delta x \, [F_3(z_2/x) - F_3(z_1/x)]$$

$$= K \rho \Delta x \ln \left(\frac{x^2 + z_2^2}{x^2 + z_1^2} \right) \quad (2\text{-}22)$$

The vertical rectangular lamina is best used to model vertical or near vertical dikes. Functions G and F_3 are unsuitable for small values of x.

26

Figure 2-9

Function $F_3(z/x)$
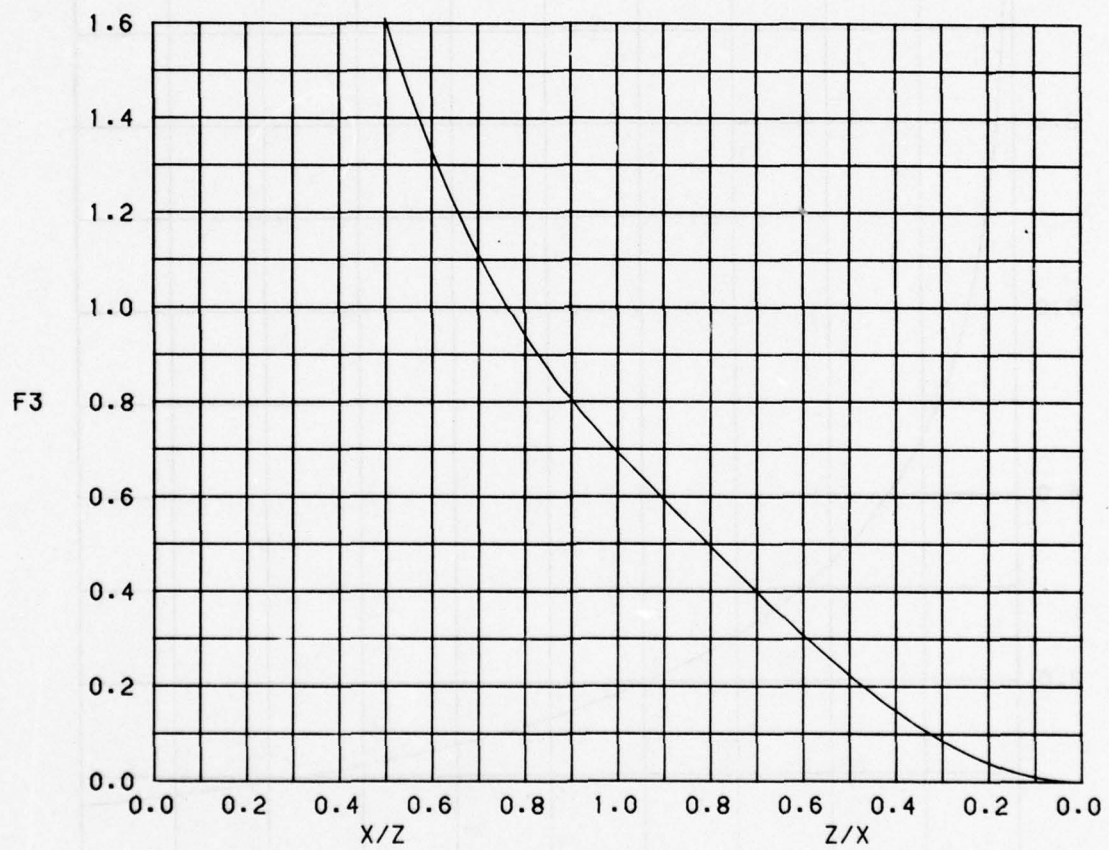
Figure 2-9 (cont'd)

$F_3(z/x)$ (cont'd)
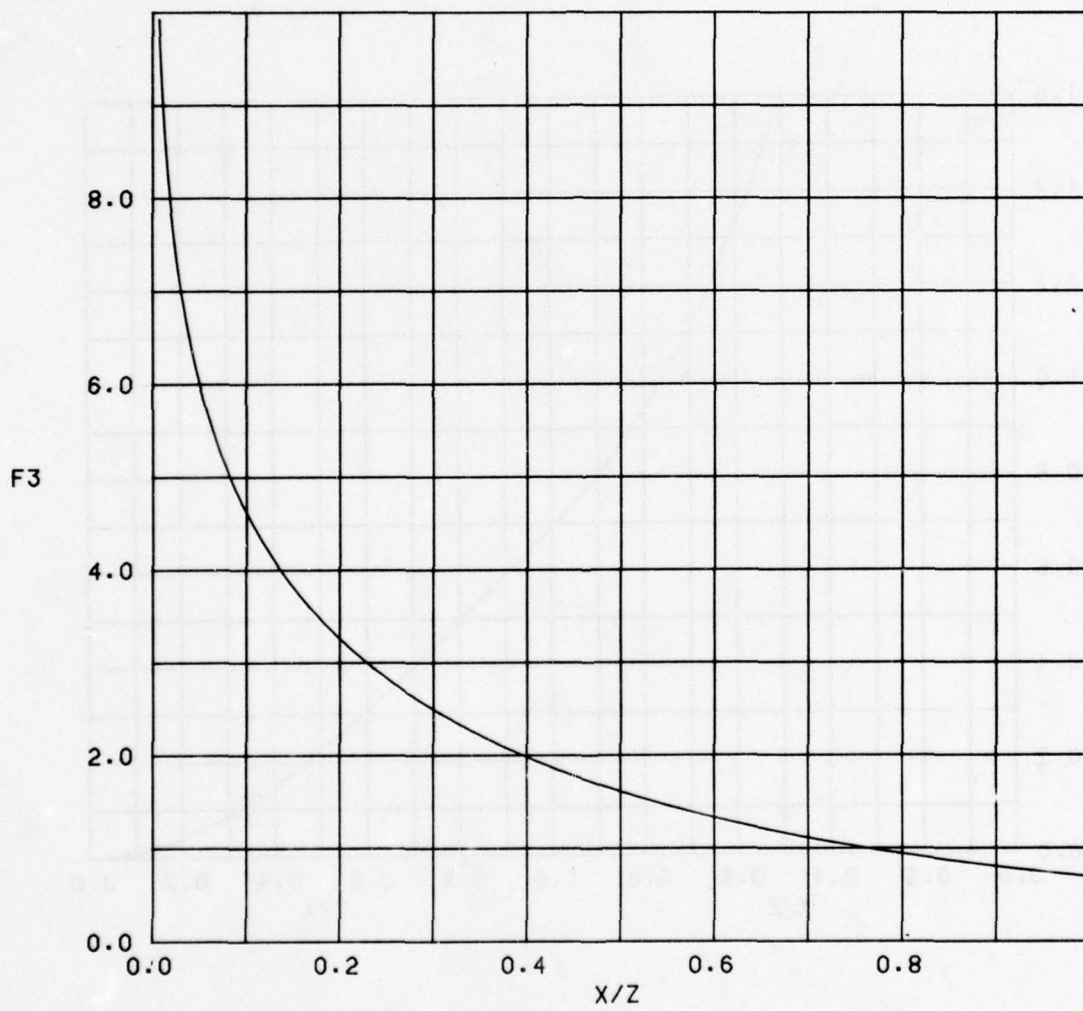
Figure 2-10

Horizontal Rectangular Lamina
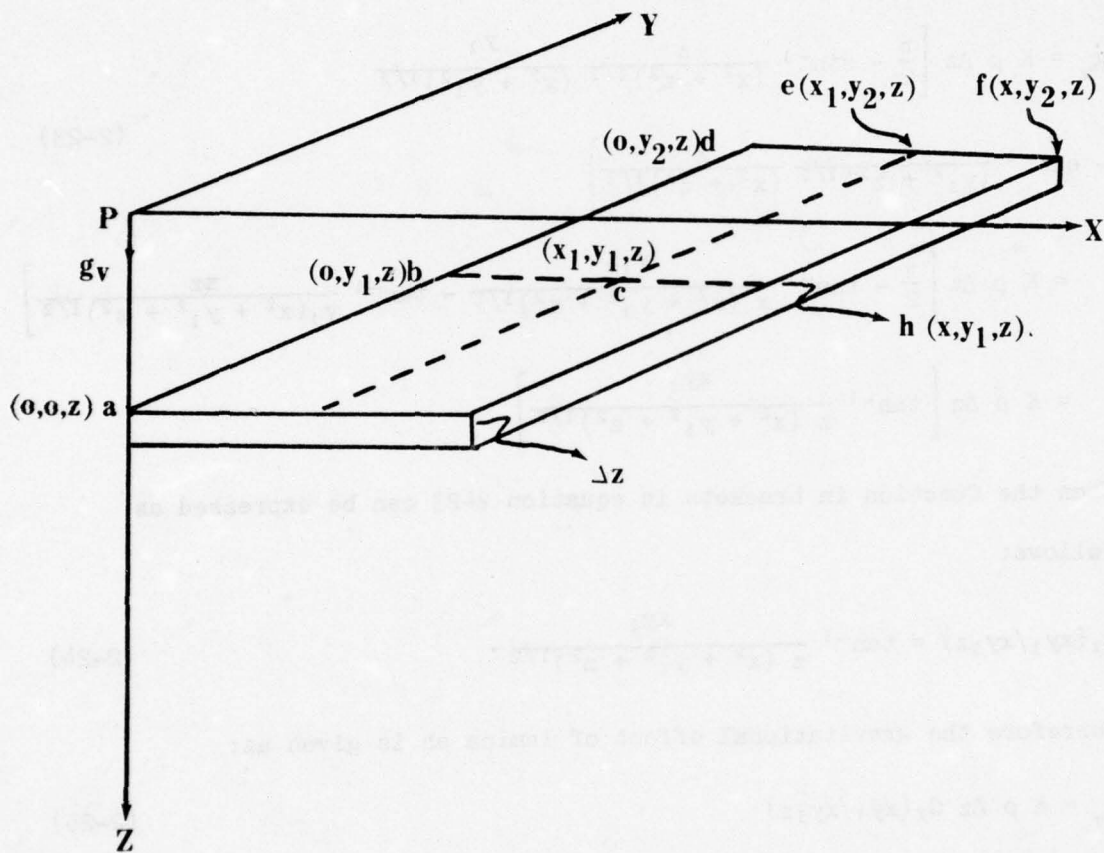
2.1.6 Horizontal Rectangular Lamina

The horizontal lamina ah in Figure 2-10 is oriented parallel to the XY plane with dimensions x, y, and Δz. Equation 2-23 then gives the gravitational effect of lamina ah.

$$
g_v = K \rho \Delta z \left[\frac{\pi}{2} - \sin^{-1} \frac{z}{(x^2 + z^2)^{1/2}} \frac{y_1}{(x^2 + y_1^2)^{1/2}} \right.
$$

$$
\left. - \sin^{-1} \frac{z}{(y_1^2 + z^2)^{1/2}} \frac{x}{(x^2 + z^2)^{1/2}} \right]
\tag{2-23}
$$

$$
= K \rho \Delta z \left[\frac{\pi}{2} - \tan^{-1} \frac{y_1 z}{x\,(x^2 + y_1^2 + z^2)^{1/2}} - \tan^{-1} \frac{xz}{y_1(x^2 + y_1^2 + z^2)^{1/2}} \right]
$$

$$
= K \rho \Delta z \left[\tan^{-1} \frac{xy_1}{z\,(x^2 + y_1^2 + z^2)^{1/2}} \right]
$$

Then the function in brackets in equation 2-23 can be expressed as follows:

$$
G_2(xy_1/xy_1z) = \tan^{-1} \frac{xy_1}{z\,(x^2 + y_1^2 + z^2)^{1/2}}
\tag{2-24}
$$

Therefore the gravitational effect of lamina ah is given as:

$$
g_v = K \rho \Delta z \, G_2(xy_1/xy_1z)
\tag{2-25}
$$

The gravitational effect of an arbitrary horizontal lamina such as cf is then given as:

$$
g_v = K \rho \Delta z \, [G_2(xy_2/xy_2z) - G_2(xy_1/xy_1z) + G_2(x_1y_1/x_1y_1z) - G_2(x_1y_2/x_1y_2z)]
$$
$$
\ldots (2\text{-}26)
$$

where $G_2{'} = (\pi/2) - G_2$ is plotted in Figure 2-11. The horizontal rectangular lamina is used to approximate sills or layered sedimentary features.

30

Figure 2-11

Function G_2' (x_1y_1/x_1y_1z)

31
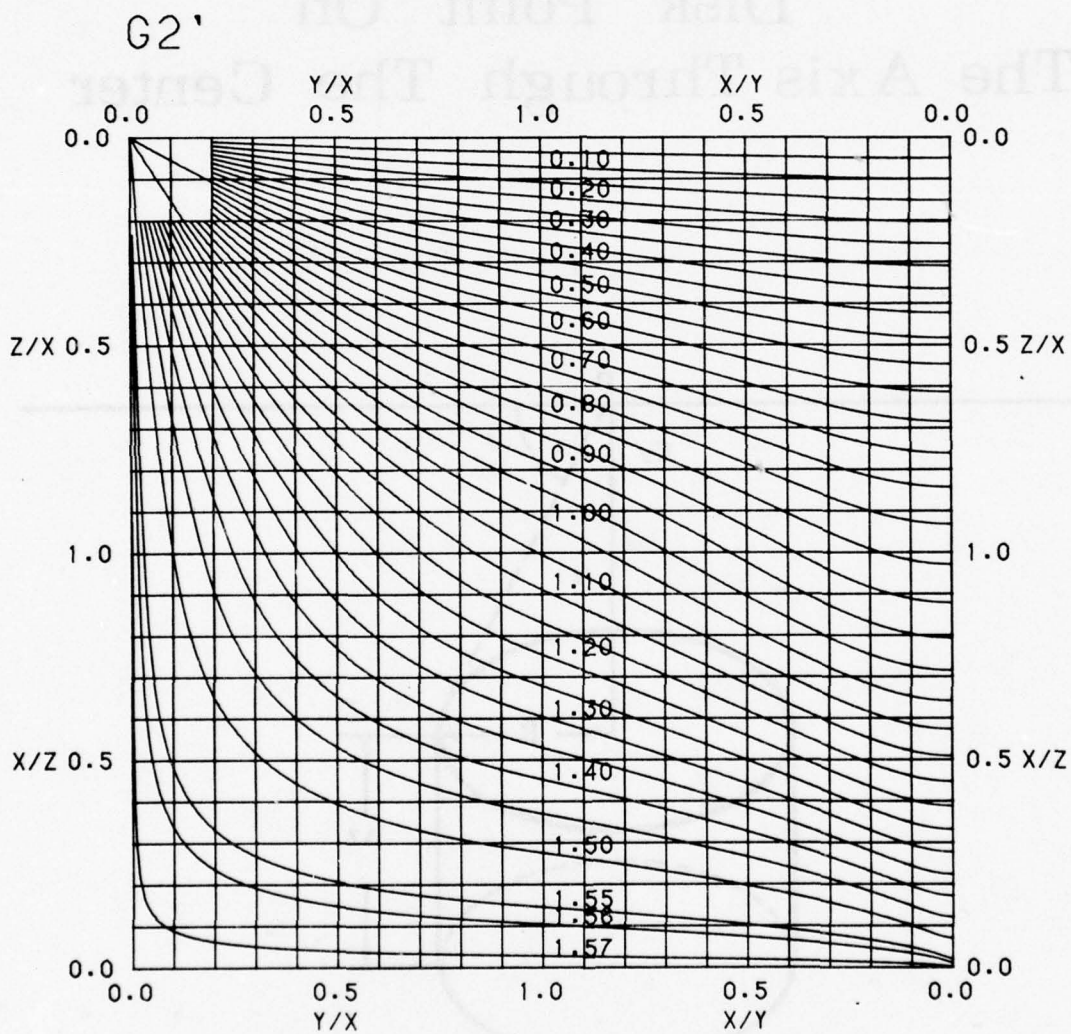
Figure 2-12

Thin Circular Horizontal
Disk Point On
The Axis Through The Center
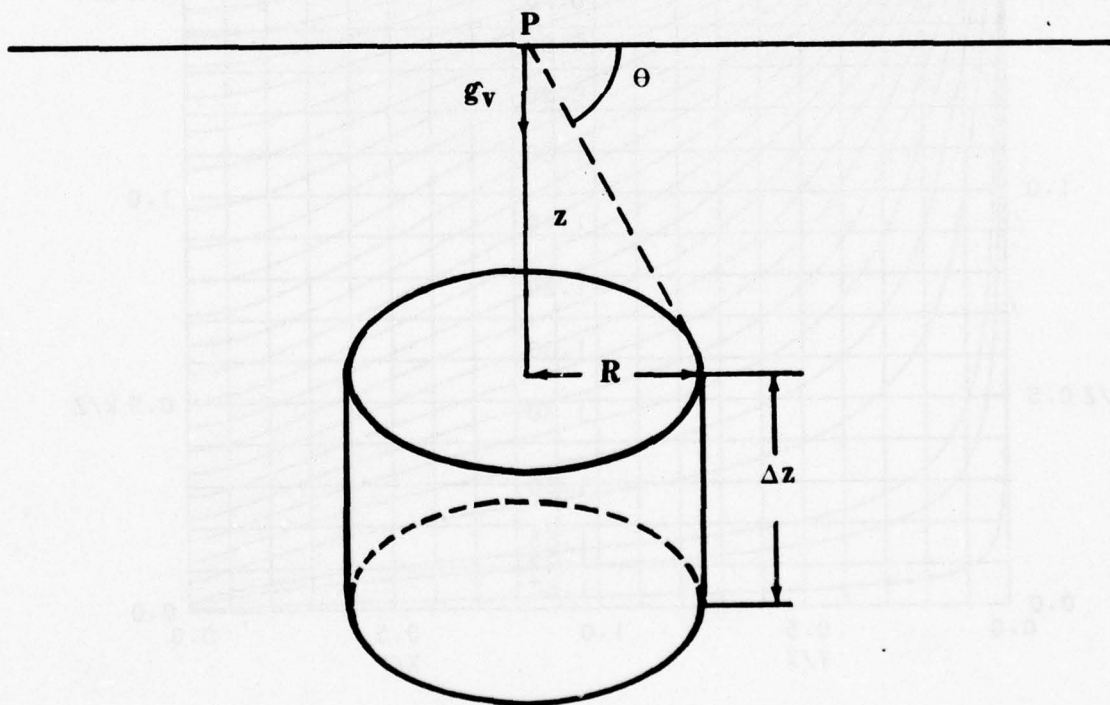
Figure 2-13

Thin Circular Horizontal Disk, General Expression
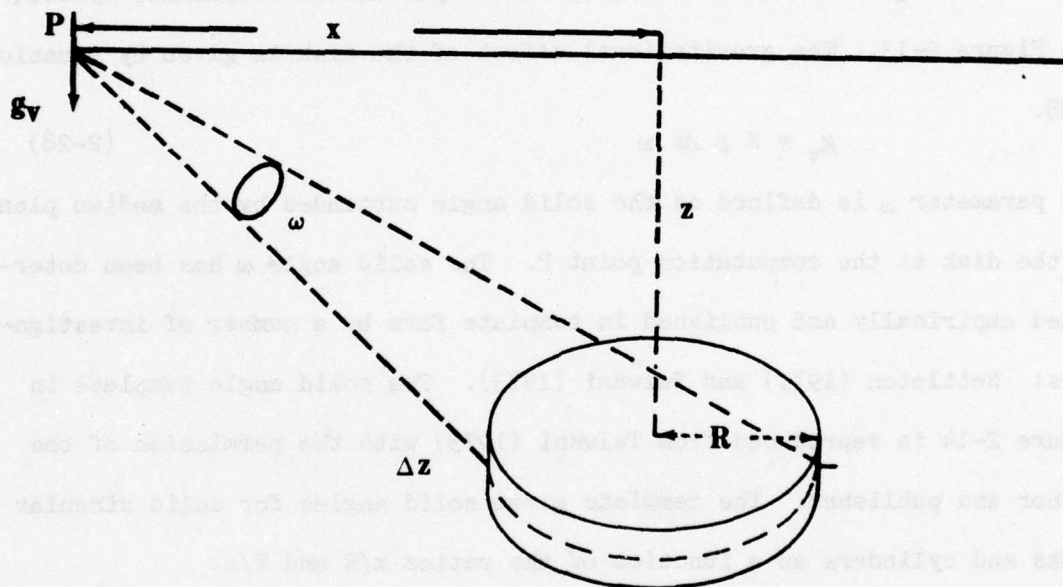
2.1.7 <u>Thin Circular Horizontal Disk, Points on the Axis Through</u>
<u>the Center</u>

The disk is defined in a cylindrical coordinate system as shown
in Figure 2-12. The gravitational effect of the disk is given by equation
2-27.

$$g_v = 2 \pi K \rho \Delta z \left[1 - \frac{z}{(z^2 + R^2)^{1/2}} \right] \qquad (2\text{-}27)$$
$$= 2 \pi K \rho \Delta z (1 - \sin\theta)$$

2.1.8 <u>Thin Circular Horizontal Disk, General Expression</u>

Again the disk is defined in a cylindrical coordinate system,
see Figure 2-13. The gravitational effect of the disk is given by equation
2-28.

$$g_v = K \rho \Delta z \, \omega \qquad (2\text{-}28)$$

The parameter ω is defined as the solid angle subtended by the median plane
of the disk at the computation point P. The solid angle ω has been deter-
mined empirically and published in template form by a number of investiga-
tors: Nettleton (1971) and Talwani (1973). The solid angle template in
Figure 2-14 is reproduced from Talwani (1973) with the permission of the
author and publisher. The template gives solid angles for solid circular
disks and cylinders as a function of the ratios x/R and R/z.

Equation 2-27 is an approximation based on the assumption that
all mass of the disk or cylinder is concentrated on the median plane.
Nettleton (1971) shows the approximation to be in error by -2% for
$\Delta z < (1/2)$ z and $R/z = 1$.

The thin disk has the same application as the horizontal rectangular
lamina with the added advantage of computational ease.

34

Figure 2-14

Solid Angle Chart – Function G_4
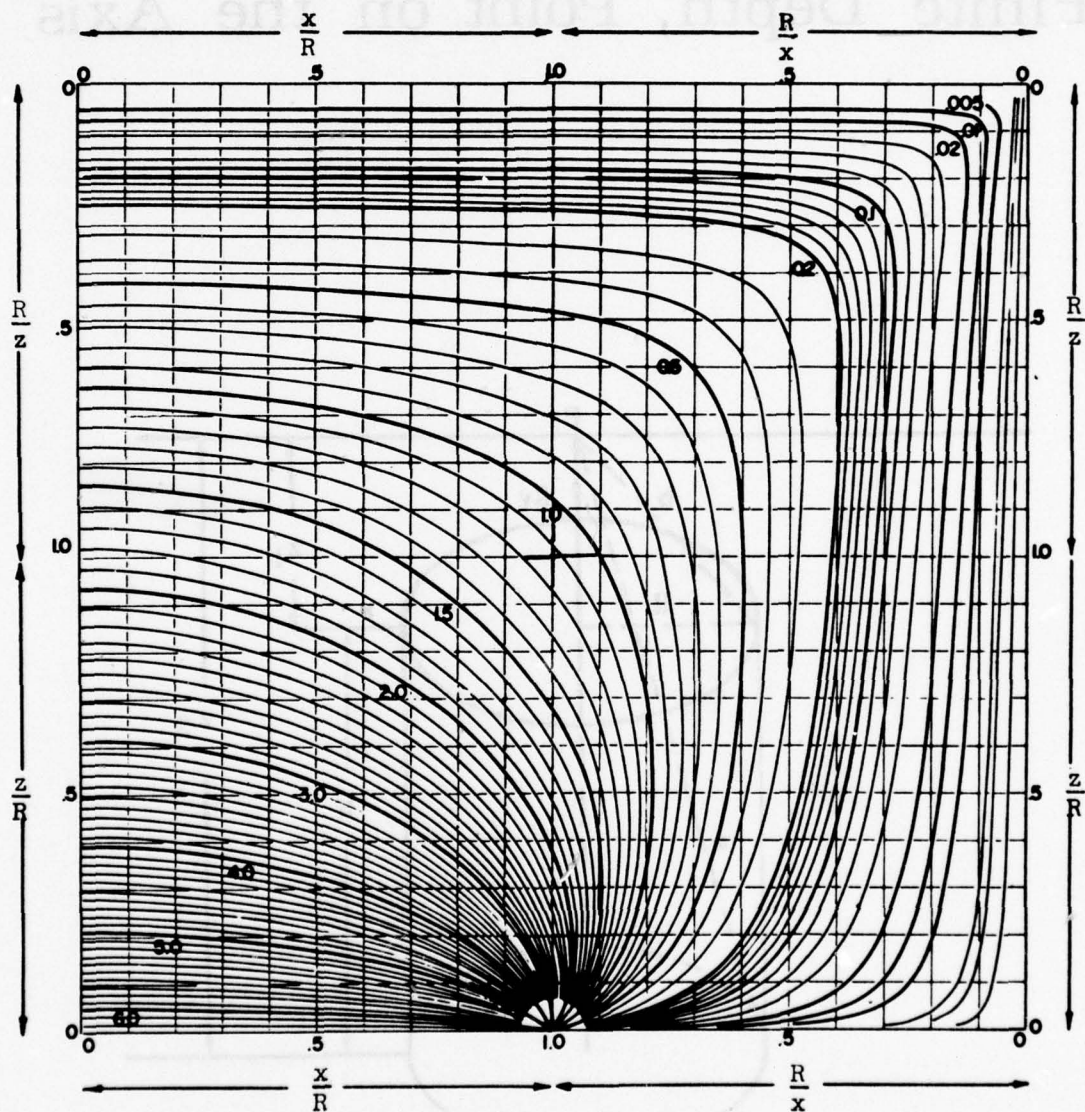
Figure 2–15

Vertical Right Circular Cylinder of Finite Depth, Point on the Axis
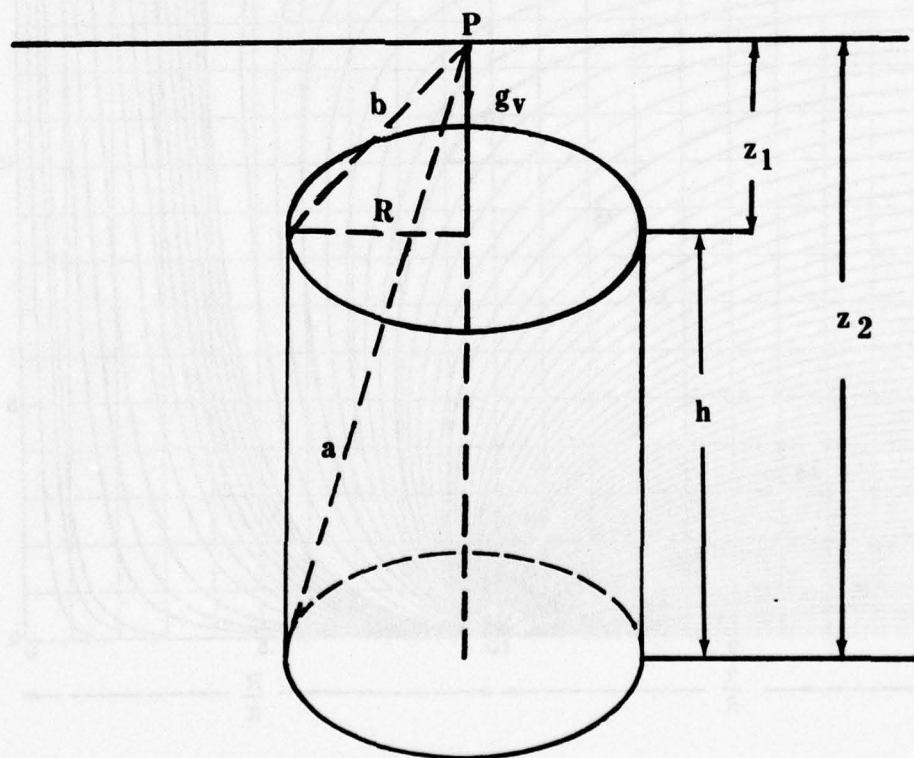
2.1.9 Vertical Right Circular Cylinder of Finite Depth, Point on the Axis

The right circular cylinder in Figure 2-15 is defined in a cylindrical coordinate system. Equation 2-29 then gives the gravitational effect of the cylinder:

$$g_v = 2 \pi K \rho [(z_2 - z_1) - (z_2^2 + R^2)^{1/2} + (z_1^2 + R^2)^{1/2}] \quad (2-29)$$

$$= 2 \pi K \rho (h - a + b)$$

where:

$$h = (z_2 - z_1)$$
$$a = (z_2^2 + R^2)^{1/2} \quad (2-30)$$
$$b = (z_1^2 + R^2)^{1/2}$$

If $z_1 = 0$, then equation 2-29 is simplified to:

$$g_v = 2 \pi K \rho [R + z_2 - (R^2 + z_2^2)^{1/2}] \quad (2-31)$$

For $z_2 = \infty$, equation 2-29 then becomes:

$$g_v = 2 \pi K \rho [(R^2 + z_1^2)^{1/2} - z_1] \quad (2-32)$$

Then, for $z_1 = 0$, $z_2 = \infty$, equation 2-29 further reduces to:

$$g_v = 2 \pi K \rho R \quad (2-33)$$

2.1.10 Vertical Right Circular Cylinder, General Expression

The coordinate system used to define the cylinder is shown in Figure 2-16. The gravitational effect of the cylinder is then given by equation 2-34.

$$g_v = K \rho R G_5 \quad (2-34)$$

The function G_5 is a very complex hyperbolic sine function which is impractical to evaluate.

Figure 2-17 gives G_5 in template form as a function of the

Figure 2-16

Vertical Right Circular Cylinder, General Expression
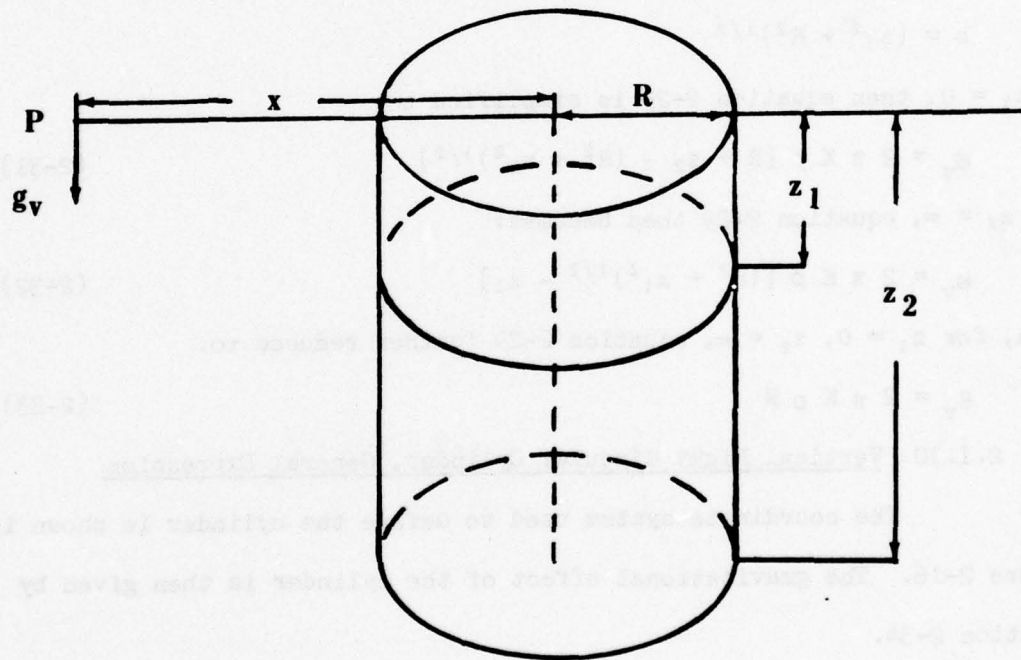
Figure 2-17

Function G_5
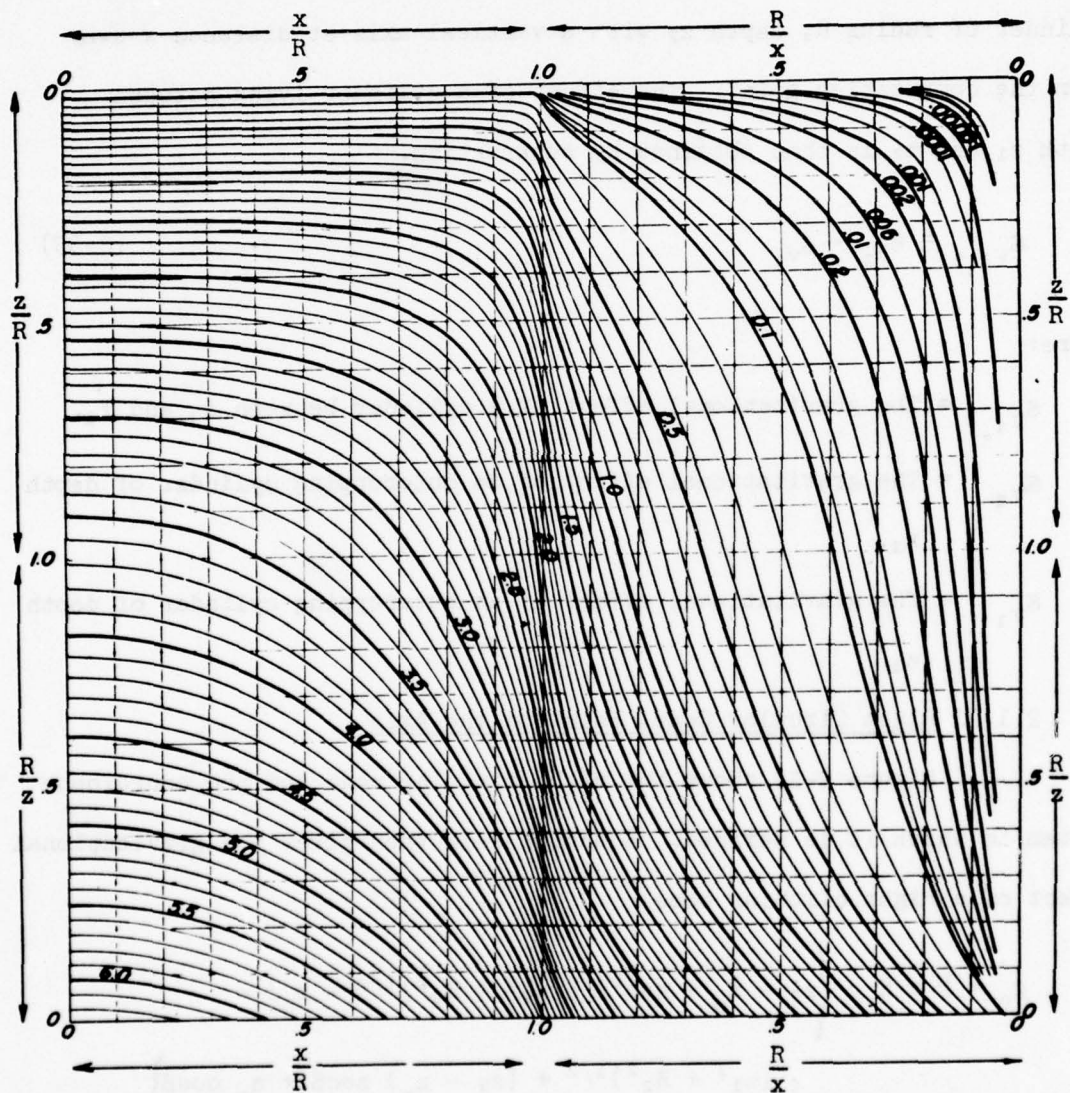
ratios x/R and R/z. The template is taken from Talwani (1973), and is reproduced with the permission of the author and publisher.

The function G_5 is given for an outcropping vertical circular cylinder of radius R, depth z_2 with a vertical axis at distance x away from the computation point. The effect of a cylinder lying between depth z_1 and z_2 is then obtained by subtraction.

$$g_{V_{1,2}} = g_{V_2} - g_{V_1} \qquad (2\text{-}35)$$

where:

$g_{V_{1,2}}$ = The gravitational effect of a cylinder between z_1 and z_2.

g_{V_2} = The gravitational effect of an outcropping cylinder of depth z_2.

g_{V_1} = The gravitational effect of an outcropping cylinder of depth z_1.

2.1.11 Right Circular Cone, Point on the Axis

Figure 2-18 shows the right circular cone and the coordinate system in which it is defined. Equation 2-36 then gives the gravitational effect of a right circular cone.

$$g_V = 2\pi K \rho \left\{ z_2 - z_o - \cos^2\beta \left[(z_2^2 + R_2^2)^{1/2} - z_o \right] - \right.$$
$$\left. z_o \cos\beta \sin^2\beta \ln \frac{(z_2^2 + R_2^2)^{1/2} + (z_2 - z_o)\sec\beta + z_o\cos\beta}{z_o(1 + \cos\beta)} \right\} \quad (2\text{-}36)$$

If $z_o = 0$, equation 2-36 is simplified as follows:

Figure 2-18

Right Circular Cone, Point on the Axis
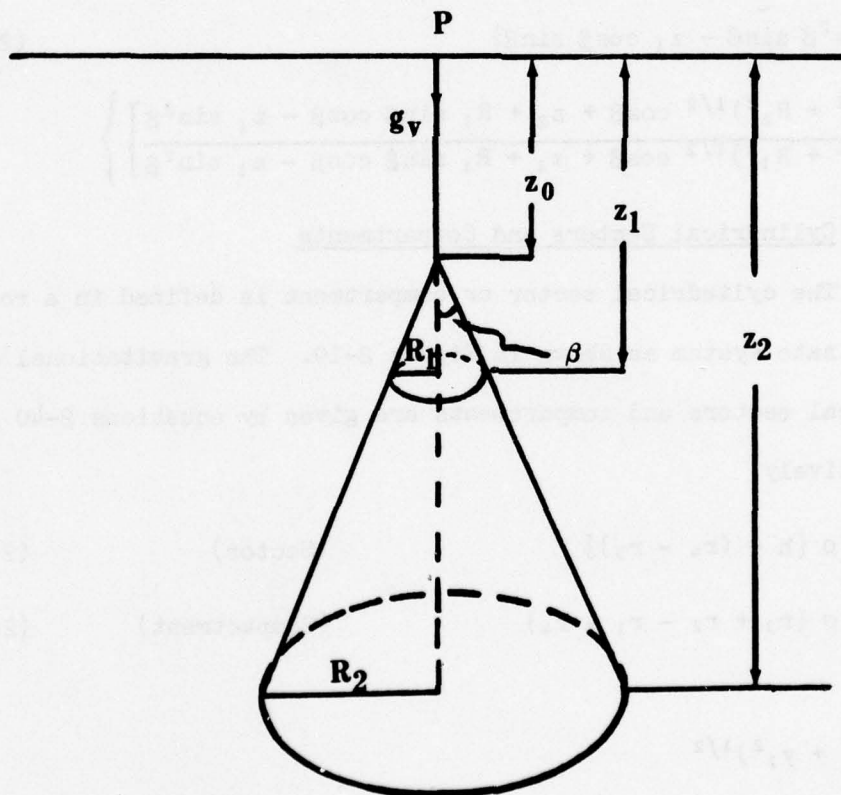
$$g_v = 2 \pi K \rho z_2 \left[1 - \frac{z_o}{(z_2{}^2 + R_2{}^2)^{1/2}} \right]$$

$$= 2 \pi K \rho z_2 (1 - \cos\beta) \tag{2-37}$$

where:

$$R_1 = (z_1 - z_o) \tan\beta$$

$$R_2 = (z_2 - z_o) \tan\beta \tag{2-38}$$

Equation 2-39 gives the effect of a conical section between z_1 and z_2.

$$g_v = 2 \pi K \rho \left\{ z_2 - z_1 - \cos^2\beta \left[(z_2{}^2 + R_2{}^2)^{1/2} - z_1{}^2 + R_1{}^2)^{1/2} \right] \right.$$

$$+ (R_1 \cos^2\beta \sin\beta - z_1 \cos\beta \sin\beta) \tag{2-39}$$

$$\left. \left[x \ln \frac{(z_2{}^2 + R_2{}^2)^{1/2} \cos\beta + z_2 + R_1 \sin\beta \cos\beta - z_1 \sin^2\beta}{(z_1{}^2 + R_1{}^2)^{1/2} \cos\beta + z_1 + R_1 \sin\beta \cos\beta - z_1 \sin^2\beta} \right] \right\}$$

2.1.12 Cylindrical Sectors and Compartments

The cylindrical sector or compartment is defined in a rectangular coordinate system as shown in Figure 2-19. The gravitational effect of cylindrical sectors and compartments are given by equations 2-40 and 2-41 respectively.

$$g_v = K \alpha \rho [h - (r_4 - r_5)] \qquad \text{(Sector)} \tag{2-40}$$

$$g_v = K \alpha \rho (r_3 + r_2 - r_1 - r_4) \qquad \text{(Compartment)} \tag{2-41}$$

where:

$$d_1 = (x_1{}^2 + y_1{}^2)^{1/2}$$

$$d_2 = (x_2{}^2 + y_2{}^2)^{1/2} \tag{2-42}$$

$$r_1 = (d_1{}^2 + z^2)^{1/2}$$

42

Figure 2-19

Cylindrical Sectors and Compartments
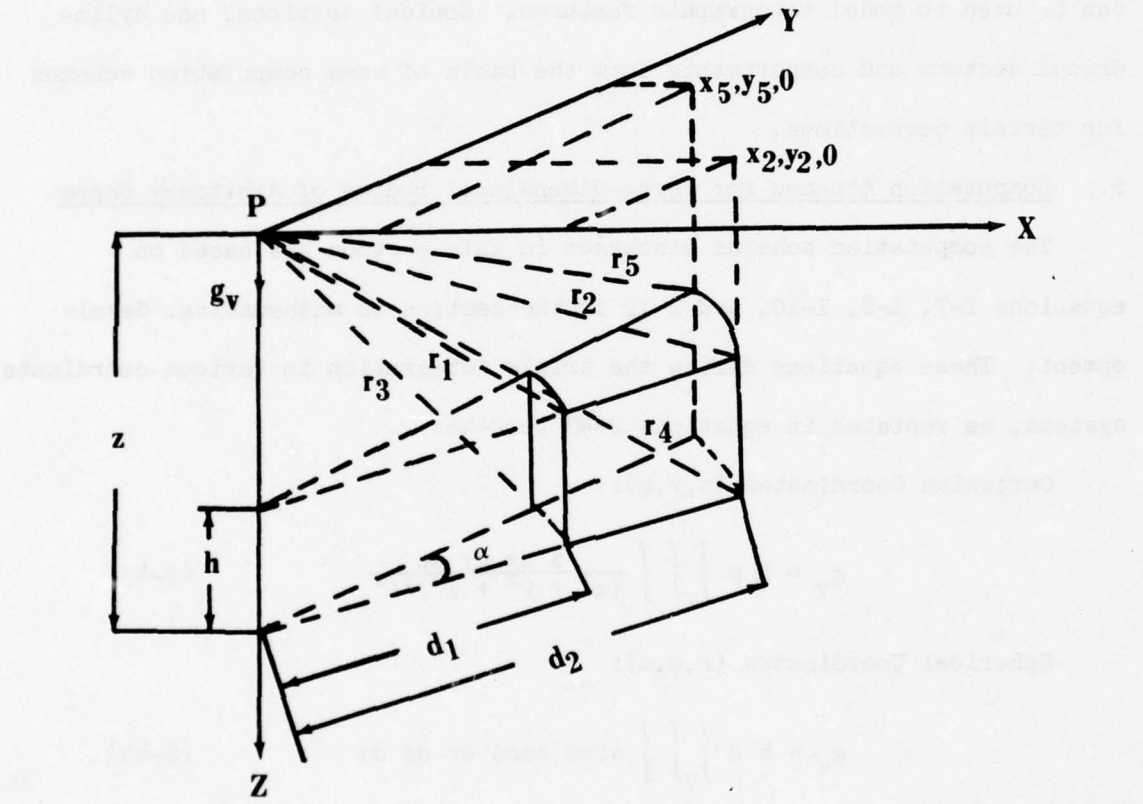
$$r_2 = r_5 = (d_2{}^2 + z^2)^{1/2}$$

$$r_3 = [d_1{}^2 + (h + z)^2]^{1/2}$$

$$r_4 = [d_2{}^2 + (h + z)^2]^{1/2}$$

(2-42)
cont.

Right circular cylinders are used to model igneous plugs and intrusions of finite cross-sectional areas, whereas, right circular cones can be used to model topographic features. Conical sections, and cylindrical sectors and compartments form the basis of some computation schemes for terrain corrections.

2.2 Computation Schemes for Three-Dimensional Bodies of Arbitrary Shape

The computation schemes discussed in this section are based on equations 1-7, 1-8, 1-10, and 1-12 in the section on mathematical development. These equations define the triple integration in various coordinate systems, as restated in equations 2-43 to 2-46:

Cartesian Coordinates (x,y,z):

$$g_v = K \rho \int_V \int \int \frac{z \; dx \; dy \; dz}{(x^2 + y^2 + z^2)^{3/2}} \qquad (2\text{-}43)$$

Spherical Coordinates (r,ϕ,α):

$$g_v = K \rho \int_V \int \int \sin\phi \; \cos\phi \; dr \; d\phi \; d\alpha \qquad (2\text{-}44)$$

Cylindrical Coordinates (R,z,α):

$$g_v = K \rho \int_V \int \int \frac{R \; z \; dz \; dR \; d\alpha}{(R^2 + z^2)^{3/2}} \qquad (2\text{-}45)$$

Conical Coordinates (R,ϕ,α):

$$g_v = K \rho \int_V \int \int \sin\phi \; dR \; d\phi \; d\alpha \qquad (2\text{-}46)$$

where the parameters x, y, z, r, R, φ, and α are defined in Figure 1-3.
The triple integration can be carried out in several ways.

The most obvious computation schemes involve summations over volume
elements, horizontal line elements, or vertical line elements. The
summation over the volume elements is a triple numerical integration
based on equation 2-2, whereas, the summation over the horizontal or
vertical line elements involves a single analytical integration based
on either equation 2-8 or equation 2-11 and a double numerical
integration. Though such computation schemes are arithmetically
simple, they suffer from two disadvantages. First, the schemes require
the body be divided into a large number of volume or line elements.
Second, the effect of a unit volume or line element is inversely pro-
portional to its distance from the origin. Therefore, the volume
or line elements must be of variable size in different parts of the body
to maintain a uniform degree of accuracy. The numerical integrations
in volume or line element computation schemes may be improved by replac-
ing the simple summation with some numerical quadrature technique such
as Simpson's Rule.

The most commonly used computation schemes for three-dimensional
bodies involve various combinations of analytical and numerical inte-
grations to compute the combined effects of horizontal laminae, vertical
laminae, cylindrical wedges, or vertical prisms.

2.2.1 Schemes Based on Rectangular Vertical Laminae

The three-dimensional body is divided into a suitable

Figure 2- 20

Vertical Lamina, YZ Plane
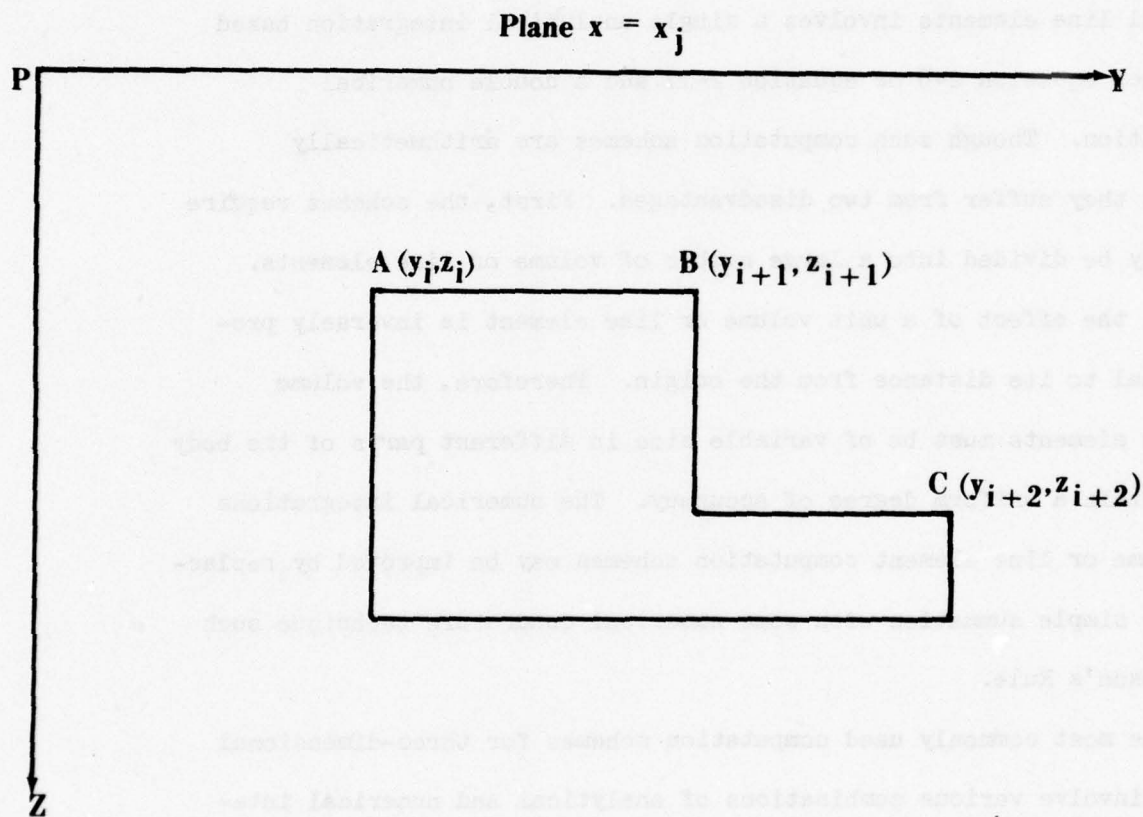
Plane $x = x_j$

number of vertical laminae. Then, each lamina in the plane $x = x_j$ is approximated by a suitable polygon ABC...A with rectangular corners and thickness Δx, Figure 2-20. The gravitational effect of lamina ABC...A is then stated in terms of $G(y/x, z/x)$, as given in equation 2-47.

$$g_v = K \rho \Delta x [G(y_i/x_j, a_i/x_j) - G(y_{i+1}/x_j, z_{i+1}/x_j) +$$
$$G(y_{i+2}/x_j, z_{i+2}/x_j) \ldots \ldots] \tag{2-47}$$

Thus, the analytical surface integration is carried out in y and z with the numerical integration carried out along x. The vertical lamina method is applicable to horizontally elongated bodies, but it should not be used to bodies outcropping near the computation point.

2.2.2 Schemes Based on Rectangular Horizontal Laminae

The three-dimensional body is divided into a suitable number of horizontal laminae. Then, an arbitrary lamina in the $z = z_j$ plane is approximated by the polygon ABC...A with rectangular corners and thickness Δz, Figure 2-21. The gravitational effect of lamina ABC...A is then stated in terms of $G_2 (xy/xyz)$ as given in equation 2-48.

$$g_v = K \rho \Delta z [G_2 (x_i y_i / x_i y_i z_j) - G_2 (x_{i+1} y_{i+1} / x_{i+1} y_{i+1} z_j)$$
$$+ G_2 (x_{i+2} y_{i+2} / x_{i+2} y_{i+2} z_j) \ldots ..] \tag{2-48}$$

The analytical surface integration is carried out in x and y and the numerical integration carried out over depth z.

2.2.3 Schemes Based on Arbitrary Horizontal Polygonal Laminae

The equations presented in this section are based on the

Figure 2–21

Horizontal Lamina, XY Plane
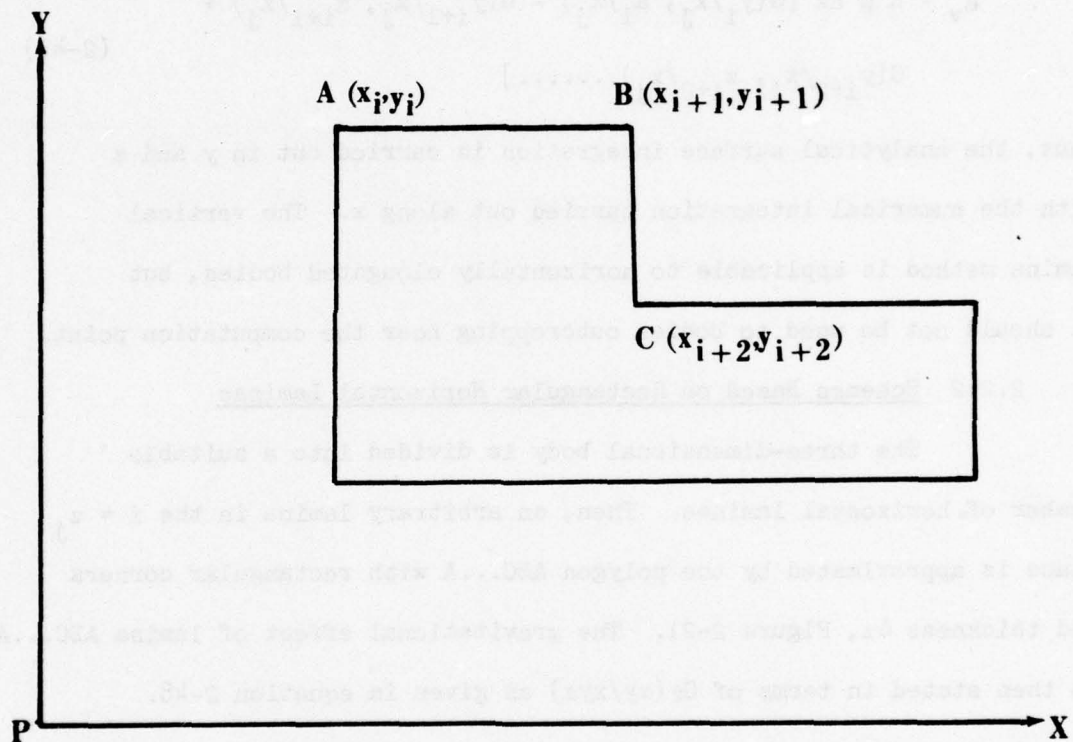
Figure 2-22

Arbitrary Horizontal
Polygonal Lamina
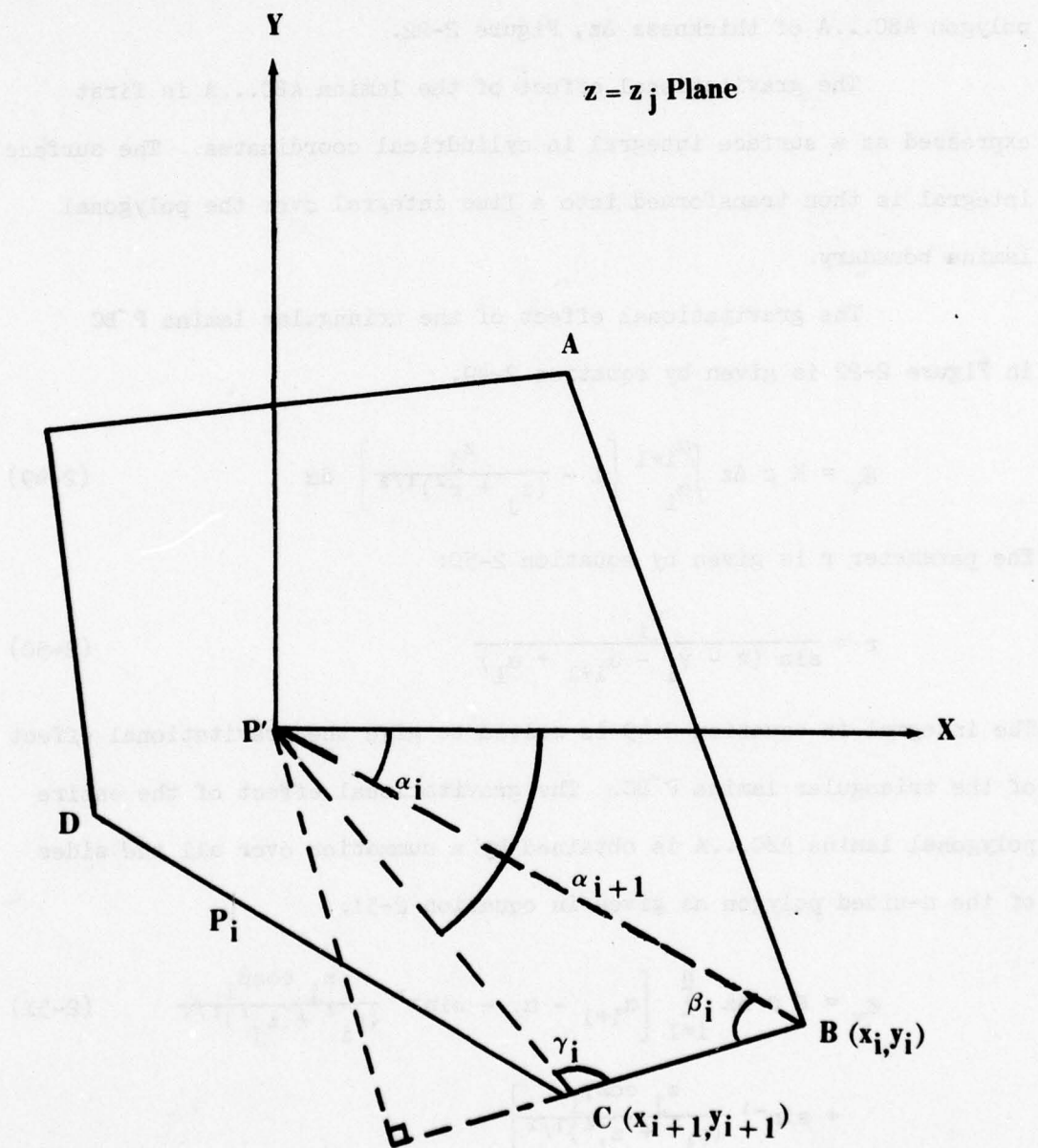
original derivations by Talwani and Ewing (1960). The complete step-by-step derivation is also given by Clermont (1967).

The body is approximated by a suitable number of polygonal laminae. A given lamina in the $z = z_j$ plane is approximated by the polygon ABC...A of thickness Δz, Figure 2-22.

The gravitational effect of the lamina ABC...A is first expressed as a surface integral in cylindrical coordinates. The surface integral is then transformed into a line integral over the polygonal lamina boundary.

The gravitational effect of the triangular lamina P´BC in Figure 2-22 is given by equation 2-49.

$$g_v = K \rho \Delta z \int_{\alpha_i}^{\alpha_{i+1}} \left[1 - \frac{z_j}{(z_j + r^2)^{1/2}} \right] d\alpha \qquad (2\text{-}49)$$

The parameter r is given by equation 2-50:

$$r = \frac{p_i}{\sin (\pi - \gamma_i - \alpha_{i+1} + \alpha_i)} \qquad (2\text{-}50)$$

The integral in equation 2-49 is solved to give the gravitational effect of the triangular lamina P´BC. The gravitational effect of the entire polygonal lamina ABC...A is obtained by a summation over all the sides of the n-sided polygon as given in equation 2-51.

$$g_v = K \rho \Delta z \sum_{i=1}^{n} \left[\alpha_{i+1} - \alpha_i - \sin^{-1} \frac{z_j \cos\beta_i}{(p_i^2 + z_j^2)^{1/2}} \right. \qquad (2\text{-}51)$$
$$\left. + \sin^{-1} \frac{z_j \cos\gamma_i}{(p_i^2 + z_j^2)^{1/2}} \right]$$

50

Equation 2-51 is rewritten in terms of x_i, y_i, and x_{i+1}, y_{i+1} for convenience in computer application, as shown in equation 2-52.

$$g_v = K \rho \Delta z \sum_{i+1}^{n} \left[s \cos^{-1} t_i - \sin^{-1} \frac{z_j q_i s}{(p_i^2 + z_j^2)^{1/2}} \right.$$

$$\left. + \sin^{-1} \frac{z_j f_i s}{(p_i^2 + z_j^2)^{1/2}} \right]$$

(2-52)

where:

$$r_i = (x_i^2 + y_i^2)^{1/2}$$

$$r_{i+1} = (x_{i+1}^2 + y_{i+1}^2)^{1/2}$$

$$r_{i,i+1} = [(x_i - x_{i+1})^2 + (y_i - y_{i+1})^2]^{1/2}$$

$$t_i = \cos(\alpha_{i+1} - \alpha_i) = \frac{x_i x_{i+1} + y_i y_{i+1}}{r_i r_{i+1}}$$

$$p_i^2 = \frac{(y_{i+1} x_i - y_i x_{i+1})^2}{r_{i,i+1}^2}$$

(2-53)

$$q_i = \cos\beta_i = \frac{x_i (x_i - x_{i+1}) + y_i (y_i - y_{i+1})}{r_i r_{i,i+1}}$$

$$f_i = \frac{x_{i+1} (x_i - x_{i+1}) + y_{i+1} (y_i - y_{i+1})}{r_{i+1} r_{i,i+1}}$$

$$s = +1 \text{ if } \sin(\alpha_{i+1} - \alpha_i) > 0$$

$$s = -1 \text{ if } \sin(\alpha_{i+1} - \alpha_i) < 0$$

The total gravitational effect is again obtained by numerical integration along the z axis. This numerical integration can be performed

using quadratic fitting techniques or Lagrange interpolation. Clermont (1967) gives a fully documented FORTRAN computer program based on equation 2-49.

Horizontal laminae are particularly applicable to modeling three-dimensional bodies due to the fact that the gravitational effect of a horizontal lamina changes quite slowly as the distance from the computation point increases.

2.2.4 Schemes Based on Cylindrical Wedges

The three-dimensional body is divided into cylindrical sectors or compartments. Each compartment intersects the RZ plane in the rectangular cross-section ABCD and subtends the angle $\Delta\alpha$ at the Z-axis as shown in cylindrical coordinates in Figure 2-23.

The gravitational effects of cylindrical sectors and compartments are given by equations 2-40 and 2-41, respectively. Equations 2-40 and 2-41 are restated in cylindrical coordinates in equations 2-54 and 2-55.

$$g_V = \Delta\alpha \ K \ \rho \ [(R_2{}^2 + z_1{}^2)^{1/2} - z_1 - (R_2{}^2 + z_2{}^2)^{1/2} + z_2)] \ (Sector)$$

..... (2-54)

and,

$$g_V = \Delta\alpha \ K \ \rho \ [(R_2{}^2 + z_1{}^2)^{1/2} - (R_2{}^2 + z_2{}^2)^{1/2} - (R_1{}^2 + z_1{}^2)^{1/2}$$

$$+ \ (R_1{}^2 + z_2{}^2)^{1/2}] \ (Compartment) \quad\quad (2-55)$$

The numerical integration through the total angle α around the z-axis is best performed by some numerical technique of quadrature such as Simpson's Rule.

Cylindrical Wedge

53
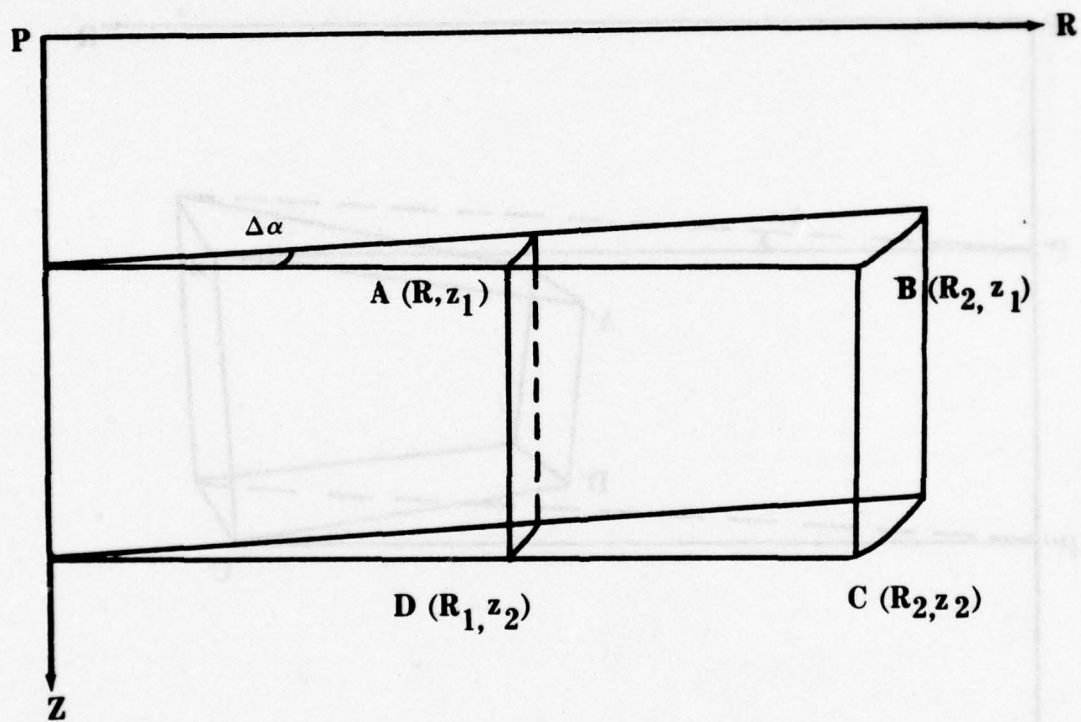
Figure 2-24

Arbitrary Cylindrical Wedge
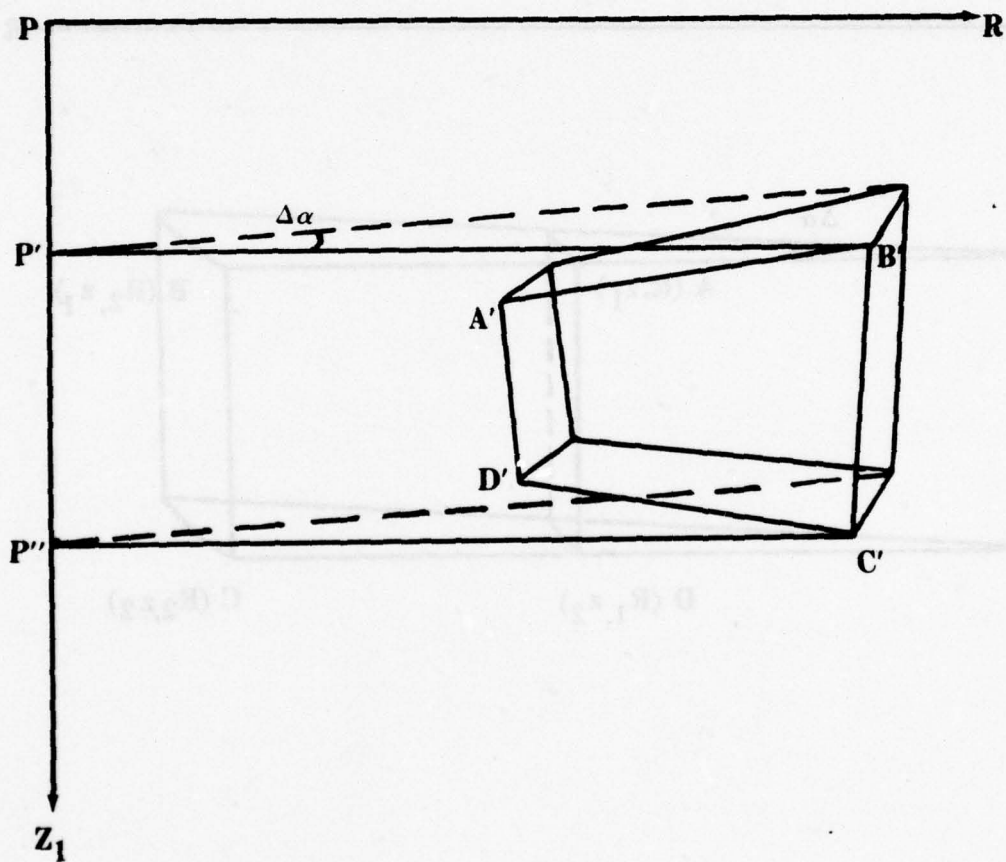
Figure 2–25
Cross – Section of Arbitrary Cylindrical Wedge
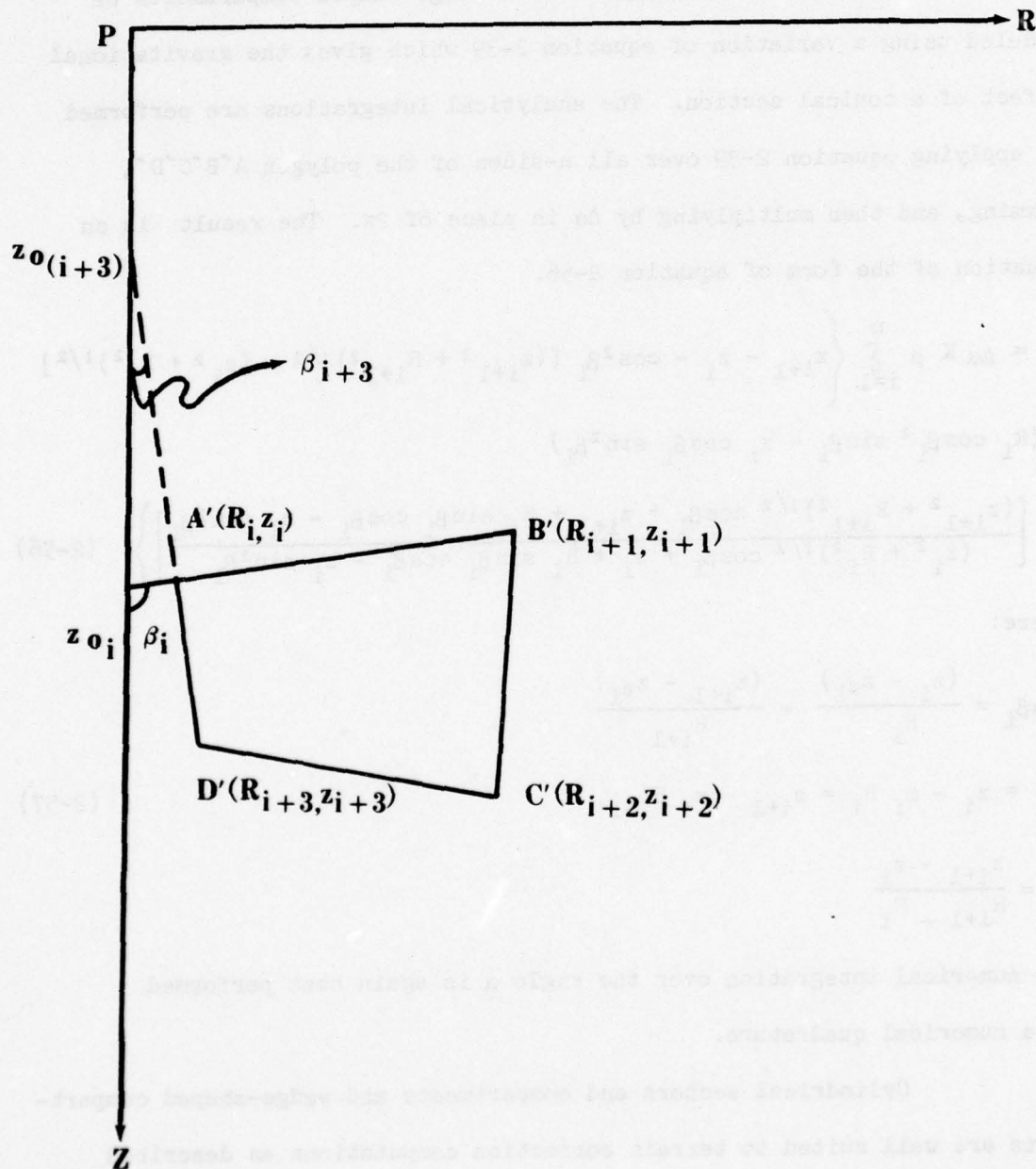
An arbitrary wedge-shaped compartment is shown in Figure 2-24 subtending the angle $\Delta\alpha$ at the z-axis. The compartment intersects the RZ plane in the n-sided polygon $A'B'C'D'$ as shown in Figure 2-25.

Talwani (1973) suggests such wedge-shaped compartments be modeled using a variation of equation 2-39 which gives the gravitational effect of a conical section. The analytical integrations are performed by applying equation 2-39 over all n-sides of the polygon $A'B'C'D'$, summing, and then multiplying by $\Delta\alpha$ in place of 2π. The result is an equation of the form of equation 2-56.

$$g_v = \Delta\alpha \, K \, \rho \sum_{i=1}^{n} \left\{ z_{i+1} - z_i - \cos^2\beta_i \left[(z_{i+1}^2 + R_{i+1}^2)^{1/2} - (z_i^2 + R_i^2)^{1/2} \right] \right.$$

$$+ (R_i \cos\beta_i^2 \sin\beta_i - z_i \cos\beta_i \sin^2\beta_i)$$

$$\left. \ln \left[\frac{(z_{i+1}^2 + R_{i+1}^2)^{1/2} \cos\beta_i + z_{i+1} + R_i \sin\beta_i \cos\beta_i - z_i \sin^2\beta_i}{(z_i^2 + R_i^2)^{1/2} \cos\beta_i + z_i + R_i \sin\beta_i \cos\beta_i - z_i \sin^2\beta_i} \right] \right\} \qquad (2\text{-}56)$$

where:

$$\tan\beta_i = \frac{(z_i - z_{0_i})}{R_i} = \frac{(z_{i+1} - z_{0_i})}{R_{i+1}}$$

$$z_{0_i} = z_i - m_i R_i = z_{i+1} - m_i R_{i+1} \qquad (2\text{-}57)$$

$$m_i = \frac{z_{i+1} - z_i}{R_{i+1} - R_i}$$

The numerical integration over the angle α is again best performed by a numerical quadrature.

Cylindrical sectors and compartments and wedge-shaped compartments are well suited to terrain correction computations as described

56

by Takin and Talwani (1966).

2.2.5 Schemes Based on Right Rectangular Prisms

The three-dimensional body is divided into a suitable number
of rectangular parallelopipeds or prisms. The gravitational effect
of each prism is computed by an exact expression such as equation 2-58.
The total gravitational effect of the three-dimensional body is then
the algebraic sum of the prisms making up the body.

The prism Po, in Figure 2-26 is defined by opposite corners
P $(0,0,0)$ and o (x_1,y_1,z_1). The gravitational effect of Po is given by
equation 2-58, expressed in rectangular coordinates.

$$
\begin{aligned}
g_v = K \rho \Bigg[& z_1 \Bigg\{ \frac{\pi}{2} - \sin^{-1} \frac{z_1}{(x_1{}^2 + z_1{}^2)^{1/2}} \frac{y_1}{(x_1{}^2 + y_1{}^2)^{1/2}} \\
& - \sin^{-1} \frac{z_1}{(y_1{}^2 + z_1{}^2)^{1/2}} \frac{x_1}{(x_1{}^2 + y_1{}^2)^{1/2}} \Bigg\} \\
& + x_1 \Bigg\{ \frac{1}{2} \ln \frac{[(x_1{}^2 + y_1{}^2 + z_1{}^2)^{1/2} - y_1][(x_1{}^2 + y_1{}^2)^{1/2} + y_1]}{[(x_1{}^2 + y_1{}^2 + z_1{}^2)^{1/2} + y_1][(x_1{}^2 + y_1{}^2)^{1/2} - y_1]} \Bigg\} \\
& + y_1 \Bigg\{ \frac{1}{2} \ln \frac{[(x_1{}^2 + y_1{}^2 + z_1{}^2)^{1/2} - x_1][(x_1{}^2 + y_1{}^2)^{1/2} + x_1]}{[(x_1{}^2 + y_1{}^2 + z_1{}^2)^{1/2} + x_1][(x_1{}^2 + y_1{}^2)^{1/2} - x_1]} \Bigg\} \Bigg] \quad (2\text{-}58)
\end{aligned}
$$

The complex functions in brackets are rewritten in functional notation
as follows:

57

Figure 2-26

Rectangular Parallelopiped (Prism)
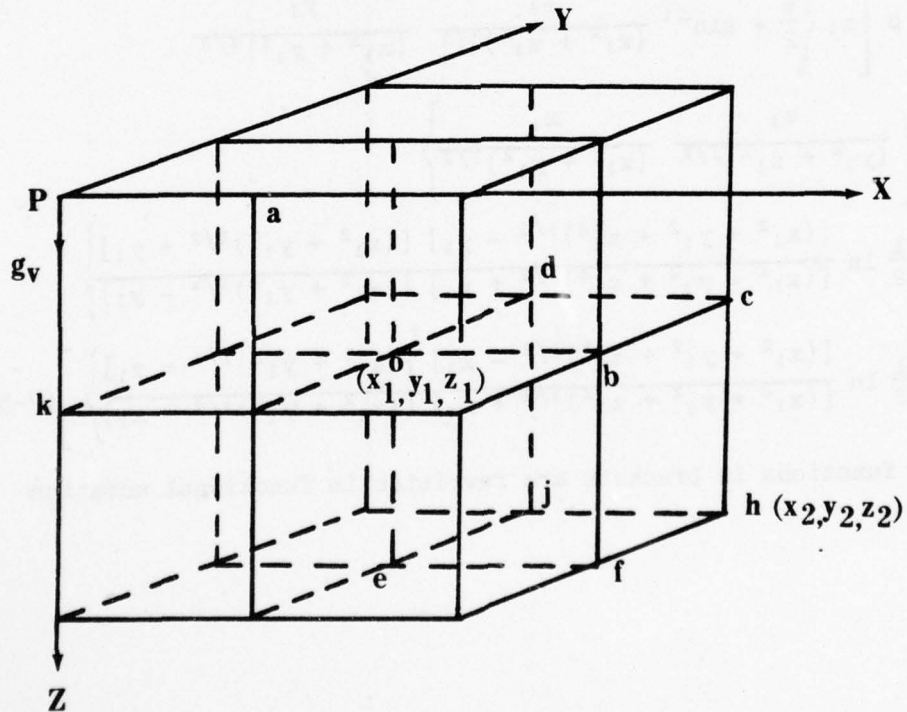
$$G_3(y_i/x_i,\ z_i/x_i) = \left[\left\{ \frac{\pi}{2} - \sin^{-1} \frac{z_i}{(x_i{}^2 + z_i{}^2)^{1/2}} \frac{y_i}{(x_i{}^2 + y_i{}^2)^{1/2}} \right. \right.$$

$$- \sin^{-1} \frac{z_i}{(y_i{}^2 + z_i{}^2)^{1/2}} \frac{x_i}{(x_i{}^2 + y_i{}^2)^{1/2}} \Bigg\}$$

$$+ \frac{x_i}{z_i} \left\{ \frac{1}{2} \ln \frac{[(x_i{}^2 + y_i{}^2 + z_i{}^2)^{1/2} - y_i]\,[(x_i{}^2 + y_i{}^2)^{1/2} + y_i]}{[(x_i{}^2 + y_i{}^2 + z_i{}^2)^{1/2} + y_i]\,[(x_i{}^2 + y_i{}^2)^{1/2} - y_i]} \right\}$$

$$+ \frac{y_i}{z_i} \left\{ \frac{1}{2} \ln \frac{[(x_i{}^2 + y_i{}^2 + z_i{}^2)^{1/2} - x_i]\,[(x_i{}^2 + y_i{}^2)^{1/2} + x_i]}{[(x_i{}^2 + y_i{}^2 + z_i{}^2)^{1/2} + x_i]\,[(x_i{}^2 + y_i{}^2)^{1/2} - x_i]} \right\} \Bigg] \qquad (2\text{-}59)$$

Then equation 2-58 is simplified to the form of equation 2-60:

$$g_v = K\,\rho\,z_1\,G_3(y_1/x_1,\ z_1/x_1) \qquad \cdot(2\text{-}60)$$

where the function G_3 is evaluated directly from Figure 2-27 for given ratios of x, y and z.

The gravitational effect of an arbitrary rectangular prism oh is computed by adding and subtracting the gravitational effects of eight prisms as shown by equation 2-61.

$$g_{oh} = g_{Ph} - g_{Pf} + g_{Pe} - g_{Pj} - g_{Pc} + g_{Pb} - g_{Po} + g_{Pd} \qquad (2\text{-}61)$$

The subscripts denote opposite corners of the prisms in Figure 2-26.

Nagy (1966) presented refined versions of equation 2-58 suitable for modeling and terrain effect computations. These equations are advantageous because they contain none of the inherent errors associated with approximate formulas. Also, the Nagy equations are readily adaptable to computer applications.

59

Figure 2-27

Function G_3
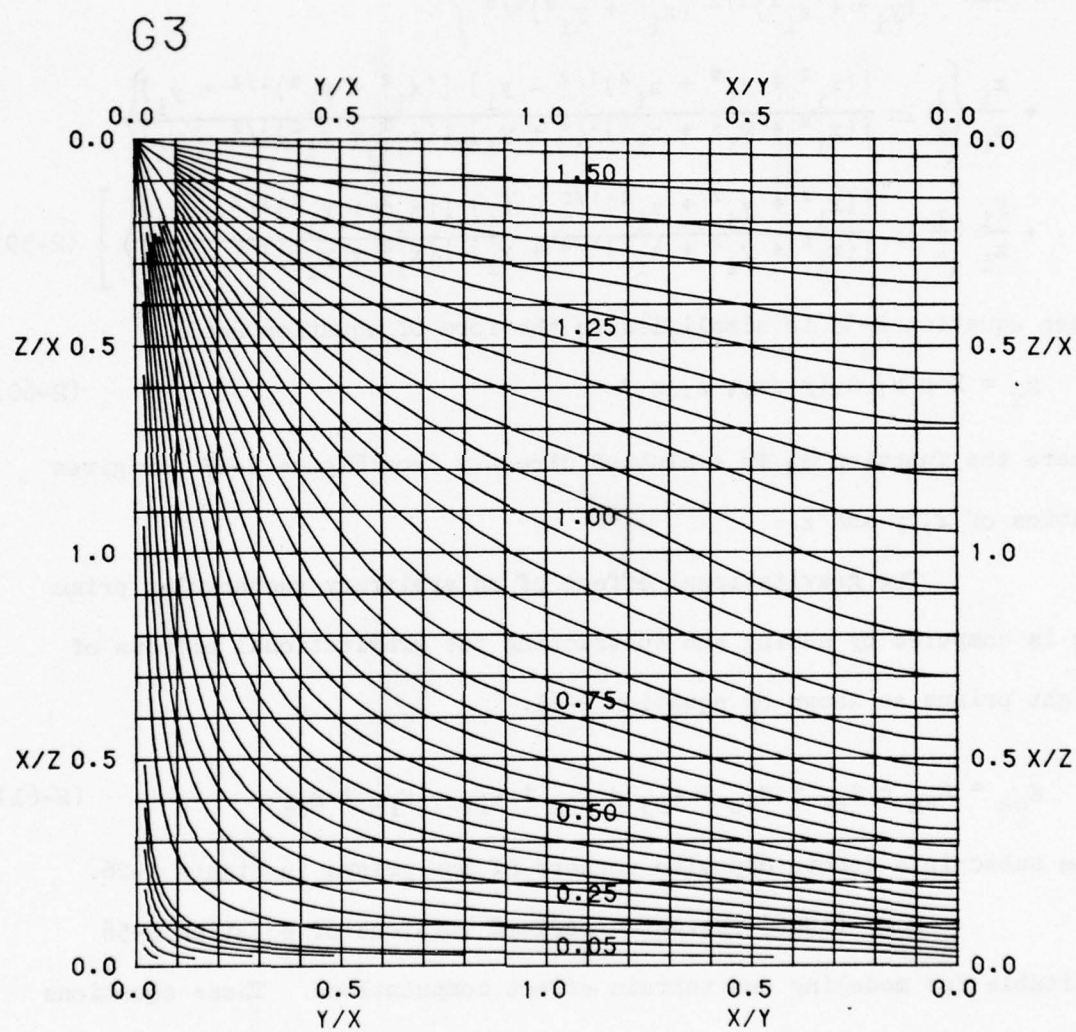
3.   TWO-DIMENSIONAL ATTRACTION FORMULAS

3.1   Some Simple Two-Dimensional Attraction Formulas

The equations presented in this section are derived from equation 1-14 in the section on mathematical development.   The two-dimensional bodies are defined in a rectangular coordinate system in x and z. The angles ϕ_n are measured clockwise from the x-axis.

3.1.1   Infinite Horizontal Rectangular Prism

Figure 3-1 gives the geometrical and angular relationships of an infinite horizontal rectangular prism.   The gravitational effect is then given by equation 3-1.

$$g_v = 2 K \rho \left[x_2 \ln \frac{r_4}{r_3} - x_1 \ln \frac{r_2}{r_1} + z_2 (\phi_2 - \phi_4) - z_1 (\phi_1 - \phi_3) \right] \quad (3-1)$$

where:

$$r_1 = (x_1{}^2 + z_1{}^2)^{1/2}$$

$$r_2 = (x_1{}^2 + z_2{}^2)^{1/2}$$

$$r_3 = (x_2{}^2 + z_1{}^2)^{1/2}$$

$$r_4 = (x_2{}^2 + z_2{}^2)^{1/2} \quad\quad (3-2)$$

$$\phi_1 = \frac{\pi}{2} - \tan^{-1} \frac{x_1}{z_1}$$

$$\phi_2 = \frac{\pi}{2} - \tan^{-1} \frac{x_1}{z_2}$$

$$\phi_3 = \frac{\pi}{2} - \tan^{-1} \frac{x_2}{z_1}$$

$$\phi_4 = \frac{\pi}{2} - \tan^{-1} \frac{x_2}{z_2}$$

Figure 3-1

Infinite Horizontal
Rectangular Prism
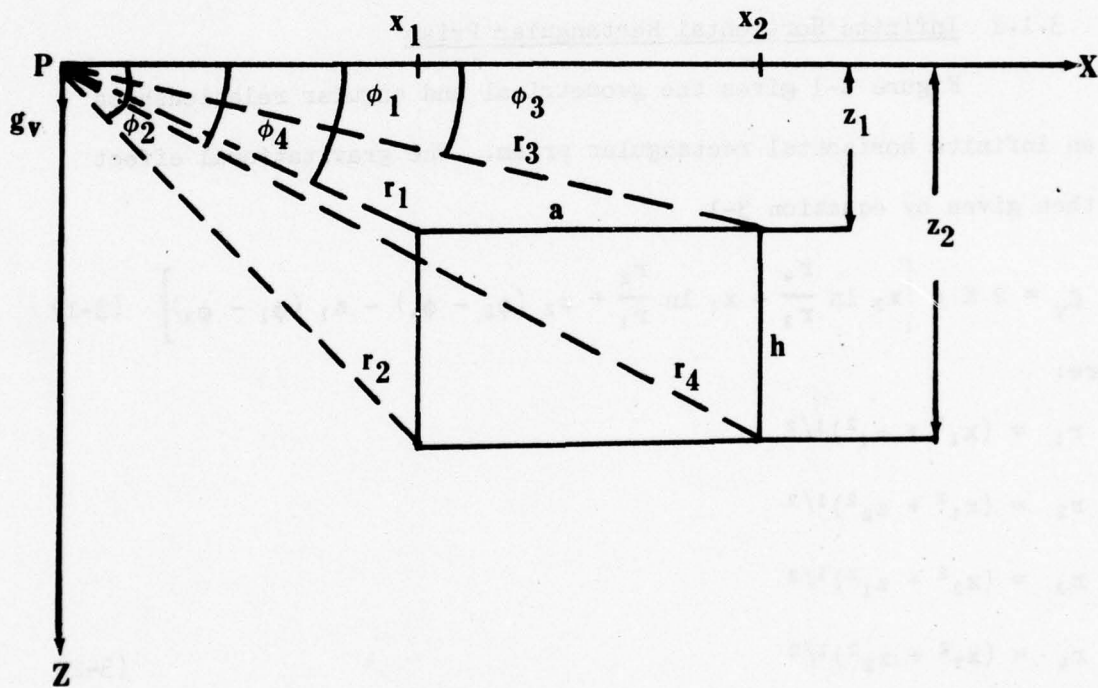
When the prism becomes thin (i.e., $h \lll z_1 \simeq z_2$), the vertical component is closely approximated by:

$$g_V \simeq 2 K \rho h [\phi_1 - \phi_3]$$ (3-3)

The right rectangular prism can be used to model vertical dikes which meet the two-dimensional criterion.

3.1.2 Infinite Horizontal Right Triangular Prism

The geometrical and angular relationships are defined in Figure 3-2. Equation 3-4 then gives the gravitational effect.

$$g_V = 2 K \rho \left\{ - [x_2 \sin i + z_1 \cos i] \left[\sin i \, \ln \frac{r_2}{r_1} + \cos i \, (\phi_2 - \phi_1) \right] \right.$$
$$\left. + x_2 \, \ln \frac{r_4}{r_1} + z_2 \, (\phi_2 - \phi_4) \right\}$$ (3-4)

where:

$$r_1 = (x_2{}^2 + z_1{}^2)^{1/2}$$

$$r_2 = (x_1{}^2 + z_2{}^2)^{1/2}$$

$$r_4 = (x_2{}^2 + z_2{}^2)^{1/2}$$

$$\phi_1 = \frac{\pi}{2} - \tan^{-1} \frac{x_2}{z_1}$$

$$\phi_2 = \frac{\pi}{2} - \tan^{-1} \frac{x_1}{z_2}$$

$$\phi_4 = \frac{\pi}{2} - \tan^{-1} \frac{x_2}{z_2}$$ (3-5)

$$\cos i = \frac{a}{(a^2 + h^2)^{1/2}}$$

$$\sin i = \frac{h}{(a^2 + h^2)^{1/2}}$$

63

Figure 3-2

Infinite Horizontal Right Rectangular Prism
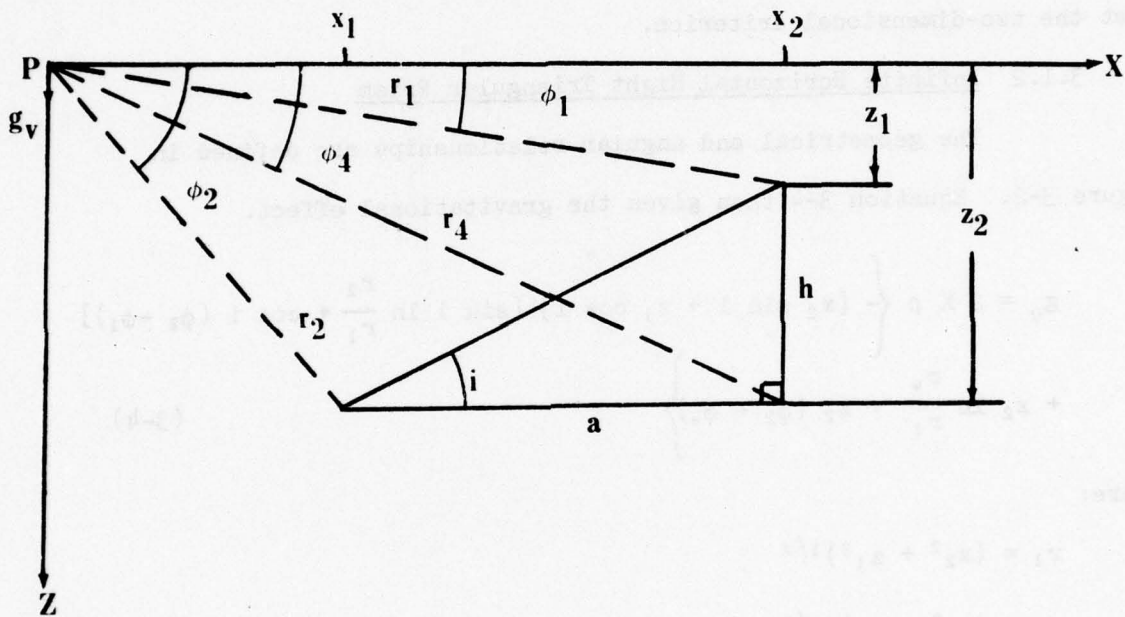
The infinite right triangular prism is used to model bodies which are generally asymmetrical in cross-section.

3.1.3 Symmetrical Anticline of Infinite Extent

The symmetrical anticline is formed by the sum of two right triangular prisms of infinite extent as shown in Figure 3-3. The gravitational effect is given by equation 3-6.

$$g_v = 2 K \rho \left\{ - [x_1 \sin i] \left[\sin i \ln \frac{r_2}{r_3} + \cos i \left(\phi_2 + \phi_3 - 2\phi_1 \right) \right] \right.$$
$$\left. - z_1 \cos i \left[\sin i \ln \frac{r_2 r_3}{r_1^2} + \cos i \left(\phi_2 - \phi_3 \right) \right] + z_2 \left(\phi_2 - \phi_3 \right) \right\} \quad (3\text{-}6)$$

where:

$$r_1 = (x_1^2 + z_1^2)^{1/2}$$

$$r_2 = [(x_1 - a)^2 + z_2^2]^{1/2}$$

$$r_3 = [(x_1 + a)^2 + z_2^2]^{1/2}$$

$$\phi_1 = \frac{\pi}{2} - \tan^{-1} \frac{x_1}{z_1}$$

$$\phi_2 = \frac{\pi}{2} - \tan^{-1} \frac{x_1 - a}{z_1} \qquad\qquad (3\text{-}7)$$

$$\phi_3 = \frac{\pi}{2} - \tan^{-1} \frac{x_1 + a}{z_1}$$

$$\cos i = \frac{a}{(a^2 + h^2)^{1/2}}$$

$$\sin i = \frac{h}{(a^2 + h^2)^{1/2}}$$

Figure 3-3

Symmetrical Anticline of Infinite Extent

$x_1 - a$ x_1 $x_1 + a$

P   X

g_v

z_1

r_1 ϕ_1

ϕ_3

z_2

ϕ_2

r_2

r_3

h

i i

a a

Z
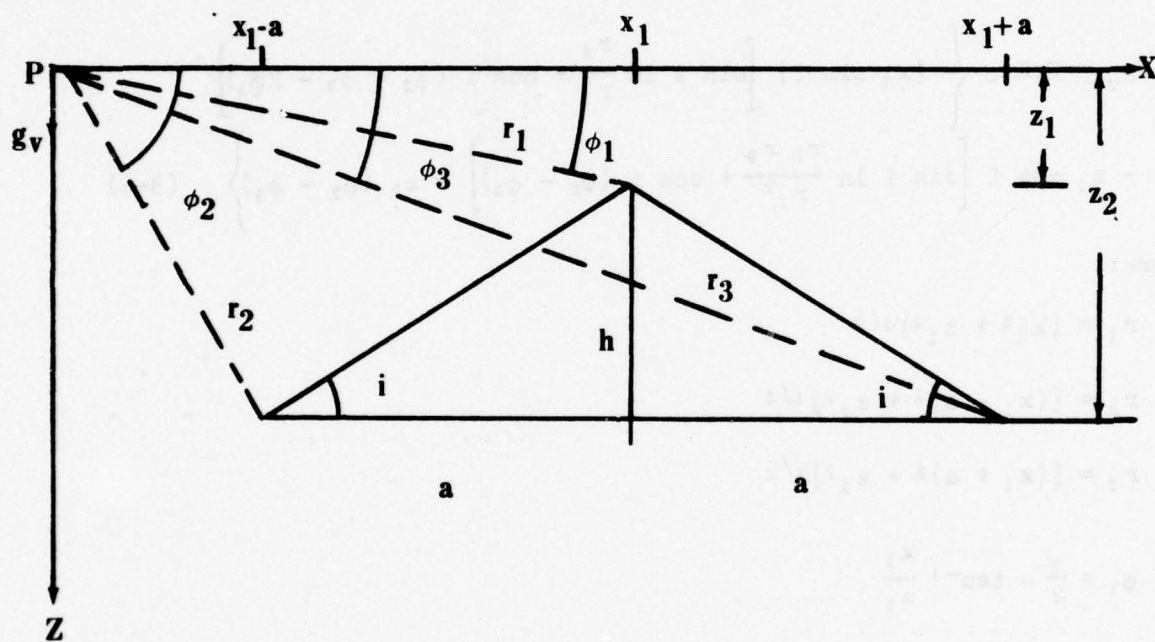
3.1.4 Vertical Offset of Infinite Extent

The geometrical and angular relationships are given in Figure 3-4. Equation 3-8 gives the gravitational effect.

$$g_v = 2 K \rho [z_2 \phi_2 - z_1 \phi_1 - x_1 \ln \frac{r_2}{r_1}]$$ (3-8)

where:

$$r_1 = (x_1{}^2 + z_1{}^2)^{1/2}$$

$$r_2 = (x_1{}^2 + z_2{}^2)^{1/2}$$

$$\phi_1 = \frac{\pi}{2} - \tan^{-1} \frac{x_1}{z_1}$$ (3-9)

$$\phi_2 = \frac{\pi}{2} - \tan^{-1} \frac{x_1}{z_2}$$

For an $h \lll z_1 \simeq z_2$, equation 3-8 becomes:

$$g_v = 2 K \rho_s h [\phi]$$ (3-10)

where:

$$\phi = \frac{\pi}{2} - \tan^{-1} \frac{x_1}{z}$$ (3-11)

3.1.5 Inclined Offset of Infinite Extent

Figure 3-5 gives the geometrical and angular relationships. The gravitational effect is given by equation 3-12.

$$g_v = 2 K \rho \left\{ - [x_1 \sin i + z_1 \cos i] [\sin i \ln \frac{r_2}{r_1} + \cos i (\phi_2 - \phi_1)] \right.$$
$$\left. + z_2 \phi_2 - z_1 \phi_1 \right\}$$ (3-12)

where:

Figure 3-4

Vertical Offset of Infinite Extent
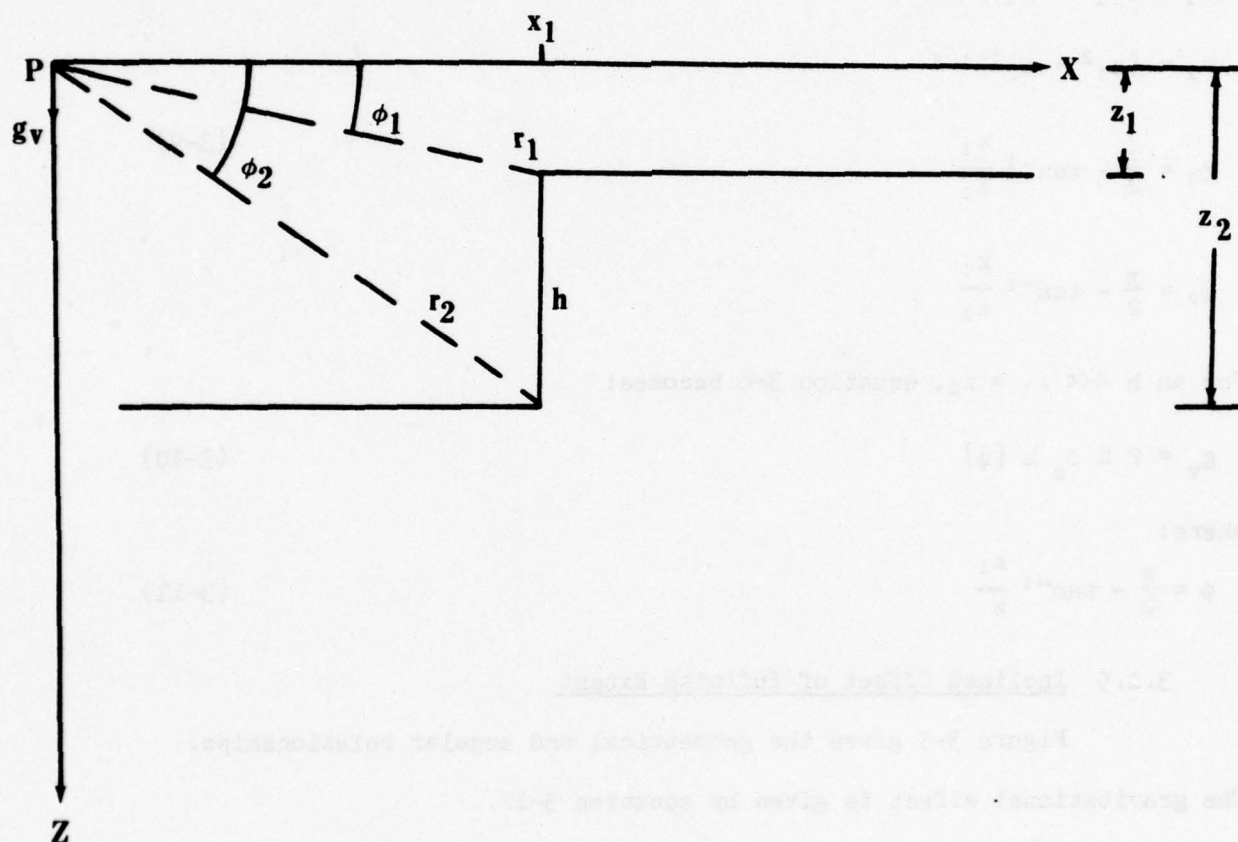
$$r_1 = (x_1{}^2 + z_1{}^2)^{1/2}$$

$$r_2 = [(x_1 - a)^2 + z_2{}^2]^{1/2}$$

$$\cos i = \frac{a}{(a^2 + h^2)^{1/2}} \; , \; \sin i = \frac{h}{(a^2 + h^2)^{1/2}} \qquad (3\text{-}13)$$

$$\phi_1 = \frac{\pi}{2} - \tan^{-1} \frac{x_1}{z_1}$$

$$\phi_2 = \frac{\pi}{2} - \tan^{-1} \frac{x_1 - a}{z_2}$$

Geldart, Gill, and Sharma (1966) give an excellent discussion of gravity anomalies of two-dimensional faults.

3.1.6 Inclined Prism of Infinite Extent

The inclined bed of infinite extent is formed by the difference of two offset slopes as shown in Figure 3-6. Equation 3-14 gives the gravitational effect.

$$g_v = 2 \, K \, \rho \left\{ - \, [x_1 \sin i + z_1 \cos i] \, [\sin i \, \ln \frac{r_2 \, r_3}{r_1 \, r_4} \right.$$

$$+ \cos i \, (\phi_2 - \phi_1 + \phi_3 - \phi_4)] + a \sin i \, [\ln \frac{r_4}{r_3} + \cos i \, (\phi_4 - \phi_3)]$$

$$\left. + z_2 \, (\phi_2 - \phi_4) - z_1 \, (\phi_1 - \phi_3) \right\} \qquad (3\text{-}14)$$

where:

69

Figure 3-5

Inclined Offset of Infinite Extent
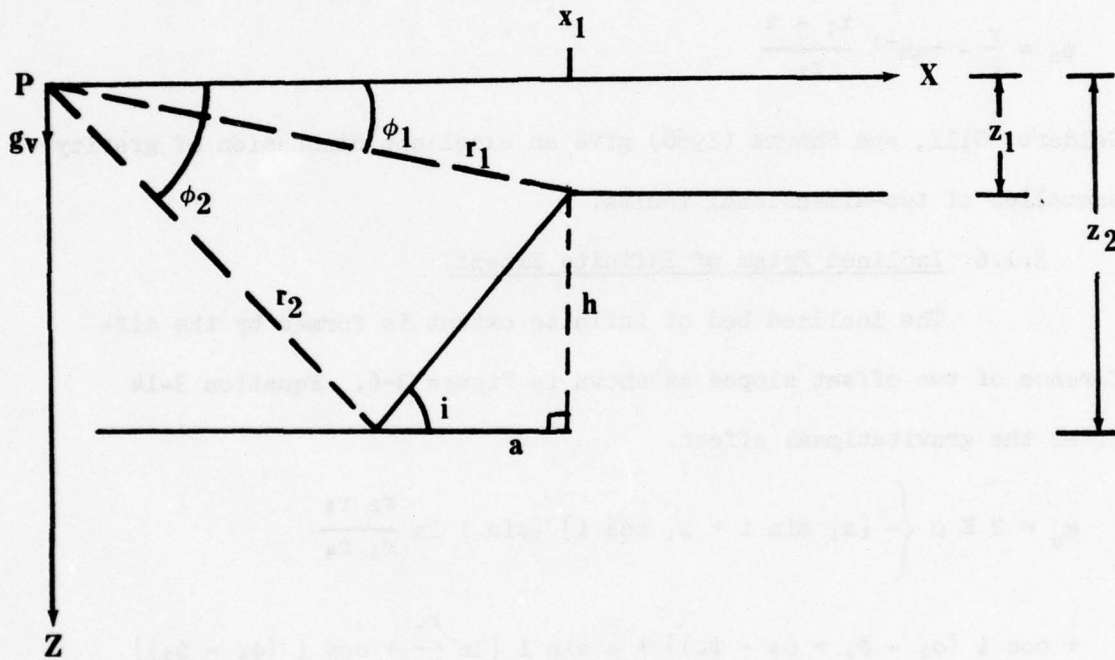
$$r_1 = (x_1{}^2 + z_1{}^2)^{1/2}$$

$$r_2 = [(x_1 - c)^2 + z_2{}^2]^{1/2}$$

$$r_3 = [(x_1 + a)^2 + z_1{}^2]^{1/2}$$

$$r_4 = [(x_1 + a - c)^2 + z_2{}^2]^{1/2}$$

$$\phi_1 = \frac{\pi}{2} - \tan^{-1} \frac{x_1}{z_1}$$

$$\phi_2 = \frac{\pi}{2} - \tan^{-1} \frac{x_1 - c}{z_2} \tag{3-15}$$

$$\phi_3 = \frac{\pi}{2} - \tan^{-1} \frac{x_1 + a}{z_1}$$

$$\phi_4 = \frac{\pi}{2} - \tan^{-1} \frac{x_1 + a - c}{z_2}$$

$$\cos i = \frac{c}{[c^2 + (z_2 - z_1)^2]^{1/2}}$$

$$\sin i = \frac{z_2 - z_1}{(c^2 + (z_2 - z_1)^2)^{1/2}}$$

The infinite inclined prism is used to model inclined dikes or similar structures.

3.1.7 Two-Dimensional Criterion

There are no geologic or geophysical structures that are truly two-dimensional. However, structures do exist that are sufficiently elongated in a single horizontal direction to be considered two-dimensional. The use of two-dimensional approximations in modeling and interpretation

71

Figure 3–6

Inclined   Prism of Infinite Extent
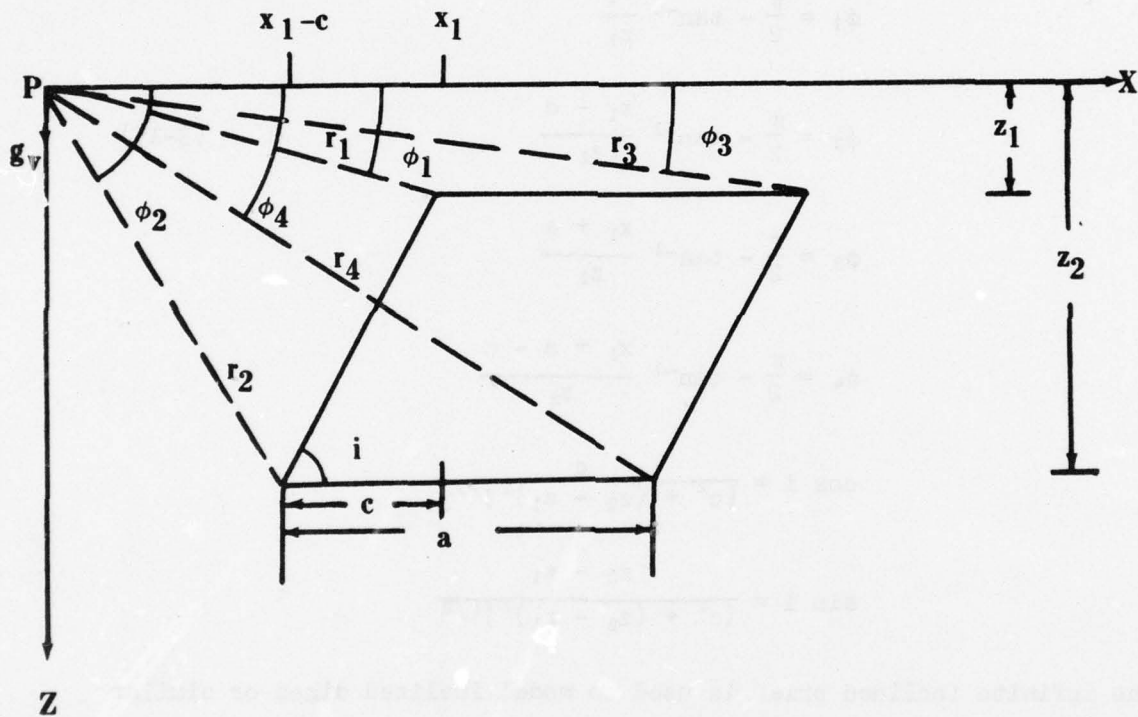
is based on the fact that the gravitational effect of more distant masses becomes negligible. It is important to estimate the error resulting from making the assumption of two-dimensionality.

The maximum error resulting from a two-dimensional assumption can be estimated by substituting a finite horizontal line element for the two-dimensional body as shown in Figure 3-7. The distance r is measured, in the xz plane, from the computation point or origin to the point on the cross-section of the two-dimensional body farthest from the origin.

$$\tilde{r} = [(x + \Delta x)^2 + (z + \Delta z)^2]^{1/2} \tag{3-16}$$

If the cross-sectional area of the body is small, Δx and Δy will be negligible. Then, r becomes the distance in the xz plane from the origin to the line element and is computed from equation 3-17.

$$r \simeq (x^2 + z^2)^{1/2} \tag{3-17}$$

Then, for a given point on the X-axis, r is dependent on z and the maximum percentage error p, in making the two-dimensional assumption is then estimated by equation 3-18:

$$p = (1 - e) \; 100\% \tag{3-18}$$

where:

$$e = \frac{y}{(r^2 + y^2)^{1/2}} \tag{3-19}$$

Table 3-1 gives the values of p for various ratios of y and r.

73

Figure 3-7

Two – Dimensional Criterion
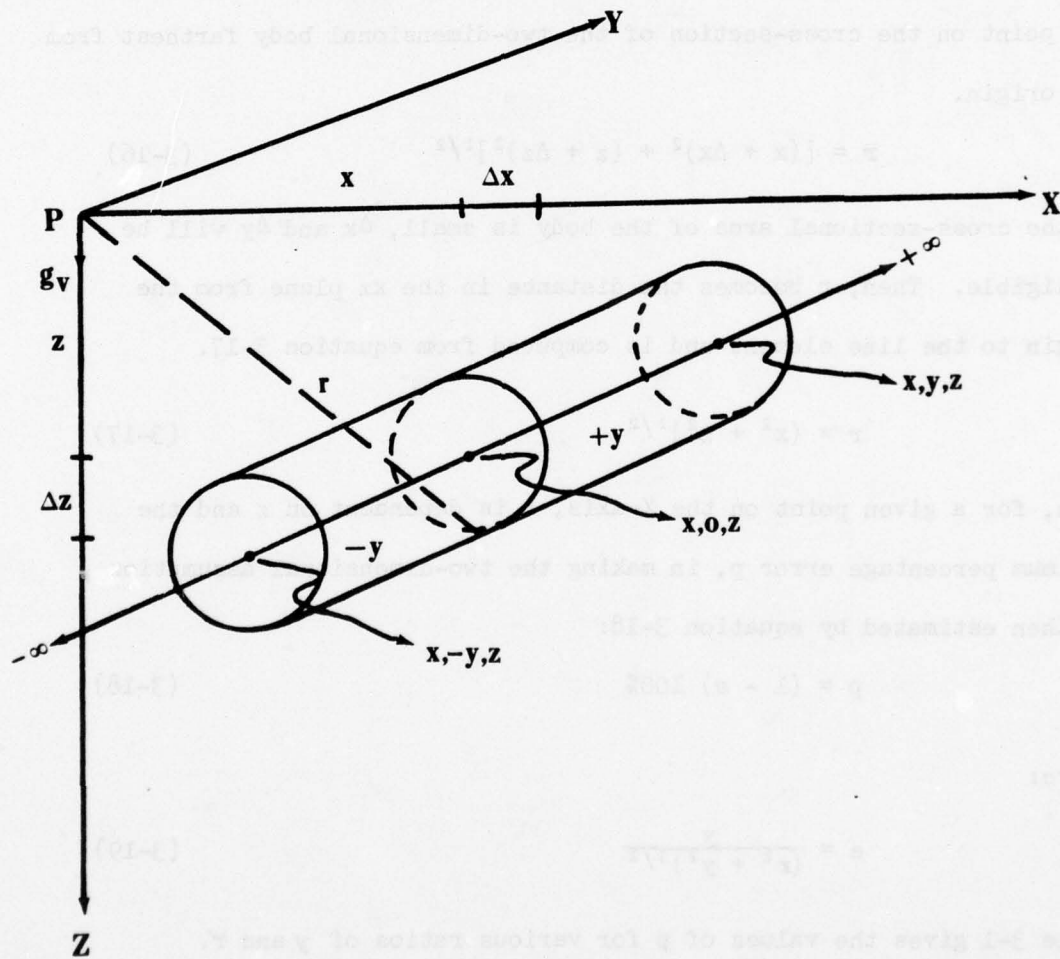
TABLE 3-1

Two-Dimensional Criterion

y	0	.5r	r	1.5r	2r	3r	4r	5r	10r	∞
p%	100	55.3	29.3	16.8	10.6	5.1	3.0	1.9	0.5	0

3.2 Computation Schemes for Two-Dimensional Bodies of Arbitrary Shape

The equations presented in this section form the basis for many automated modeling and inversion schemes. Such schemes are used to model two-dimensional bodies of arbitrary shapes and variable density contrast.

3.2.1 Equations for Surface Integration

The gravitational effect of a two-dimensional body of arbitrary cross-sectional area A_s is obtained by integrating the effects of infinite horizontal line elements of area dA over A_s, Figure 3-8. The general form of the integral is restated in equation 3-20.

$$g_v = 2 \ K \ \rho \int_{A_s} \int \frac{z}{(x^2 + z^2)} \ dA \qquad (3-20)$$

Equation 3-20 is expressed in different coordinate systems as follows:

Cartesian Coordinates, (x, z):

$$g_v = 2 \ K \ \rho \int_{A_s} \int \frac{z \ dx \ dz}{(x^2 + z^2)} \qquad (3-21)$$

Polar Coordinates, (r, θ):

$$g_v = 2 \ K \ \rho \int_{A_s} \int \sin\theta \ d\theta \ dr \qquad (3-22)$$

75

Figure 3-8

Two – Dimensional Body of Cross – Sectional Area, A_S
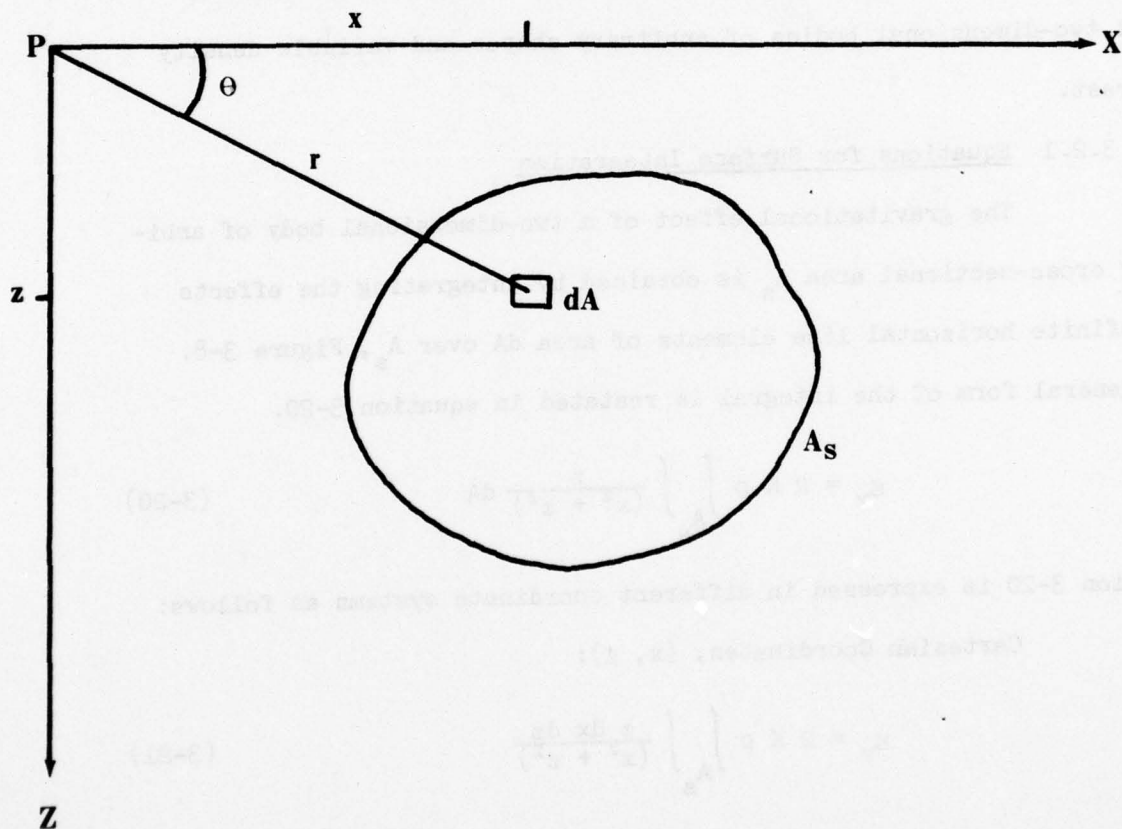
Angular Coordinates, (x, θ):

$$g_v = 2 K \rho \int_{A_s} \int \tan\theta \, d\theta \, d\mathbf{x} \qquad (3\text{-}23)$$

Angular Coordinates, (z, θ):

$$g_v = 2 K \rho \int_{A_s} \int d\theta \, dz \qquad (3\text{-}24)$$

The above equations can be evaluated by a simple summation of the effects of individual horizontal line elements over the area A_s. However, the gravitational effect of a line element increases very rapidly as its distance from the origin decreases.

3.2.2 Equations in Terms of Line Integrals

It is more practical and convenient to solve the two-dimensional problem in terms of line integrals rather than surface integrals, Hubbert (1948). Equations 3-22, 3-23 and 3-24 are rewritten as line integrals in equations 3-25 through 3-28 where the line integral L is in the cross-sectional plane of the body.

For the polar coordinates, (r, θ) figure 3-9:

$$g_v = 2 K \rho \, \Delta r \int_L \sin\theta \, d\theta$$

$$= 2 K \rho_s \, \Delta r \, [(\cos\theta_2 - \cos\theta_1) + (\cos\theta_4 - \cos\theta_3) + \ldots]$$

$$= 2 K \rho_s \, \Delta r \sum_{i=1}^{n} (\cos\theta_{i+1} - \cos\theta_i) \qquad (3\text{-}25)$$

77

Figure 3-9

Polar Coordinates r, θ
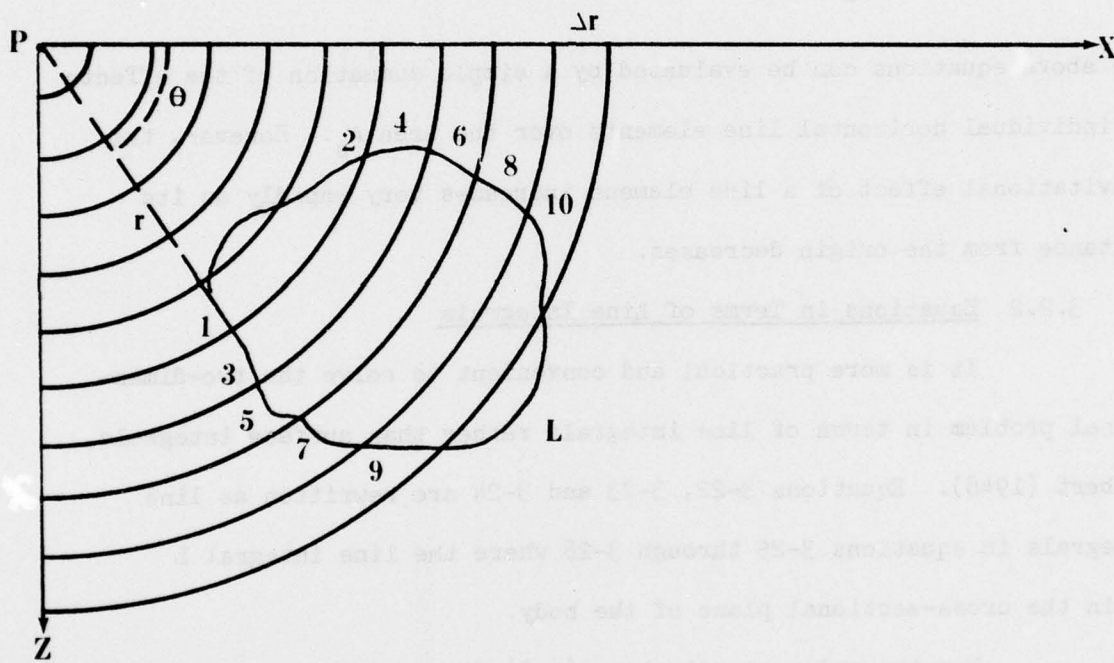
For the angular coordinates, (x, θ) figure 3-10:

$$g_v = 2 \, K \, \rho \, \Delta x \int_L \tan\theta \, d\theta$$

$$= 2 \, K \, \rho \, \Delta x \, \ln\left[\frac{\cos\theta_2}{\cos\theta_1} + \ln\frac{\cos\theta_4}{\cos\theta_3} + \ldots\right]$$

$$= 2 \, K \, \rho \, \Delta x \sum_{i=1}^{n}\left[\ln\frac{\cos\theta_{i+1}}{\cos\theta_i}\right] \tag{3-26}$$

Equation 3-24 is the simplest and most convenient to use. The integral can be expressed in terms of Δz or $\Delta\theta$ as is shown in equations 3-27 and 3-28.

For the angular coordinates, (z, θ) figures (3-11) and (3-12):

$$g_v = 2 \, K \, \rho \, \Delta z \int_L d\theta$$

$$= 2 \, K \, \rho \, \Delta z \, [(\theta_2 - \theta_1) + (\theta_4 - \theta_3) + \ldots]$$

$$= 2 \, K \, \rho \, \Delta z \sum_{i=1}^{n} (\theta_{i+1} - \theta_i) \tag{3-27}$$

Or, by changing the order of integration, equation 3-24 becomes:

$$g_v = 2 \, K \, \rho \, \Delta\theta \int_L dz$$

$$= 2 \, K \, \rho \, \Delta\theta \, [(z_2 - z_1) + (z_4 - z_3) + \ldots]$$

$$= 2 \, K \, \rho \, \Delta\theta \sum_{i=1}^{n} (z_{i+1} - z_i) \tag{3-28}$$

Any of the integration schemes defined by equations 3-25 through 3-28 can be used to numerically evaluate the line integral L.

79

Angular Coordinates X, θ
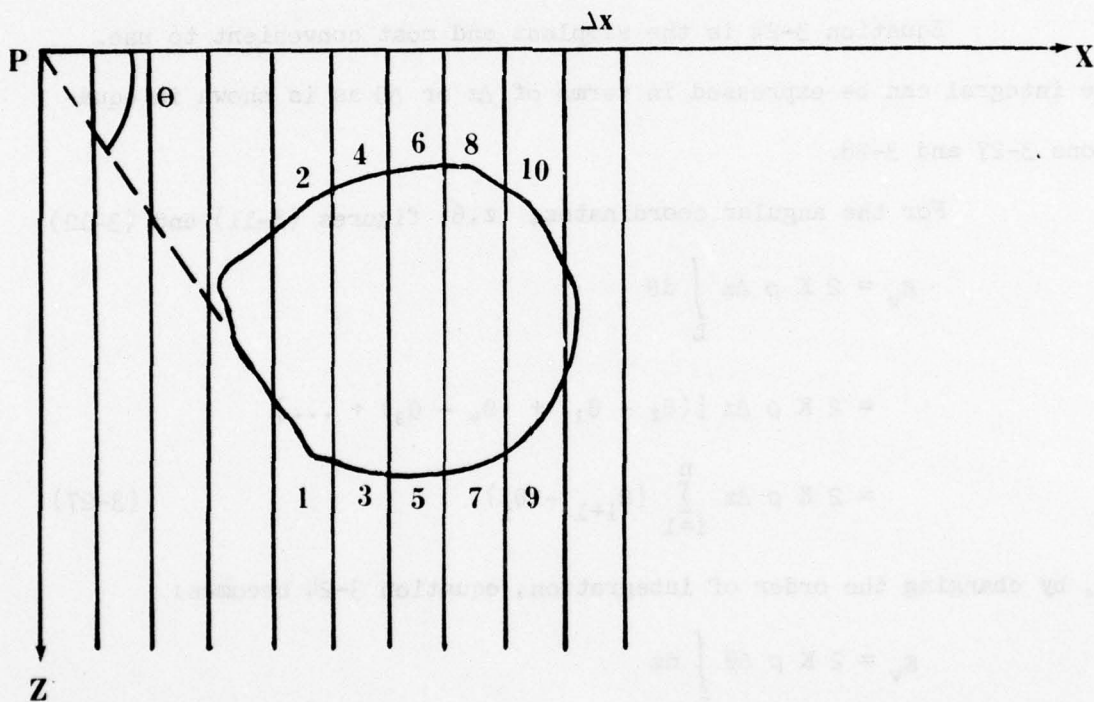
Figure 3-11

Angular Coordinates θ, Z
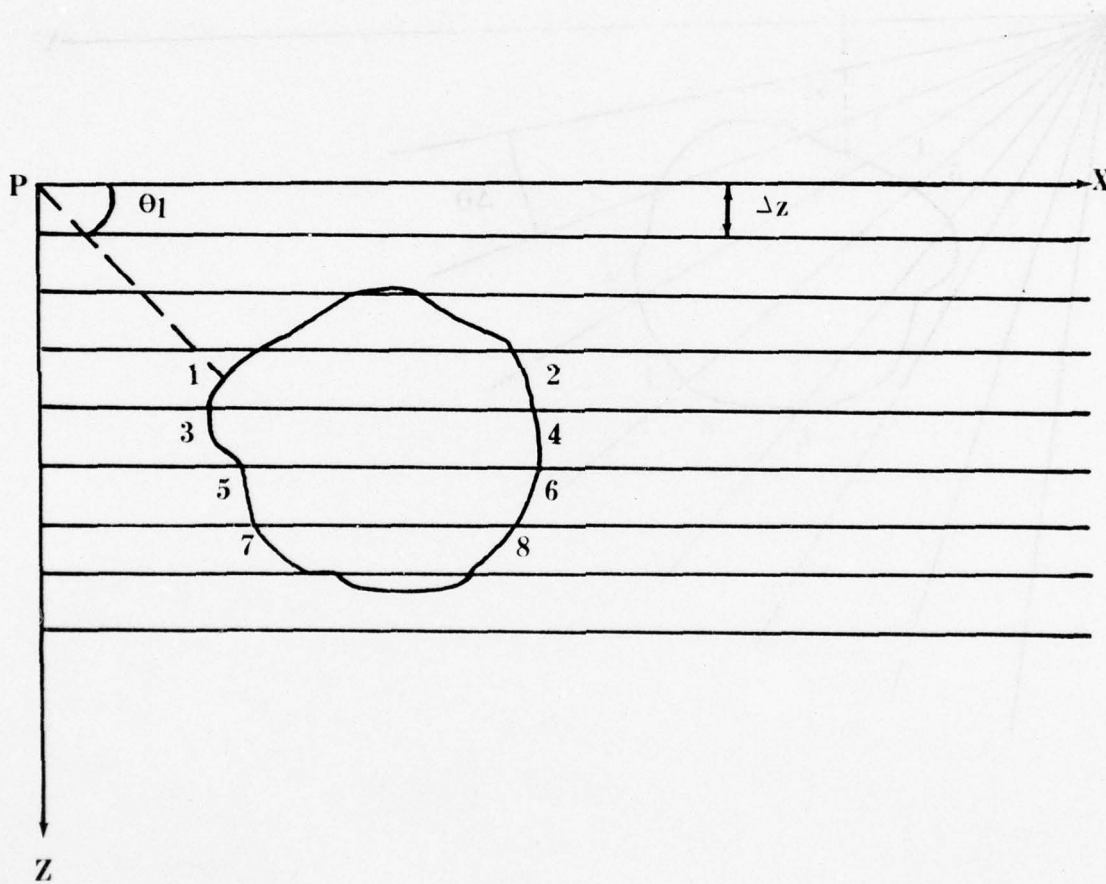
Figure 3-12

Angular Coordinates Z, θ
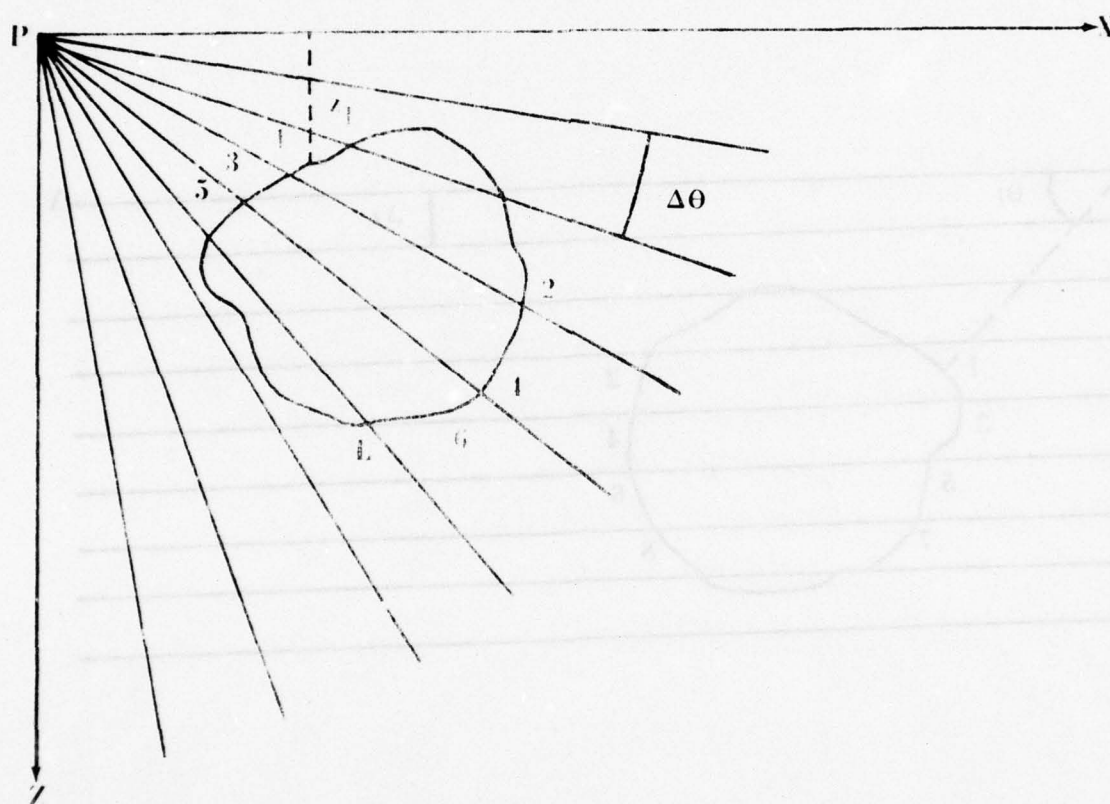
However, the most commonly used schemes are based on the approach of Talwani, Worzel and Landisman, (1959). It is a practical and convenient approach in which the two-dimensional cross-section is approximated by an n-sided polygon.

3.2.3 Gravitational Effect of an n-Sided Polygon

The gravitational effect of an arbitrary two-dimensional body of triangular cross-section PCD, Figure 3-13, is given by equation 3-29.

$$g_v = 2 K \rho \int_{\theta_i}^{\theta_{i+1}} z \, d\theta \tag{3-29}$$

The gravitational effect of the polygon ABCD...A is obtained by integrating equation 3-29 for each triangular cross-section and summing the results, as in equation 3-30.

$$g_v = 2 K \rho \sum_{i=1}^{N} \left\{ \frac{x_i z_{i+1} - z_i x_{i+1}}{(x_i - x_{i+1})^2 + (z_i - z_{i+1})^2} \right.$$

$$\left. \left[(z_{i+1} - z_i) \ln \frac{r_{i+1}}{r_i} + (x_i - x_{i+1}) (\theta_{i+1} - \theta_i) \right] \right\} \tag{3-30}$$

Figure 3-13

Arbitrary n − Sided Polygon

X_{i+1}

X_i

P

θ_i

θ_{i+1}

A

B

D

Z_i

Z_{i+1}

X

Z
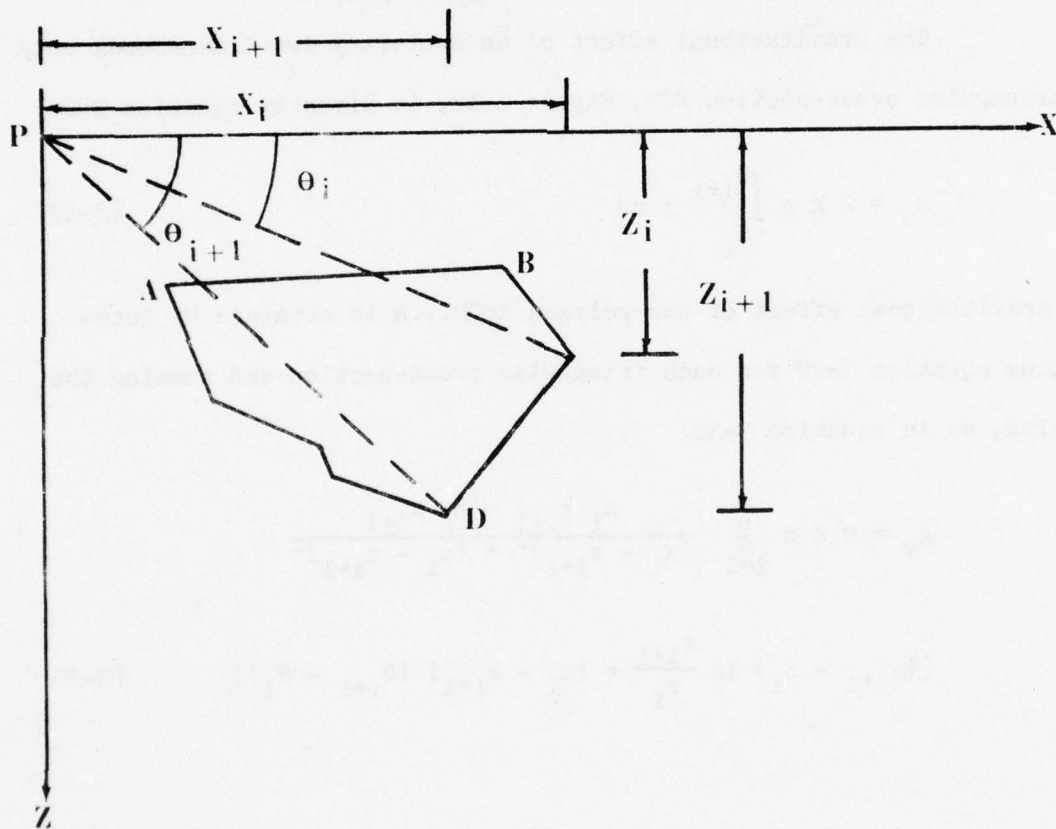
4. DENSITY DETERMINATION

4.1 Density and Porosity Defined

Density is defined as the ratio of mass to volume. If a given rock sample is 100% solid state rock material, density is defined by equation 4-1:

$$\rho = \frac{M}{V} \qquad (4\text{-}1)$$

In reality, rock specimens are composed of solid state rock material, and liquid, and/or air filled pore space. Therefore, equation 4-1 must be rewritten as:

$$\rho = \frac{(M_1 + M_2 + M_3)}{(V_1 + V_2 + V_3)} \qquad (4\text{-}2)$$

where:

M_1, M_2, M_3 = The masses of the solid state, liquid, and air spaces, respectively.

V_1, V_2, V_3 = The volumes of the solid state, liquid, and air spaces, respectively.

Equation 4-2 points out the inherent ambiguity in density determination. Therefore, in practice it is necessary to define density in terms of some limiting relationships.

Precise laboratory measurements yield accurate values of the dry and saturated densities ρ_d and ρ_s as defined in equations 4-3 and 4-4:

$$\rho_d = \frac{M_1 + M_3}{V_1 + V_3} \qquad (4\text{-}3)$$

$$\rho_s = \frac{M_1 + M_2}{V_1 + V_2} \qquad (4\text{-}4)$$
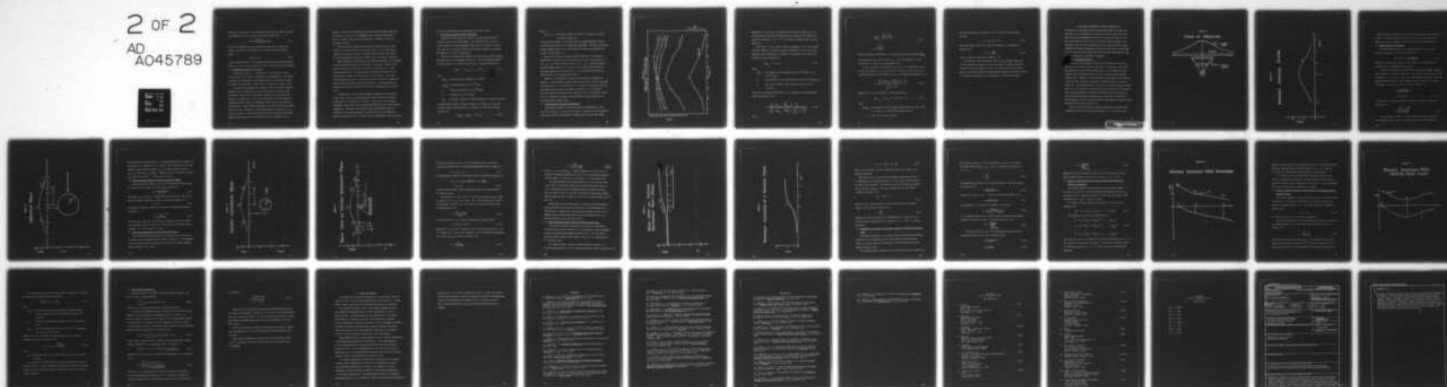
Porosity p is the ratio of the volume of liquid and air space in a given rock sample to the total volume as given in equation 4-5.

$$p\% = \frac{V_2 + V_3}{V_1 + V_2 + V_3} (100) \qquad (4-5)$$

The true rock sample density ρ_v depends on mineralogic composition, porosity and degree of saturation and is defined by the following range:

$$\rho_d \leq \rho_v \leq \rho_s \qquad (4-6)$$

Ideally, large numbers of rock samples are measured and processed statistically to yield a best estimate of the true density of the rock samples.

4.2 <u>Generalized Density Relationships</u>

Generalized density relationships are best discussed in terms of rock types (i.e., igneous, metamorphic and sedimentary). The density of igneous and metamorphic rocks depends mainly on mineralogic composition because the porosity of these rocks is usually less than 2% - 4%.

The density relationships in sedimentary rocks are highly variable. Carbonate rocks containing few or no solution cavities are the only sedimentary rocks in which mineralogic composition is generally more important than porosity. Pick, Picha and Vyskočil (1973) estimate the following porosity ranges of sedimentary rocks, based on the degree of consolidation. Unconsolidated sedimentary rocks have porosities ranging from 25% to 90%. Sedimentary rocks consolidated by diagenesis (i.e., static processes of lithification) have porosities tending towards 18%, whereas, sedimentary rocks consolidated by severe orogenesis (i.e.,

dynamic processes of lithification) have porosities averaging about 4%. In general, the density of sedimentary rocks increases with depth of burial. However, this general relationship is variable and must be determined locally.

Residual gravity anomalies are caused by lateral density or mass variations in the earth's crust and upper mantle. If the earth were composed of material in layers of laterally uniform mass, there would be no residual gravity anomalies no matter what the vertical variation.

Many gravimetric investigations are primarily dependent on a knowledge of mass distribution and/or local isostatic conditions. However, mass distributions may be difficult to determine and express due to some inherent ambiguities. Regional-residual separation techniques may not realistically separate the regional and residual fields. Also, mass distributions may be subtle continuous functions of position rather than clearly defined discrete functions of position. Such ambiguities can significantly affect the results of gravitational modeling and interpretation.

An examination of the general integral equations for the gravitational effect of two or three-dimensional bodies shows that density is independent of the geometry of the body. In fact, the other unknown parameters, depth and size are indirectly dependent on the initial density assumptions. Therefore, the initial density approximations must be determined by methods independent of geometry such as the laboratory methods already mentioned. However, densities determined in the laboratory

may not be representative of large masses of rocks in situ.

4.3 Nettleton's Method of Density Profiling

Nettleton (1939) describes a method of determining "effective" densities from gravity measurements. The effective density is the in situ density of large topographic masses due to a variety of influences such as: mineralogic composition, porosity changes in rock type, and degree of isostatic compensation.

Gravity and elevation measurements are made along a profile usually perpendicular to the topographic structure. Free-air gravity anomalies are then computed at n observation points j=1, n, using equation 4-7:

$$\left(\Delta g_f\right)_j = \left(g_{obs}\right)_j - \gamma_j + \delta g_f h_j \qquad (4-7)$$

where:

$\left(\Delta g_f\right)_j$ = Free-air gravity anomaly at j^{th} point

$\left(g_{obs}\right)_j$ = Observed gravity at the jth point

γ_j = Theoretical gravity at the jth point

h_j = Elevation at the jth point

δg_f = Free-air reduction (0.3086 mgals/meter, elevation in meters)

A geophysically realistic range of densities is chosen, ρ_1 to ρ_m, and a Bouguer gravity anomaly profile is computed for each density using equation 4-8.

$$\left(\Delta g_b\right)_{ij} = \left(\Delta g_f\right)_j - 2\pi K \rho_i h_j \qquad (4-8)$$

88

where:

$2\pi K \rho_i h_j$ = The Bouguer reduction for the ith density at the jth observation point, i=1, m.

If the elevation range is large, the Free-air gravity anomalies should be terrain corrected for the surrounding topography. The resulting Bouguer gravity anomaly profiles are plotted against distance and compared with elevation, as in Figure 4-1.

Equation 4-8 shows the Bouguer gravity anomalies to be directly proportional to elevation for all densities less than the true density (i.e., $\rho_i < \rho_v$) and the inverse holds for $(\rho_i > \rho_v)$. Thus, the Bouguer gravity anomaly profile for the correct density is the one reflecting the least dependency on elevation (i.e., the profile should be nearly flat directly over the topographic feature).

Figure 4-1 illustrates the method as applied over a hypothetical seamount. Bouguer gravity anomaly profiles are plotted for four densities. The profiles for ρ = 1.7 gm/cm^3 and ρ = 2.2 gm/cm^3 clearly show a direct relationship with elevation, whereas the profile for ρ = 2.4 gm/cm^3 shows an inverse relationship with elevation. Thus, the effective density is ρ_v = 2.3 gm/cm^3 which agrees with the density used in constructing the hypothetical seamount model.

4.4 Jung's Method of Density Determination

Jung (1943) expresses the Nettleton method in mathematical terms that can be applied to surface distributions of points as well as profiles. Gravity and elevation measurements are made over the area under study.

Figure 4-1

Density Profiling

km

1.5
2.0
2.5
3.0
3.5
4.0
4.5

$\rho = 2.4$
$\rho = 2.3$
$\rho = 2.2$
$\rho = 1.7$

Elevation

40 35 30 25 20 15 10 5

Kilometers

200 190 180 170 160 150 140 130 120 110 100 90 80 70

Milligals
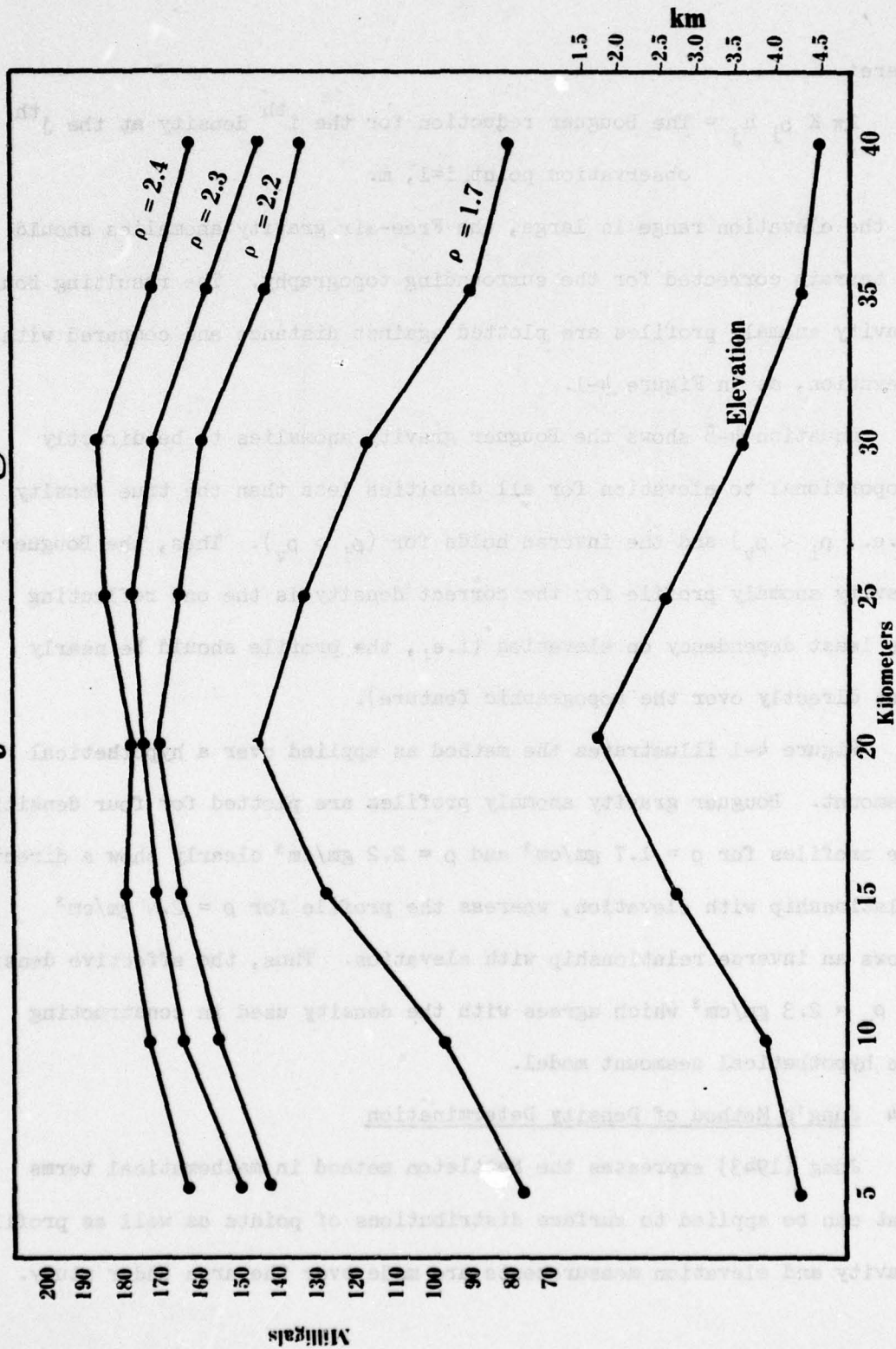
Equation 4-7 is then used to compute Free-air gravity anomalies at the n-observation points and the Bouguer gravity anomalies are computed for one of the densities ρ_i (i=1, m) in the range of geophysically realistic densities.

The method of least squares regression analysis is used to determine effective density. The Bouguer gravity anomalies for each of the given densities can be expressed as a function of elevation in the form of a regression line by equation 4-9:

$$\left(\Delta g_b\right)_{ij} = a_i + b_i \, h_j \qquad (4-9)$$

where:

$\left(\Delta g_b\right)_{ij}$ = The Bouguer gravity anomaly for the ith density ρ_i at the jth point

a_i = The intercept of the regression line for the ith density ρ_i

b_i = The slope constant of the regression line for the ith density ρ_i

First, the correlation coefficient, r_i, is computed for each regression line using equation 4-10:

$$r_i = \frac{\sum_{j=1}^{n} \left[\left(\Delta g_b\right)_{ij} - \overline{\left(\Delta g_b\right)}_i\right]\left[h_j - \bar{h}\right]}{\sqrt{\sum_{j=1}^{n} \left[\left(\Delta g_b\right)_{ij} - \overline{\left(\Delta g_b\right)}_i\right]^2} \; \sqrt{\sum_{j=1}^{n} \left[h_j - \bar{h}\right]^2}} \qquad (4-10)$$

where:

$$\left(\overline{\Delta g_b} \right)_i = \frac{\sum\limits_{j=1}^{n} \left(\Delta g_b \right)_{ij}}{n}$$

(4-11)

$$\overline{h} = \frac{\sum\limits_{j=1}^{n} h_j}{n}$$

If the correlation coefficient, r_i is equal to zero, the anomalies $\left(\Delta g_b \right)_{ij}$ are uncorrelated for a given density ρ_i. Thus, the density ρ_i is the real effective density of the topographic mass.

If the correlation coefficient is not equal to or sufficiently close to zero, the density ρ_i is not the effective density. Then, for $r_i \neq o$, the slope constant of the regression line b_i is computed by equation 4-12.

$$b_i = \frac{\sum\limits_{j=1}^{n} \left[\left(\Delta g_b \right)_{ij} - \left(\overline{\Delta g_b} \right)_i \right] \left[h_j - \overline{h} \right]}{\sum\limits_{j=1}^{n} [h_j - \overline{h}]^2}$$

(4-12)

Equation 4-9 is then rewritten in the following form:

$$\left(\Delta g_b \right)_{tj} = \left(\Delta g_b \right)_{ij} + 2\pi K h_j \left(\rho_t - \rho_i \right)$$

(4-13)

where:

$\left(\Delta g_b \right)_{tj}$ = The Bouguer gravity anomaly computed using the true effective density ρ_t at the $j^{\underline{th}}$ computation point

ρ_t = The true effective density.

The slope constant b_i in equation 4-13 is defined by the following equation:

$$b_i = 2\pi \, K \, (\rho_t - \rho_i) \qquad (4\text{-}14)$$

Then, the correct value of the effective density ρ_t is computed by equation 4-15:

$$\rho_t = \rho_i + \frac{b_i}{2\pi K} \qquad (4\text{-}15)$$

where, b_i has been computed by equation 4-12.

The Nettleton and Jung methods both give the effective densities of the topographic structures or masses between the highest and lowest elevations over the profile or area. The methods do not work well in areas of low relief, areas of complex lateral density variations or areas of considerable basement relief underlying the sedimentary layers.

5. SOME SIMPLE TECHNIQUES FOR DEPTH DETERMINATION

The purpose of this section is to present some simple techniques and formulas for the determination of depth and possible shapes and sizes. There is no unique mathematical solution to the determination of the mass distribution of the source of a residual gravity anomaly field. Therefore, some realistic assumptions and/or estimations must be made regarding the unknown parameters: depth, size and shape. Such assumptions are generalizations but yield realistic first approximations when detailed knowledge of structure is lacking.

Cone of Solutions Defined

Nettleton (1971) suggests the "Cone of Solutions" as an initial approach to the inverse problem. The "Cone of Solutions" states that the spherical or point mass of given density is the deepest possible singular mass configuration that can cause a given residual gravity anomaly field. However, other lenticular or rectangular mass configurations with that density are possible at shallower depths, as shown in Figure 5-1. All possibilities in the "Cone of Solutions" should preserve mass (i.e., the product of volume and density contrast must be the same). The following paragraphs describe some inversion techniques based on some possible simple mass configurations in the "Cone of Solutions." Each technique is then illustrated using the hypothetical residual gravity anomaly profile shown in Figure 5-2.

Skeels (1963) shows that the deepest geophysically feasible mass configuration must be a "vertical-sided mass" (i.e., infinite prism

Figure 5-1

Cone of Solutions

Anomaly
Profile

Regional

Cone of
Solutions
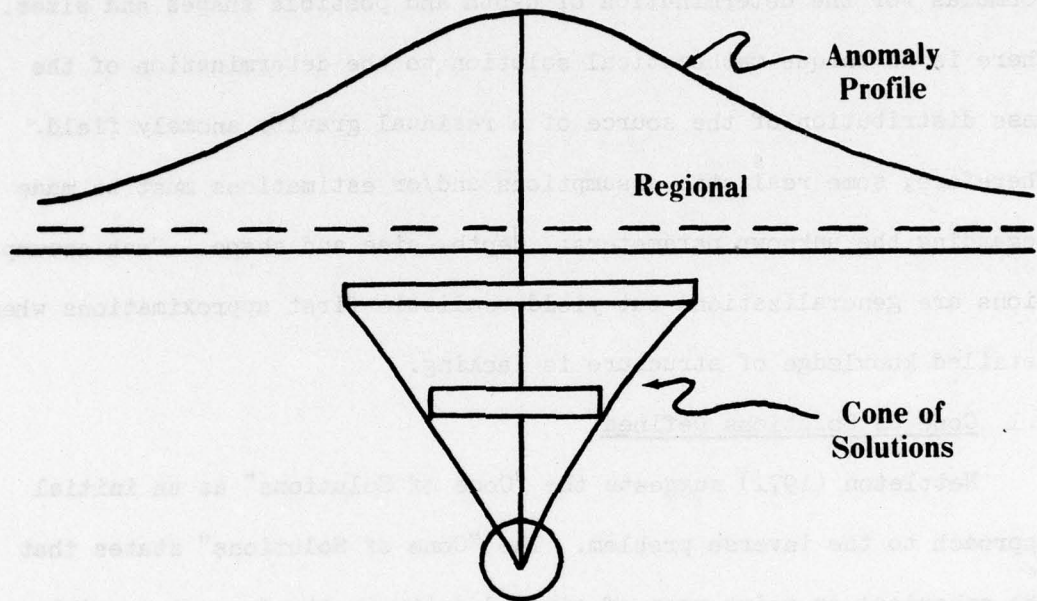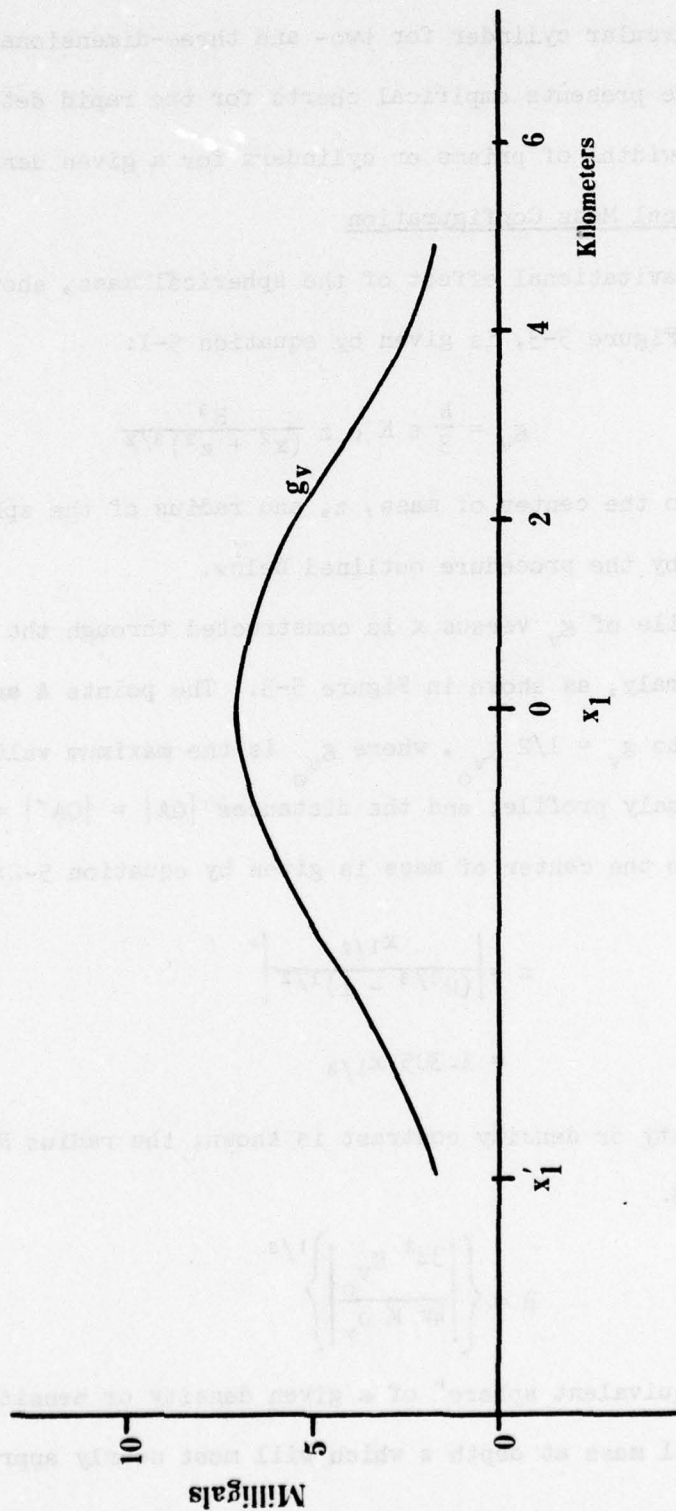
or right circular cylinder for two- and three-dimensional cases, respectively). He presents empirical charts for the rapid determination of depths and widths of prisms or cylinders for a given density contrast.

5.2 Spherical Mass Configuration

The gravitational effect of the spherical mass, shown in cross-section in Figure 5-3, is given by equation 5-1:

$$g_v = \frac{4}{3} \pi K \rho z \frac{R^3}{(x^2 + z^2)^{3/2}}$$
(5-1)

The depth to the center of mass, z, and radius of the sphere, R, are determined by the procedure outlined below.

A profile of g_v versus x is constructed through the maximum residual gravity anomaly, as shown in Figure 5-3. The points A and A′ on the x-axis correspond to $g_v = 1/2 \ g_{v_o}$, where g_{v_o} is the maximum value on the residual gravity anomaly profile; and the distances $|OA| = |OA′| = x_{1/2}$. Then, the depth to the center of mass is given by equation 5-2:

$$z = \left| \frac{x_{1/2}}{(2^{2/3} - 1)^{1/2}} \right|$$

$$= 1.305 \ x_{1/2}$$
(5-2)

If the density or density contrast is known, the radius R is given by equation 5-3.

$$R = \left\{ \left| \frac{3z^2 \ g_{v_o}}{4\pi K \rho_v} \right| \right\}^{1/3}$$
(5-3)

The "equivalent sphere" of a given density or density contrast is the spherical mass at depth z which will most nearly approximate the

98

Figure 5-3

Spherical Mass

Sphere in Cross-Section
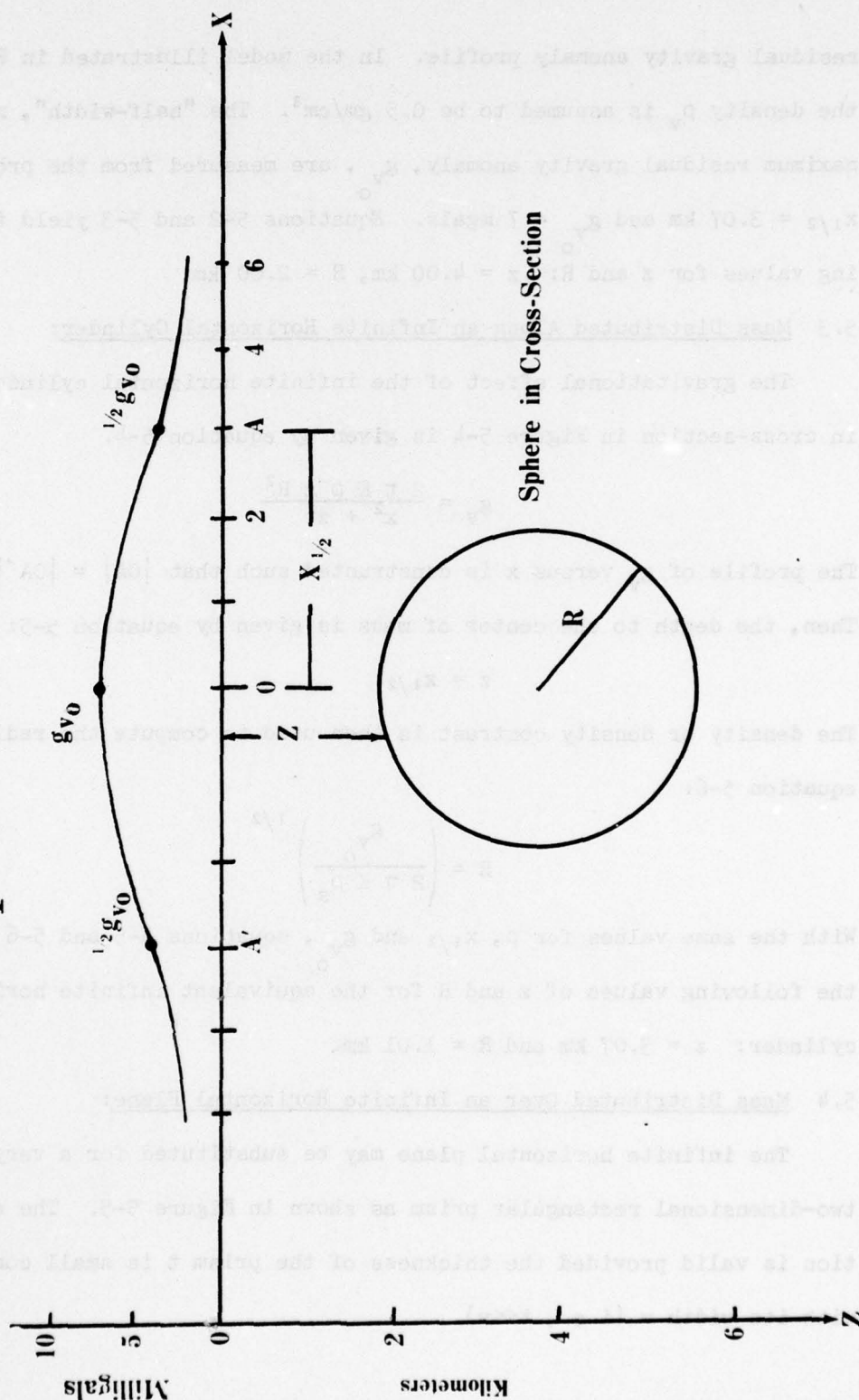
residual gravity anomaly profile. In the model illustrated in Figure 5-3, the density ρ_v is assumed to be 0.5 gm/cm^3. The "half-width", $x_{1/2}$, and maximum residual gravity anomaly, g_{v_o}, are measured from the profile: $x_{1/2}$ = 3.07 km and g_{v_o} = 7 mgals. Equations 5-2 and 5-3 yield the following values for z and R: z = 4.00 km, R = 2.00 km.

5.3 Mass Distributed Along an Infinite Horizontal Cylinder:

The gravitational effect of the infinite horizontal cylinder shown in cross-section in Figure 5-4 is given by equation 5-4.

$$g_v = \frac{2 \pi K \rho z R^2}{x^2 + z^2} \tag{5-4}$$

The profile of g_v versus x is constructed such that $|OA| = |OA'| = x_{1/2}$. Then, the depth to the center of mass is given by equation 5-5:

$$z = x_{1/2} \tag{5-5}$$

The density or density contrast is then used to compute the radius by equation 5-6:

$$R = \left(\frac{g_{v_o}}{2 \pi K \rho_s} \right)^{1/2} \tag{5-6}$$

With the same values for ρ, $x_{1/2}$ and g_{v_o}, equations 5-5 and 5-6 yield the following values of z and R for the equivalent infinite horizontal cylinder: z = 3.07 km and R = 1.01 km.

5.4 Mass Distributed Over an Infinite Horizontal Plane:

The infinite horizontal plane may be substituted for a very thin two-dimensional rectangular prism as shown in Figure 5-5. The approximation is valid provided the thickness of the prism t is small compared with its width w (i.e., t<<w).

100

Figure 5-4

Infinite Cylindrical Mass

Mass Over an Infinite Horizontal Plane
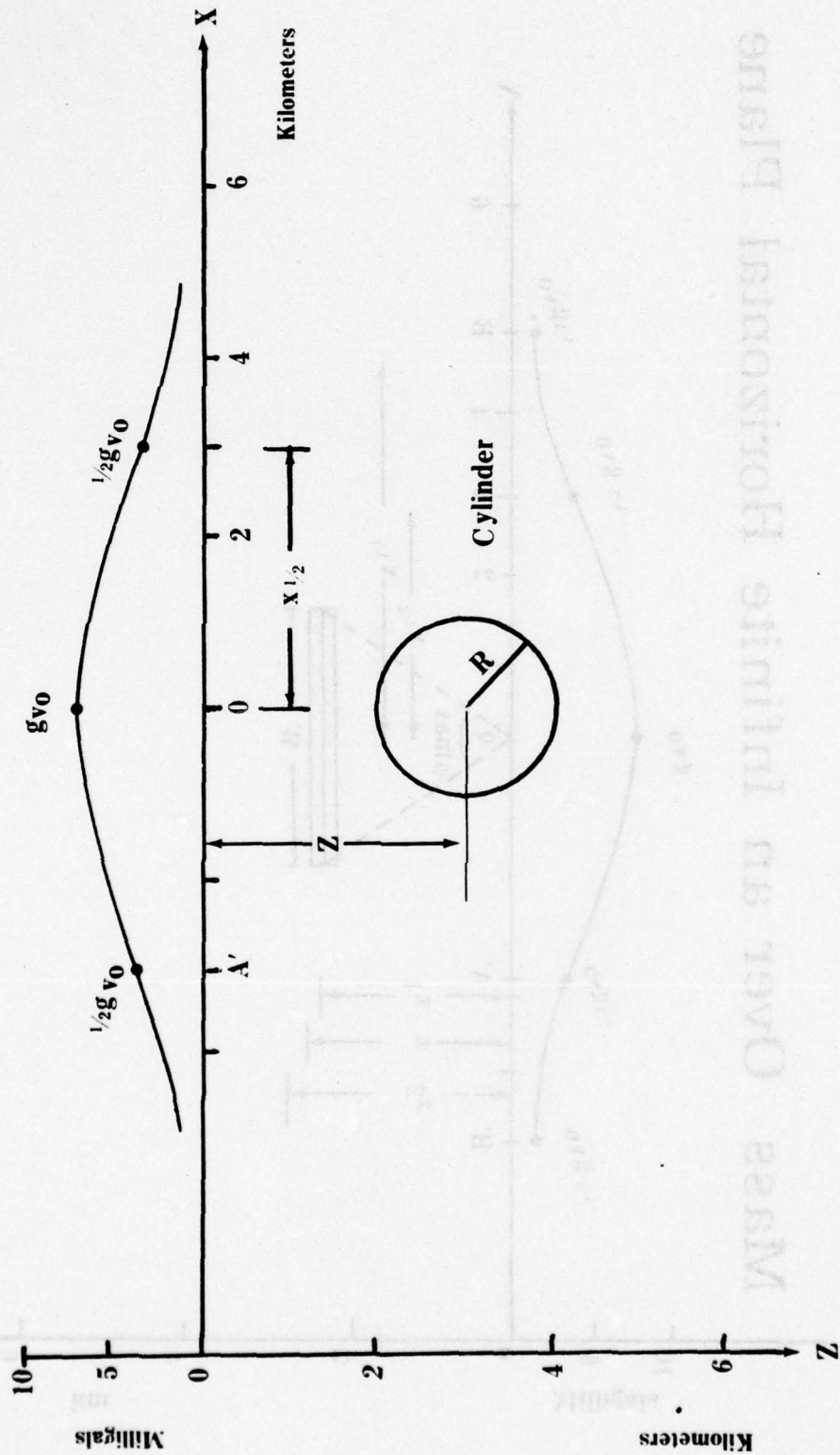
Figure 5-5
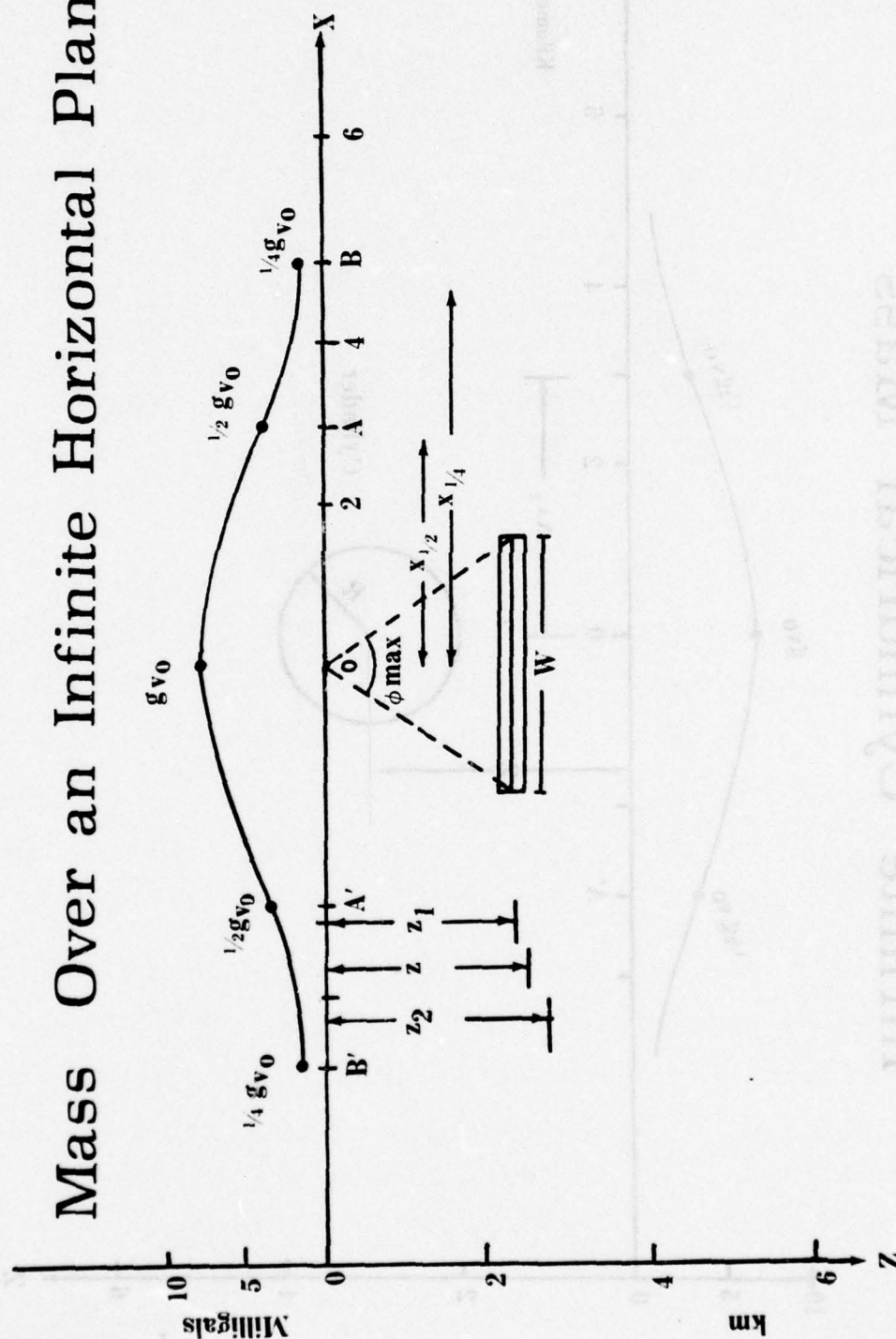
The surface density constant, μ, of the infinite plane is defined in terms of the surface density of the two-dimensional prism by equation 5-7.

$$\mu = \rho (z_2 - z_1) \tag{5-7}$$

The gravitational effect of the infinite plane is defined by equation 5-8:

$$g_V = 2 K \mu \left[\tan^{-1} \left(\frac{x + w}{z} \right) - \tan^{-1} \left(\frac{x}{z} \right) \right]$$

$$= 2 K \mu \phi \tag{5-8}$$

where x is the distance from the computation point to the near edge of the infinite plane.

The points A, A´, and B and B´ on the x-axis correspond to $g_V = (1/2) g_{V_O}$ and $g_V = (1/4) g_{V_O}$, respectively. Then, the distances $|OA| = |OA´| = x_{1/2}$ and $|OB| = |OB´| = x_{1/4}$. The depth to the infinite plane is then given by equation 5-9:

$$z = \frac{(x_{1/4}^2 - x_{1/2}^2)}{2x_{1/2}} \tag{5-9}$$

Then, the width, W, of the plane is determined by equation 5-10.

$$W = 2 (x_{1/2}^2 - z^2)^{1/2} \tag{5-10}$$

Equation 5-7 can be used to compute μ only if values are known for z_1 and z_2. However, if z_1 and z_2 aren't known, μ, can be evaluated from equation 5-8 using z and g_{V_O} as shown in equation 5-10:

$$\mu = \frac{g_{V_O}}{2 K \phi \, \text{max}} \tag{5-11}$$

$$\mu = \frac{g_{v_o}}{4 \, K \, \tan^{-1}\left(\dfrac{W}{2z}\right)}$$

<div align="right">(5-11)
(cont.)</div>

With $x_{1/2}$ = 3.07 km and g_{v_o} = 7 mgals, equations 5-9, 5-10 and 5-11 yield the following values for z, W and μ for the equivalent horizontal infinite plane: z = 2.53 km, W = 3.449 km, μ = .43973 gm/cm^3 (km).

The spherical mass and infinite plane are the two limiting cases in the "Cone of Solutions", whereas the infinite horizontal cylinder is an intermediate case for an assumed density or density contrast. Thus the center of mass of the mass configuration causing the residual gravity anomaly profile in Figure 5-2 must be at a depth between 2.53 km and 4 km.

The methods just discussed apply to symmetrical residual gravity anomaly profiles caused by either spherical or two-dimensional mass distributions. Asymmetrical residual gravity anomaly profiles must be handled by more refined techniques such as the characteristic curve method described by Grant and West (1965).

5.5 Mass Distributed Over an Infinite Horizontal Half-Plane:

The infinite horizontal half-plane may be used to approximate a vertical fault as shown in Figure 5-6. The thickness of the half-plane, is then the vertical displacement along the fault. The one-limbed residual gravity anomaly profile shown in Figure 5-7 is characteristic of a vertical fault.

The surface density constant is again defined by equation 5-7. The gravitational effect of the infinite half-plane is given by equation 5-12.

Figure 5-6

Mass Over an Infinite
Horizontal Half − Plane
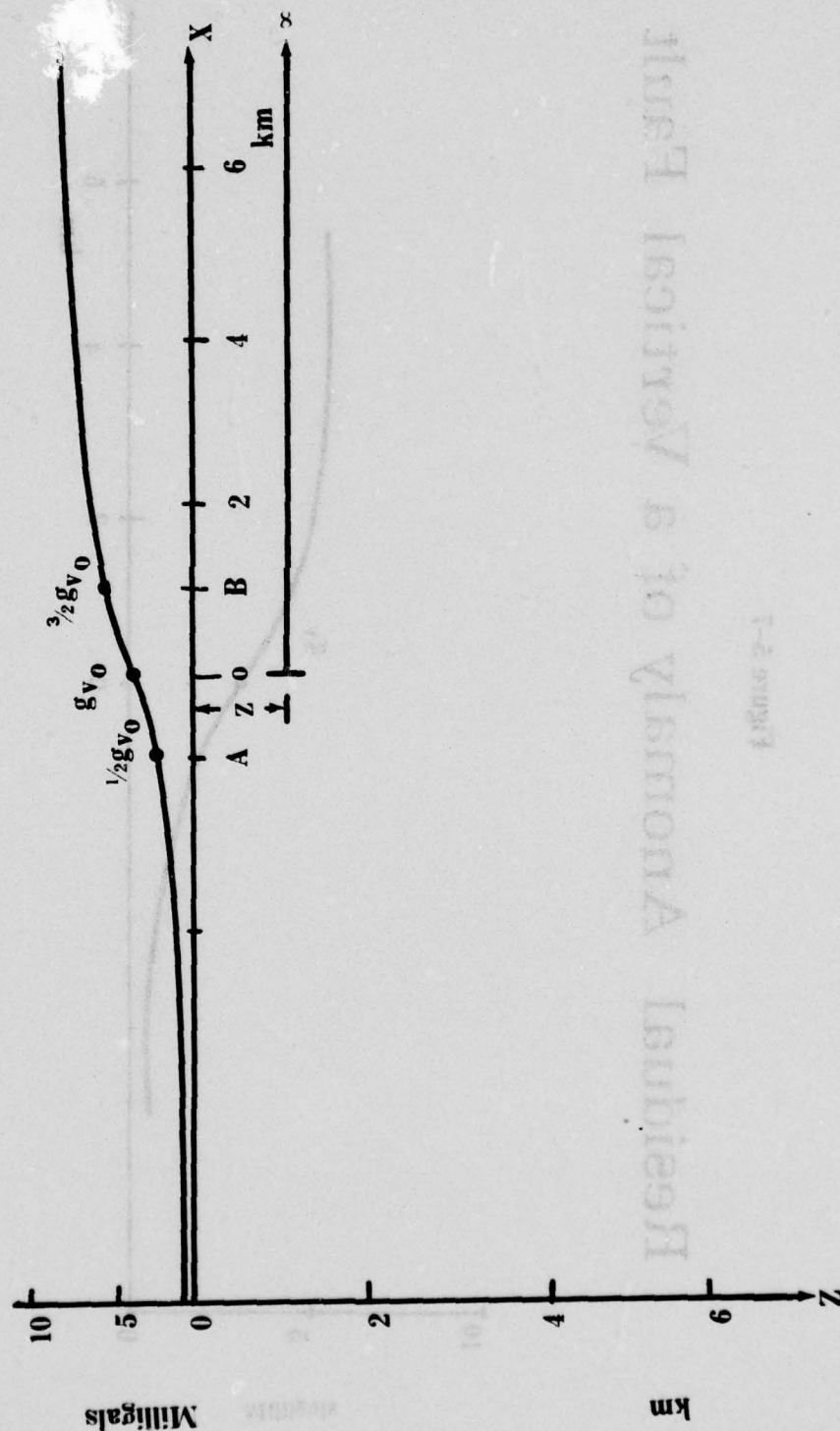
Figure 5–7

Residual Anomaly of a Vertical Fault

$$g_v = 2 \, K \, \mu \left(\frac{\pi}{2} - \tan^{-1} \frac{x}{z} \right) \qquad (5\text{-}12)$$

where x is the distance from the computation point to the edge of the infinite half-plane.

The point 0 on the x-axis must be determined graphically because it corresponds to the inflection point on the g_v profile directly above the edge of the half-plane. The points A and B on the x-axis correspond to $g_{v_A} = (1/2) \, g_{v_0}$ and $g_{v_B} = (3/2) \, g_{v_0}$, respectively, and the depth z is given by equation 5-13.

$$|OA| = |OB| \approx z \qquad (5\text{-}13)$$

Equation 5-12 is then evaluated at the inflection point to compute a value for μ, as shown in equation 5-14:

$$\mu = \frac{g_{v_0}}{K\pi} \qquad (5\text{-}14)$$

Equation 5-13 and 5-14 yield the following values of z and μ for the residual gravity anomaly profile in Figure 5-7: z = 1 km, μ = .14906 x 10^5 gm/cm^2.

5.6 Estimation of the Depth to the Upper Boundary of a Body of Arbitrary Shape:

The general solutions to the problem along with complete derivations are given by Bott and Smith (1958). The equations they derived are valid in a general sense and are applied to the hypothetical residual gravity anomaly profile.

The residual gravity anomaly profile referenced is given in Figure 5-2.

Two points g_{v_1} and g_{v_2}, with corresponding x_1 and x_2 on the x-axis, are chosen such that $g_{v_1} > g_{v_2}$. Then, λ is defined by equation 5-15 ($\lambda > 1$):

$$\lambda = \frac{g_{v_1}}{g_{v_2}} \tag{5-15}$$

The maximum possible depth to the upper boundary of the body is given by equation 5-16:

$$z \leq \frac{|x_1 - x_2|}{\lambda^{2/3} - 1} \lambda^{1/3} \tag{5-16}$$

Equation 5-17 gives z for m > 1 where m is given by equation 5-18:

$$z \leq \frac{w}{(m^{2/3} - 1)^{1/2}} \tag{5-17}$$

The parameter w is an arbitrary interval on the x-axis.

$$m = \frac{2g_v(x)}{[g_{v(x+w)} + g_{v(x-w)}]} \tag{5-18}$$

If the maximum values of the residual gravity anomaly and horizontal gradient are known, the depth z is given by equation 5-19:

$$z \leq .86 \frac{g_{v(max)}}{\left|\frac{\partial g_v}{\partial x}\right|_{max}} \tag{5-19}$$

The same derivations yield the corresponding equations for two-dimensional bodies, with m and λ already defined.

$$z \leq \frac{|x_1 - x_2|}{\lambda - 1} \lambda^{1/2} \tag{5-20}$$

$$z \leq \frac{w}{(m-1)^{1/2}} \tag{5-21}$$

108

$$z \leq .65 \frac{g_v(max)}{\left|\dfrac{\partial g_v}{\partial x}\right|\,max} \tag{5-22}$$

Equations 5-15 and 5-16 yield a value of $z \leq 5.1$ km for the residual gravity anomaly profile in Figure 5-2, where $|x_1 - x_2| = 5$ km.

5.7 Depth to a Density Interface Along a Profile With Gravity and Borehole Information:

The density interface and associated residual gravity anomaly are shown in Figure 5-8. There are boreholes along the profile at x_2, x_3 and x_n, and the interface outcrops at x_1, such that the depths of the interface $z(x_1)$, $z(x_2) \ldots z(x_n)$ are known.

The interface is then expressed in the form of a series as in equation 5-23.

$$z(x) = A_o + A_1(g_v) + A_2(g_v)^2 + \ldots + A_n(g_v)^n \tag{5-23}$$

The equations are set up as in equation 5-24.

$$z_1 = A_o + A_1(g_{v_1}) + A_2(g_{v_1})^2 + \ldots + A_i(g_{v_1})^i$$
$$z_2 = A_o + A_1(g_{v_2}) + A_2(g_{v_2})^2 + \ldots + A_i(g_{v_2})^i \tag{5-24}$$
$$\cdot \quad \cdot \quad \cdot \quad \cdot \quad \cdot$$
$$\cdot \quad \cdot \quad \cdot \quad \cdot \quad \cdot$$
$$z_n = A_o + A_1(g_{v_n}) + A_2(g_{v_n})^2 + \ldots + A_i(g_{v_n})^i$$

The solution of the set of equations yields the coefficients A_1, $A_2 \ldots A_i$. The solution is unique when the number of coefficients equals the number of observation points (i.e., $i = n$) and can be solved as simultaneous equations.

109

Figure 5-8

Density Interface With Boreholes
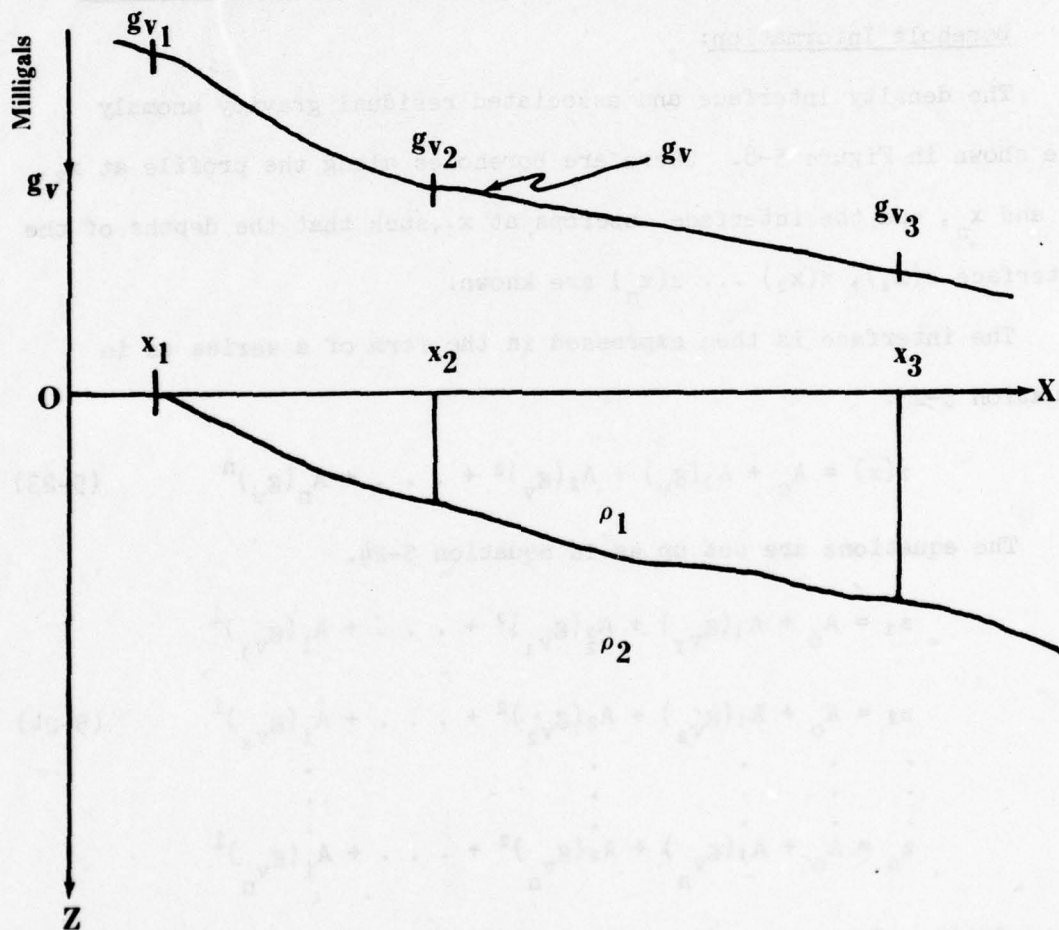
However, the solution is not unique when the number of observation points is greater than the number of coefficients (i.e., $n > i$). The best fit solution is then obtained by the method of least squares.

If the depth is known at many points along the profile, it may suffice to graphically interpolate the shape between the known depths, using the residual gravity anomaly profile as control. Both the graphical and analytical methods are independent of density.

5.8 Depth to a Density Interface Along a Profile From Residual Gravity Anomalies Alone:

The residual gravity anomaly profile and density interface are shown in Figure 5-9. The method requires that the densities ρ_1 and ρ_2 be known or reasonably approximated. The density contrast is defined by equation 5-25:

$$\rho_c = \rho_1 - \rho_2 \qquad (5\text{-}25)$$

For basin structures, $\rho_2 > \rho_1$ and ρ_c is negative.

The first approximation to the shape of the interface is determined by computing depths z_i at n-observation points along the x-axis by equation 5-26:

$$z_i = \frac{g_{v_i}}{2 \pi K \rho_c} \qquad (5\text{-}26)$$

The theoretical gravity anomalies $\left(g_{v_k} \right)_i$ are computed for the current depths using appropriate equations, i.e., Talwani's equation for the gravitational effect of two-dimensional n-sided polygon, equation 3-31.

Figure 5-9

Density Interface With
Gravity Data Alone
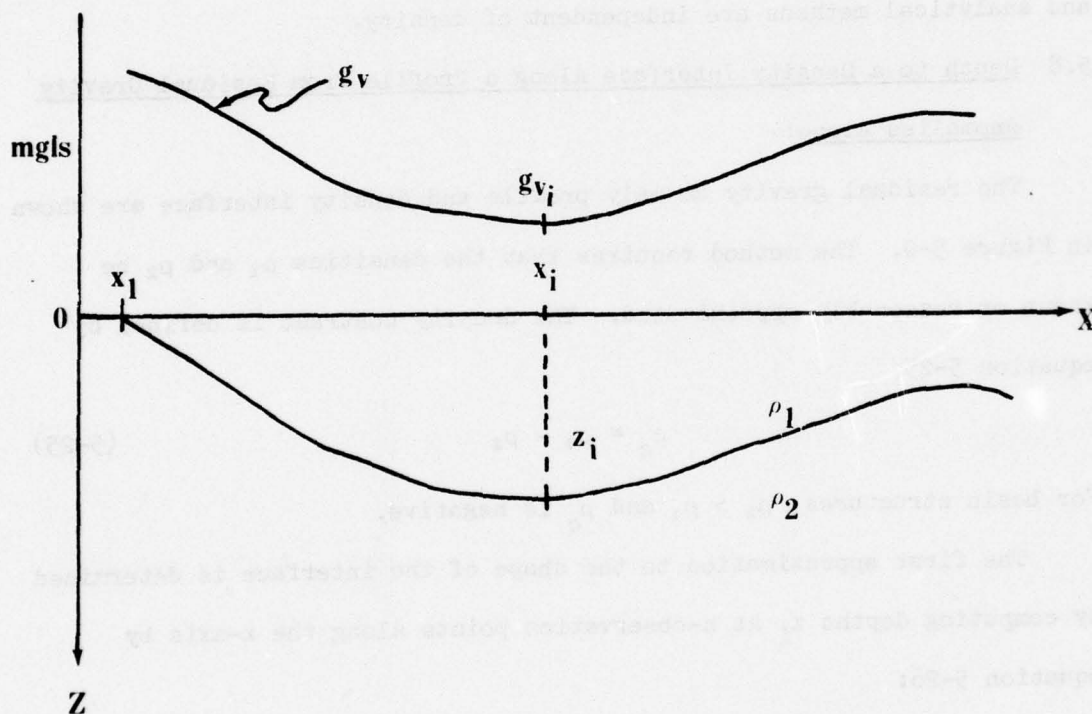
The theoretical and observed residual gravity anomalies are compared and differences computed using equation 5-27.

$$\left(\delta g_k\right)_i = g_{v_i} - \left(g_{v_k}\right)_i \qquad (5\text{-}27)$$

where:

$\left(\delta g_k\right)_i$ = Difference between the observed and computed residual gravity anomalies at the ith observation point for k^{th} iteration.

g_{v_i} = Observed residual gravity anomaly at the ith observation point.

$\left(g_{v_k}\right)_i$ = Computed residual gravity anomaly at the ith observation point for the kth iteration.

Updated values for the depths are then computed using the gravity differences as shown in equation 5-28.

$$z_{ki} = z_{(k-1)i} + \frac{\left(\delta g_{v_k}\right)_i}{2 \pi K \rho_c} \qquad (5\text{-}28)$$

where:

z_{ki} = The updated depth at the ith observation point for the kth iteration.

The procedure is iterated until the gravity differences meet some minimum criterion. Qureshi and Mula (1971) present a complete derivation and discussion of the method based on algorithms suitable for use with digital computers.

5.9 Calculation of Excess Mass:

The excess mass, M, is computed using the integral equation 5-29 which is based on Gauss' theorem.

$$\int_{-\infty}^{\infty} \int_{-\infty}^{\infty} g_v \,(x,y) \; dx \; dy = 2 \,\pi \, KM \qquad (5-29)$$

Equation 5-29 is entirely independent of shape and density.

In theory the integrations must be carried over the entire XY plane. However, the actual ranges of integrations are -X to X and -Y to Y when the origin is placed near the center of the residual gravity anomaly in the XY plane. The ranges in X and Y represent the limits of data or the distances at which the residual gravity anomalies become negligible. Equation 5-29 is rewritten with a remainder term.

$$2 \,\pi \, K \, M = \int_{-X}^{X} \int_{-Y}^{Y} g_v \,(x,y) \; dx \; dy + R \,(X,Y) \qquad (5-30)$$

If the center of mass of M is at $(\bar{x}, \bar{y}, \bar{z})$, the remainder term is approximated by equation 5-31, provided that $|\bar{x}| \ll X$ and $|\bar{y}| \ll Y$:

$$R(X,Y) = 2 \,\pi \, K \, M - 4 \, G \, M \, \tan^{-1} \frac{XY}{\bar{z} \,(X^2 + Y^2)^{1/2}} \qquad (5-31)$$

Equation 5-32 is then derived by substituting equation 5-31 into equation 5-30:

$$M = \frac{\displaystyle\int_{-X}^{X} \int_{-Y}^{Y} g_v(x,y) \; dx \; dy}{4 \; K \;\; \tan^{-1} \dfrac{XY}{\bar{z} \,(X^2 + Y^2)^{1/2}}} \qquad (5-32)$$

The value for $\bar{z}$ is estimated by the half-width method from equation 5-2 for three-dimensional bodies (i.e., $\bar{z} = 1.305 X_{1/2}$). Equation 5-5 is used to compute $\bar{z}$ for two-dimensional bodies, $\bar{z} = X_{1/2}$ and equation

114

5-32 becomes:

$$M = \frac{\int_{-X}^{X} g_v (x) \, dx}{4 \, K \, \tan^{-} \frac{X}{z}} \qquad (5-33)$$

Simpson's Rule or some similar numerical quadrature method is used to evaluate the integrals in equations 5-32 and 5-33 if the observed data points are evenly distributed. If the observed data points are not evenly distributed, a template method must be used as described by Grant and West (1965).

The inversion methods discussed in this section are used to compute first approximations to the unknown parameter controlling depth, size and shape.

More complex techniques are beyond the scope and purpose of this report. The reader interested in such techniques is referred to the bibliography.

115

6. CONCLUDING REMARKS

The formulas and techniques presented in this publication form the analytical basis of gravitational modeling and interpretation. In application, several theoretical and practical aspects must be considered.

The theoretical aspects refer to the inherent ambiguities due to the assumptions regarding density or mass distributions as well as size and shape. Practical aspects to be considered are: the amount and accuracy of the gravity data; the resolving power of regional-residual separation techniques; the amount of time and manpower available; the kinds of available digitizing and computer equipment; the availability and amount of the other geophysical data which can be used as control; and most important, the purpose of the investigation.

Most systems of gravitational analysis involve iterative combinations of gravitational modeling and interpretation. First approximations of the unknown parameters are made using gravity and other available geophysical data. The first approximations are then used as input in appropriate two- or three-dimensional attraction equations and the gravitational effects are computed over a profile or area.

The computed gravitational effects are compared with the observed residual gravity anomalies and adjusted at each computation point by some appropriate mathematical technique (i.e., analysis of Fourier components, Fourier convolution, method of least squares minimization or non-linear optimization). The updated model, based on the adjusted unknown parameters, is then analyzed in terms of geological and geophysical

116

possibilities. It is often necessary and useful to compute and analyze several possible models. Thus, the analytical techniques of gravitational analysis provide generalized schematic models. Detailed structure must then be hypothesized on the basis of experience and intuitive judgment.

REFERENCES

1. Bott, M. H. P.; R. Smith, "The Estimation of the Limiting Depth of Gravitating Bodies," _Geophys Prospect_, 6, p 1, 1958

2. Clermont, K, "A Computer Program for Gravitational Attraction of Arbitrary Three-Dimensional Bodies, With Application to the Crazy Mountains and Little Rocky Mountains, Montana," _Geol. Eng. Rpt # 67-1_, Princeton Univ, Princeton, 1967.

3. Dobrin, M. B., _Introduction to Geophysical Prospecting_, McGraw Hill Book Co., New York, 1960.

4. Egyed, L., "A New Method of Average Density Determination," Ann. University, Sc. Budapest, S. Geol, I, p. 33, 1957.

5. Garland, G. D., _Introduction to Geophysics_, W. B. Saunders Co., Philadelphia, PA, 1971.

6. Geldart, L. P., D. E. Gill and B. Sharma, "Gravity Anomalies of Two-Dimensional Faults," _Geophysics_, 23, pp. 372 - 379, April 1966.

7. Grant, F. S. and G. F. West, _Interpretation Theory in Applied Geophysics_, McGraw Hill Book Co., New York, 1965.

8. Hammer, S., "Approximation in Gravity, Interpretation Calculations," _Geophysics_, 39, pp. 205-222, 1974.

9. Heiland, C. A., _Geophysical Exploration_, Hafner Publishing Co., New York, 1968.

10. Hubbert, M. K., "Line-Integral Method of Computing Gravity" _Geophysics_, 13, pp. 215-225, 1948.

11. Jung, K., "Über die Bestimmung der Bodendichte aus den Schwere-messungen," _Beitr. Angew. Geoph._, 10, 1943.

12. Jung, K., _Schwerkraftverfahren in der Angewandten Geophysik_, Geest and Portig K. - G., Leipzig, 1961.

13. Linsser, H., "A Generalized Form of Nettleton's Density Determin-ation," _Geophys. Prosp._ 13, pp. 215-225, 1948.

14. Morgan, H. A. and F. S. Grant, "High-Speed Calculation of Gravity and Magnetic Profiles Across Two-Dimensional Bodies Having Arbitrary Cross-Section," _Geophys, Prosp._, 7, pp. 10-15, 1963.

15. Nagy, D., "The Gravitational Attraction of a Right Rectangular Prism," _Geophysics_, 31, pp. 362-371, 1966.

16. Nagy, D., "A Chart For the Computation of the Gravitational Attraction of a Right Rectangular Prism," _Pure and Applied Geophysics_, 102, pp. 5-14, 1973.

17. Nettleton, L. L., "Determination of Density for Reduction of Gravimetric Observations," _Geophysics_, 4, pp. 1976-183, 1939.

18. Nettleton, L. L., "Elementary Gravity and Magnetics for Geologists and Seismologists," _SEG Monograph Series #1_, 1971.

19. Pick, M., J. Picha and V. Vyskočil, _Theory of the Earth's Gravity Field_, Elsevier Publishing Co., New York, 1973.

20. Qureshi, I. R., and H. G. Mula, "Two-Dimensional Mass Distributions From Gravity Anomalies: A computer Method," _Geophysical Prosp._, V. 19, p. 180-191, 1971

21. Skeels, D. C., "An Approximate Solution of the Problem of Maximum Depth in Gravity Interpretation," _Geophysics_, V. 28, p. 724-735, 1963.

22. Strange, W. E. and G. P. Woollard, "The Use of Geologic and Geophysical Parameters in the Evaluation, Interpolation, and Prediction of Gravity," HIG-64-17, AF23 (601)-3879, Hawaii Institute of Geophysics, University of Hawaii, 1964.

23. Takin, M. and M. Talwani, "Rapid Computation of the Gravitation Attraction of Topography on a Spherical Earth," _Geophys. Prospect_, 14, (2), pp. 119-142, 1966.

24. Talwani, M., J. L. Worzel and M. Landisman, "Rapid Gravity Computations for Two-Dimensional Bodies With Application to the Mendocino Submarine Fracture Zone," _JGR_, 64, (1), pp. 49-59, 1959.

25. Talwani, M. and M. Ewing, "Rapid Computation of Gravitational Attraction of Three-Dimensional Bodies of Arbitrary Shape," Geophysics, 25, (1), pp. 203-225, 1960.

26. Talwani, M., "Computer Usage in the Computation of Gravity Anomalies," _Methods in Computational Physics, Geophysics_, V. 13, Academic Press, New York, 1973, pp. 343-389.

BIBLIOGRAPHY

1. Al-Chalabi, M., "Interpretation of Gravity Anomalies by Non-Linear Optimization," <u>Geophys Prospecting</u>, 20, 1-16, 1971.

2. Backus, G., and F. Gilbert, "The Resolving Power of Gross Earth Data," <u>Geophys. Journ. Roy. Astron. Soc.</u>, 16, 169-205, 1968.

3. Bott, M. H. P., "Solution of the Linear Inverse Problem in Magnetic Interpretation With Application to Oceanic Magnetic Anomalies," <u>Geophys. Journ. Roy. Astron. Soc.</u>, 13, 313-323, 1967.

4. Braile, L. W., G. R. Keller, and W. J. Peeples, "Inversion of Dimensional Density Distributions" <u>JGR</u>, 79, pp. 2017-2021, 1974.

5. Corbato, C. E., "A Least Squares Procedure for Gravity Interpretation," <u>Geophysics</u>, 30, pp. 228-233, 1965.

6. Daneŝ, Z. F., "On a Successive Approximation Method for Interpreting Gravity Anomalies," <u>Geophysics</u>, 25, pp. 1215-1228, 1960.

7. Dyrelius, D. and A. Vogel, "Improvement of Convergency in Iterative Gravity Interpretation," <u>Geophys. Journ Roy. Astron. Soc.</u>, 27, pp. 195-205, 1972.

8. Jackson, D. D., "Interpretation of Inaccurate, Insufficient, and Inconsistent Data," <u>Geophys. Journ. Roy. Astron. Soc.</u>, 28, pp. 97-109, 1972.

9. Johnson, W. W., "A Least-Squares Method of Interpreting Magnetic Anomalies Caused by Two-Dimensional Structures," <u>Geophysics</u>, 34, pp 65-74, 1969.

10. Majumdar, R. K. and S. H. Rao, "A Rapid Method for the Determination of Gravity and Magnetic Effects of Two=Dimensional Prismatic Bodies," <u>Gerlands Beiträge Zur Geophysik</u>, 82, pp. 235-244, 1973.

11. Nagy, D., "The Gravitational Attraction of a Right Rectangular Prism," <u>Geophysics</u>, 31, pp. 362-371, 1966.

12. Negi, J. G. and S. C. Garde, "Symmetric Matrix Method for Rapid Gravity Interpretation," <u>JGR</u>, 74, pp. 3804-3807, 1969.

13. Roy A., "Ambiguity in Geophysical Interpretation," <u>Geophysics</u>, 27, pp. 90-99, 1962.

14. Tanner, J. G., "An Automated Method of Gravity Interpretation," <u>Geophys. Journ. Roy Astron. Soc.</u>, 13, pp. 339-347, 1967.

120

15. Skeels, D. C., "Ambiguity in Gravity Interpretation," _Geophysics_, 12, pp. 43-56, 1947.

16. Vogel, A., "Least Squares in Three-Dimensional Gravity and Magnetic Interpretation," _Geoexploration_, 2, pp. 1-19, 1964.

External
Initial Distribution List
For
DMAAC RP-76-001

1. Director
   Defense Mapping Agency
   ATTN: PPS
   U. S. Naval Observatory, Bldg. 56
   Washington, D. C. 20305

2. Director
   DMA Topographic Center
   ATTN: Code 52000
   6500 Brooks Lane, N. W.
   Washington, D. C. 20315

3. Commander   2 Copies
   U. S. Naval Oceanographic Office
   ATTN: Code 3530
   Washington, D. C. 20373

4. Director   1 Copy
   DMA Inter American Geodetic Survey
   ATTN: Mr. Stephen Patchett
   Ft. Clayton, Canal Zone

5. Commander   1 Copy
   DMAAC Geodetic Survey Squadron
   F. E. Warren AFB, WY 82001

6. Mr. William Strange   1 Copy
   National Oceanic and Atmospheric Administration
   National Ocean Survey
   Rockville, Maryland 20852

7. AFGL/LW Stop #30   1 Copy
   ATTN: Mr. Dave Anthony
   L. G. Hanscom Field
   Bedford, Massachusetts 01730

8. DMA Liasison Officer   5 Copies
   USDAO
   U. S. Embassy, Box 36
   FPO New York 09510

9. University of Hawaii   1 Copy
   Hawaii Institute of Geophysics
   2525 Correa Road
   Honolulu, Hawaii   96822

10. The Ohio State University   2 Copies
    Department of Geodetic Science
    1958 Neil Avenue
    Columbus, Ohio   43210

11. Purdue University   1 Copy
    Department of Geosciences
    Lafayette, Indiana   47907

12. Dr. Ben Bryan   1 Copy
    Tennessee Valley Authority
    Geologic Branch
    51 Evans Building
    Knoxville, Tennessee   37902

13. AFSWC   1 Copy
    Kirtland AFB, NM   87117

14. Director   1 Copy
    Defense Mapping Agency
    ATTN: PRA
    U. S. Naval Observatory, Bldg. 56
    Washington, D.C.   20315

15. Mr. Harold C. Krivoy   1 Copy
    U. S. Geological Survey
    National Center, Mail Stop 955
    Reston, Virginia   22092

16. Defense Documentation Center   12 Copies
    Cameron Station, Virginia   22314

17. Dr. George P. Woollard   1 Copy
    University of Hawaii
    Hawaii Institute of Geophysics
    2525 Correa Road
    Honolulu, Hawaii   96822

18. Office of Naval Research   1 Copy
    ATTN: Dr. Alexander Malahoff/Code 483
    Marine Geology and Geophysics Program
    Arlington, Virginia   22217

19. Lamont-Doherty Geological Observatory   1 Copy
       of Columbia University
    ATTN: Dr. Manik Talwani
    Palisades, New York   10964

Internal
Initial Distribution List
For
DMAAC RP-76-001

PRP - 3 Copies

PPI - 1 Copy

RDSL - 1 Copy

AADL - 1 Copy

RD - 2 Copies

RDG - 1 Copy

RDGG - 1 Copy

RDP - 1 Copy

SECURITY CLASSIFICATION OF THIS PAGE *(When Data Entered)*

REPORT DOCUMENTATION PAGE

		READ INSTRUCTIONS BEFORE COMPLETING FORM
1. REPORT NUMBER DMAAC/RP-76-001	2. GOVT ACCESSION NO.	3. RECIPIENT'S CATALOG NUMBER
4. TITLE *(and Subtitle)* GRAVITATIONAL MODELING.		5. TYPE OF REPORT & PERIOD COVERED FINAL rept.,
		6. PERFORMING ORG. REPORT NUMBER
7. AUTHOR(s) Charles W. Beierle Walter J. Rothermel	134p.	8. CONTRACT OR GRANT NUMBER(s) Sep 76
9. PERFORMING ORGANIZATION NAME AND ADDRESS Defense Mapping Agency Aerospace Center St. Louis AFS, MO 63118		10. PROGRAM ELEMENT, PROJECT, TASK AREA & WORK UNIT NUMBERS
11. CONTROLLING OFFICE NAME AND ADDRESS Gravity Correlation Branch (RDNC) DoD Gravity Services Division Research Department		12. REPORT DATE SEPTEMBER 1975
		13. NUMBER OF PAGES 121
14. MONITORING AGENCY NAME & ADDRESS*(if different from Controlling Office)*		15. SECURITY CLASS. *(of this report)* UNCLASSIFIED
		15a. DECLASSIFICATION/DOWNGRADING SCHEDULE

16. DISTRIBUTION STATEMENT *(of this Report)*

Approved for public release;
distribution unlimited

17. DISTRIBUTION STATEMENT *(of the abstract entered in Block 20, if different from Report)*

18. SUPPLEMENTARY NOTES

19. KEY WORDS *(Continue on reverse side if necessary and identify by block number)*

Gravitational Modeling, Gravimetric Interpretation, Mass Modeling,
Mass Attraction, Two-Dimensional Modeling, Three-Dimensional Modeling

20. ABSTRACT *(Continue on reverse side if necessary and identify by block number)*

Formulas for computing the gravitational effect of some simple two-and-three-dimensional geometric figures are presented in forms suitable for use with digital computers and in many cases, programmable desk calculators. Basic computation schemes are presented for complex two-and-three-dimensional bodies of arbitrary shape. Some simple inversion rules or techniques are presented which yield approximations of depth based on simple geometric figures. Such over →

DD FORM 1473 EDITION OF 1 NOV 65 IS OBSOLETE

20. ABSTRACT (cont)

inversion techniques are particularly applicable where gravity measurements
are sparse. These techniques yield first approximations of the depth,
size and shape of the mass or masses causing a given residual gravity
anomaly. Density or density contrast is independent of depth, size and
shape and is discussed seperately. Density and porosity are defined by
appropriate equations. Generalized density relationships, based on rock
types are discussed. Equations for the determination of effective density
from gravity measurements are presented. The concluding remarks cover
some general aspects of gravitational modeling.